

Summer 2019

Investigation of Fundamental Principles of Rigid Body Impact Mechanics

Khalid Alluhydan

Southern Methodist University, kalluhyd@smu.edu

Follow this and additional works at: https://scholar.smu.edu/engineering_mechanical_etds

 Part of the Acoustics, Dynamics, and Controls Commons, Applied Mechanics Commons, Biomechanical Engineering Commons, Biomechanics and Biotransport Commons, Dynamics and Dynamical Systems Commons, Dynamic Systems Commons, Engineering Mechanics Commons, Engineering Physics Commons, Mechanics of Materials Commons, Non-linear Dynamics Commons, Ordinary Differential Equations and Applied Dynamics Commons, Structural Materials Commons, and the Structures and Materials Commons

Recommended Citation

Alluhydan, Khalid, "Investigation of Fundamental Principles of Rigid Body Impact Mechanics" (2019).
Mechanical Engineering Research Theses and Dissertations. 17.
https://scholar.smu.edu/engineering_mechanical_etds/17

This Dissertation is brought to you for free and open access by the Mechanical Engineering at SMU Scholar. It has been accepted for inclusion in Mechanical Engineering Research Theses and Dissertations by an authorized administrator of SMU Scholar. For more information, please visit <http://digitalrepository.smu.edu>.

INVESTIGATION OF FUNDAMENTAL PRINCIPLES
OF RIGID BODY IMPACT MECHANICS

Approved by:

Dr. Yildirim Hurmuzlu
Professor

Dr. MinJun Kim
Professor

Dr. Peter Raad
Professor

Dr. Edmond Richer
Associate Professor

Dr. Dario Villarreal
Assistant Professor

INVESTIGATION OF FUNDAMENTAL PRINCIPLES
OF RIGID BODY IMPACT MECHANICS

A Dissertation Presented to the Graduate Faculty of the

Bobby B. Lyle School of Engineering

Southern Methodist University

in

Partial Fulfillment of the Requirements

for the degree of

Doctor of Philosophy

with a

Major in Mechanical Engineering

by

Khalid S. Alluhydan

B.S., Southern Methodist University, 2013
M.S., Southern Methodist University, 2014

August 6, 2019

Copyright (2019)

Khalid S. Alluhydan

All Rights Reserved

ACKNOWLEDGMENTS

I would like to express my deepest respect, gratitude, and appreciation to my academic advisor and professor Dr. Yildirim Hurmuzlu. I am very grateful for your encouragement, guidance, and motivation. You've been a mentor, an academic advisor, and a father. With your help, you've made this work possible. Thank you for making me a better person, student, and researcher.

I would also like to thank my professors on my supervisory committee, Dr. Peter Raad, Dr. Edmond Richer, Dr. Minjun Kim, and Dr. Dario Villarreal, for their valuable advice and comments, which have significantly helped me to improve my work.

I would like to express the greatest respect, love, appreciation, and gratitude to my mother and father, Meznah and Suliman Alluhydan. Thank you for dedicating your lives for your family, and thank you for making me who I am today. Words can't express my gratitude for everything you've done. I hope I made you proud of me.

I want to thank my sister Raghad, and my brothers Abdullah, Mohammed, and Omar for their love and support. I also want to thank my grandmother Meznah Alluhydan for her love and support, for which I am very grateful.

Finally, I would like to express my appreciation and love for all of my friends who supported me throughout my journey. I want to thank my friends and labmates: Dr. Joe Zoghzoghy, Dr. Ahmad Alshorman, Ehab Alkhatib,

Moahd Alghuson, Assaad El Helou, Elie Salameh, Ahmad Gad, Youssef Jaber, Abdullah Jabr, Shide Bakhtiari, and Adam Cox. Special thanks to my friend and projects mate Pouria Razzaghi.

Alluhydan, Khalid S.

B.S., Southern Methodist University, 2013
M.S., Southern Methodist University, 2014

Investigation of Fundamental Principles
of Rigid Body Impact Mechanics

Advisor: Dr. Yildirim Hurmuzlu

Doctor of Philosophy degree conferred August 6, 2019

Dissertation completed April 03, 2019

In impact mechanics, the collision between two or more bodies is a common, yet a very challenging problem. Producing analytical solutions that can predict the post-collision motion of the colliding bodies require consistent modeling of the dynamics of the colliding bodies. This dissertation presents a new method for solving the two and multibody impact problems that can be used to predict the post-collision motion of the colliding bodies. Also, we solve the rigid body collision problem of planar kinematic chains with multiple contacts with external surfaces.

In the first part of this dissertation, we study planar collisions of Balls and Cylinders with an emphasis on the coefficient of restitution (COR). We conduct a set of experiments using three types of materials; steel, wood, and rubber. Then, we estimate the kinematic COR for all collision pairs. We discover unusual variations among the Ball-Ball (B-B) and Ball-Cylinder (B-C) CORs. We propose a discretization method to investigate the cause of the variations in the COR. Three types of local contact models are used for the simulation including: rigid body, bimodal linear, and bimodal Hertz models.

Based on simulation results, we discover that the bimodal Hertz model produce collision outcomes that has the greatest agreement with the experimental results. In addition, our simulations show that softer materials need to be segmented more than harder ones. Softer materials are materials with smaller stiffness values than harder ones. Moreover, we obtain a relationship between the stiffness ratio and the number of segments of softer material to produce the physically most accurate B-C CORs. We validate this relationship and the proposed method by conducting two additional sets of experiments.

In the second part of the dissertation, we study planar collisions of hybrid chains of balls and cylinders with an emphasis on the post-impact velocities. We use three types of materials including steel, wood, and rubber. We perform the collision experiments of balls and cylinders for three, four, and five-body chains and obtain their corresponding pre- and post-impact velocities. We propose a discretization method to accurately calculate the post-impact velocities of the colliding bodies in the chain. We use the bimodal Hertz contact force model and employ the Ball-Ball COR at the contacting segments to analyze the impact dynamics of the colliding objects.

A relationship between the stiffness ratio and the number of segments of softer material is used to determine the required number of segments for each ball and cylinder connected in the chain. The simulation runs show that by using this relationship, we obtain the greatest agreement of the post-impact velocities of the colliding bodies with the experimental results.

Finally, we consider the rigid body collision problem of particle based multi-branch kinematic chains with external surfaces. One end of the chain strikes an impact surface while other ends are resting on contact surfaces. The chain

consists of two types of primitive building units, a mass with a revolute joint, and a connecting rod. A solution to the problem was presented before. Yet, the uniqueness and existence of solutions were not proven for the general case.

In this chapter, we use the linear and angular momentum principles with a set of complementary equations to analytically prove that the solution exists and it is unique. The task is to find critical configuration conditions such that a contact mass has zero normal velocity, and normal impulse. We present a mathematical development that expresses the normal velocities and impulses at the contacting ends in terms of the normal impulse at the impact point. The approach not only proves uniqueness and existence, but also yields precise conditions to detect the so called critical configurations of the chain. When the chain has a critical configuration, the normal velocity and impulse at a contacting end become simultaneously equal to zero.

We apply the proposed methods to obtain critical configurations of two numerical examples: a three- and a five-mass chains. Finally, we experimentally verify the existence of the critical configuration for a three-mass chain on flat and inclined surfaces with different inclination angles.

TABLE OF CONTENTS

LIST OF FIGURES	ix
LIST OF TABLES	xi
LIST OF SYMBOLS	xii
CHAPTER	
1. Introduction & Literature Survey	1
1.1. Impact Theory	1
1.2. Coefficient of Restitution	11
1.3. Impacts with Cylinders	15
1.4. Multibody Impacts	18
1.5. Impacts of Kinematic Chains	22
1.6. Structure of the Dissertation	25
2. On Planar Impacts of Cylinders and Balls	27
2.1. Introduction	27
2.2. Experimental Setup	29
2.3. Problem Description	36
2.4. Generalized Equations of Motion	36
2.4.1. Rigid Body Method	39
2.4.2. Bimodal Contact Force Model	40
2.5. Numerical Simulation and Results	44
2.6. Verification of Results	56

3.	Planar Impacts in Hybrid Chains of Cylinders and Balls.....	59
3.1.	Introduction	59
3.2.	Experimental Setup	62
3.3.	Problem Description	67
3.3.1.	Generalized B-B-C	68
3.3.2.	Segmentation Process	75
3.4.	Numerical Simulation and Results	78
4.	On Uniqueness and Existence of Solutions to Multiple-Contact Collisions of Planar-Particle Based Kinematic Chains.....	86
4.1.	Introduction	86
4.2.	Problem Description	89
4.3.	Development of the Impact Equations	92
4.4.	Normal Impulse and Normal Velocity Relationship of the Contacting Mass	96
4.4.1.	Three-Mass system.....	105
4.4.1.1.	Three-Mass System with a Single Flat Surface	108
4.4.1.2.	Three-Mass System with two Parallel Level Surfaces	108
4.4.1.3.	Three-Mass System with an Inclined Surface.	109
4.4.2.	Five-Mass System	110
4.5.	Experimental Set-up	111
4.6.	Experimental Verification.....	115
5.	Conclusions	123
	BIBLIOGRAPHY	127

LIST OF FIGURES

Figure	Page
2.1 B-B collision experimental setup	30
2.2 B-C collision experimental setup.....	31
2.3 Experimental Contact Stiffness Testing	35
2.4 General discrete B-C model	38
2.5 Force Displacement Curves	41
2.6 Average percentage error for all categories	45
2.7 Percentage error of category 1 B-C collisions	47
2.8 Percentage error of category 2 B-C collisions	48
2.9 Percentage error of category 3 B-C collisions	49
2.10 Average percentage error for all categories	50
2.11 Numerical force displacement profile	51
2.12 Number of segments corresponding to APE_m	53
2.13 Number of segment of the softer material and stiffness ratio	55
2.14 COR versus the number of segments of the softer material	58
3.1 Three-body collision experimental setup	62
3.2 Four-body collision experimental setup	63
3.3 Five-body collision experimental setup	63
3.4 General discrete B-B-C model	68

3.5	B-B-C force displacement curves.....	72
3.6	Stiffness ratio versus the number of segments	77
3.7	Example of five-body chain combination	78
3.8	Three-body (B-B-C) APE	83
3.9	Three-body (B-C-B) APE	84
3.10	Four-body system APE	85
3.11	Five-body system APE.....	85
4.1	Multiple-Contact, Planar, Particle Based Chain	91
4.2	A Section of the Linear Chain	101
4.3	General Chain Mechanism.....	103
4.4	General Chain Mechanism with multiple contacting points	105
4.5	The Three-Masses Chain.	107
4.6	The Five-Mass Chain	110
4.7	Experimental Setup	113
4.8	Geometric properties of the three mass chain	114
4.9	Flat surface experimental and theoretical prediction of the detachment of the contact mass	116
4.10	Flat surface experimental readout for detachment of the con- tact mass.	118
4.11	Inclined surface experimental and theoretical prediction for the detachment and non-detachment of the contact mass	119
4.12	Inclined surface experimental readout for detachment of the contact mass for 25° inclination angle	121
4.13	Variation of experimental $\Delta\theta_c^e$ with the inclination angles	122

LIST OF TABLES

Table	Page
2.1 Masses and geometric values	33
2.2 Experimental COR values	34
2.3 Experimental stiffness values	36
2.4 Minimum average percentage error of each category	54
2.5 Masses and geometric values of the small balls	56
2.6 Experimental stiffness values	56
2.7 Experimental COR values with the small balls	57
3.1 Masses and geometric values	65
3.2 Experimental B-B COR values	66
3.3 Experimental stiffness values	67
3.4 Three-body (B-B-C) post-impact velocities	80
3.5 Three-body (B-C-B) post-impact velocities	81
3.6 Four-body post-impact velocities	82
3.7 Five-body post-impact velocities.....	82

LIST OF SYMBOLS

x, y, z, θ	generalized coordinates
$\dot{x}, \dot{y}, \dot{\theta}, V, v$	velocity
\dot{x}_i^-	pre-impact velocity of each segment
\dot{x}_b^-	pre-impact velocity of the ball
\dot{x}_c^-	pre-impact velocity of the cylinder
\dot{x}_i^+	post-impact velocity of each segment
\dot{x}_b^+	center of mass post-impact velocity of the ball
\dot{x}_c^+	center of mass post-impact velocity of the cylinder
$\ddot{x}, \ddot{y}, \ddot{\theta}, a$	acceleration
δ	relative displacement
δ_m	maximum displacement
δ_p	permanent indentation
m	mass
m_b	ball mass
m_c	cylinder mass
m_k	contact mass
m_{imp}	impact mass
R_b	ball radius

L_c	cylinder length
L	link length
K^i	linear internal spring
K_b^i	stiffness of the internal springs of the ball
K_c^i	stiffness of the internal springs of the cylinder
K_b	overall stiffness of the ball
K_c	overall stiffness of the cylinder
K_b^e	external contact spring of the ball
K_c^e	external contact spring of the cylinder
K_C	compression collision stiffness
K_R	restitution collision stiffness
K_S^i	internal stiffness of the soft material
K_H^i	internal stiffness of the hard material
W_C	work done during compression
W_R	work done during restitution
E_L	local energy loss
COR	coefficient of restitution
e_L	local, average experimentally measured Ball-Ball coefficient of restitution

\bar{e}_G	average experimentally measured Ball-Cylinder coefficient of restitution
e_G	equivalent mathematical Ball-Cylinder coefficient of restitution
e^*	energetic coefficient of restitution
\bar{e}	energetic coefficient of restitution at the contacting segments
j	number of segments
j_S	number of segments of the softer material
j_H	number of segments of the harder material
N	total number of segments
n	Hertz exponent
PE	percentage error
APE	average percentage error
APE_m	minimum average percentage error
r_K	stiffness ratio
\vec{F}_c, F	contact force
F_m	maximum contact force
\hat{F}, τ	impulse at the contact points
η	normal impulse at the impacting point

μ	coefficient of friction
\tilde{F}	impulse contribution of the impacting mass
$\Delta\dot{\theta}$	change in angular velocity
ϕ	surface inclination angle
\tilde{f}_i	internal impulse reaction
$\Delta\theta_c$	critical configuration
$\Delta\theta_c^t$	theoretical critical configuration
$\Delta\theta_c^e$	experimental critical configuration
L_y	elevation difference between two parallel surfaces
L_x	length from the contact mass to the end of the flat surface
\mathbf{x}	vector of the generalized coordinates
$\dot{\mathbf{x}}$	vector of the generalized velocities
$\ddot{\mathbf{x}}$	vector of the generalized accelerations
\mathbf{M}	mass matrix
\mathbf{C}	centripetal vector
\mathbf{G}	gravity terms vector
\mathbf{T}	joint moments vector
ϕ	inclination angle vector of surfaces

S	external contact surface
\mathbf{D}	contact forces terms matrix
\mathbf{F}	contact forces vector
\mathbf{a}	normal and tangential accelerations vector
$\mathbf{H}_1, \mathbf{H}_2$	general form matrices of the normal and tangential accelerations
$\bar{\mathbf{x}}$	generalized position constant vector
\mathbf{V}	velocity vector
Γ	constant matrix depends on pre-impact positions, masses, rod's lengths, and inclination angles of the contact surfaces
$\boldsymbol{\tau}$	impulses at the contact points vector
Ψ_1, Ψ_2	vectors
\mathbf{V}_y	normal velocity vector
$\hat{\mathbf{F}}_y$	normal impulse vector
α, β	vectors
ξ, γ	matrices
$\hat{i}, \hat{j}, \hat{k}$	unit vectors

*I dedicate this thesis to my mother, father, sister, grandmother, and my
brothers.*

In a great memory of my best friend, Abdullah Abdulaziz Alluhydan.

Chapter 1

Introduction & Literature Survey

1.1. Impact Theory

In mechanics, impact is a complex phenomenon in nature that occurs when two or more bodies collide [2]. Impact is also a complicated, sudden, and short term encounter for two bodies in contact [3]. The collision between two rigid bodies produces normal impulsive forces at the contact region [4]. Impact can also be characterized as changes in the velocities of colliding bodies resulting from high reaction force in which the colliding bodies experience elastic-plastic deformation and energy dissipation in different forms [5]. Impact is characterized as an impulsive motion in which the contact forces experience sudden changes [6]. Keller stated that in rigid body mechanics, a collision between two bodies with a single point of contact is considered to be instantaneous, in which bodies exert an impulsive reaction force opposing each other [7]. Impact exists in many engineering applications and problems such as multibody systems, robots, and machinery design [8]. Impacts or collisions are usually accompanied by important characteristics that must be taken into consideration including acceleration, deceleration, velocity changes, energy dissipation, and high forces [9]. Impacts can have fully plastic collisions where the relative post-impact velocity of the colliding bodies is zero [10]. The classification of impact problems, however, is built upon the system's motion before and after

the impact [11].

In general, there are four different types of impact [5]. Central impact occurs when the center of masses of the colliding bodies are aligned on the line of impact. Eccentric impact occurs when the center of masses of the colliding bodies are not aligned with the line of action or impact. Direct impact occurs when the impact occurs when the colliding bodies initial velocities lie on the line of impact. Finally, an impact is oblique if the colliding bodies initial velocities are on an angle. Impacts are considered to be continuous processes, which last for a very short period of time. These impacts cause changes in the geometry and discontinuities that might exist as a result of the collision. It is, however, important to take into account these characteristics that result from collisions in the design of mechanical systems to avoid failures or permanent damages.

Generally, there are two main methods for approaching the solution of impact problems that are: the instantaneous and continuous based methods [12]. The instantaneous method is based on the impulse momentum definition [13]. In general, the instantaneous method assumes that the colliding bodies are rigid and the period of collision is very short. It can be considered a piecewise analysis [10]. This method was first studied for the collision between two spheres with no friction by Newton [14]. Whittaker expanded Newton's work to take into account frictional effects [15]. Brach expanded Newton's work and developed an algebraic solution for the impact problem in the presence of friction [16]. He also proposed that in the presence of friction or tangential effect, the tangential definition of the coefficient of restitution can be used to describe the tangential effects on the tangential motion [17]. Wang and Ma-

son used the Routh graphical representation to solve the impact problem and proposed an analytical expression for the frictional impulse [3]. Their solution of the rigid body problem is based on the fact that the collision process is abrupt, reactions are impulsive, discontinuities in the kinetic variables exist, and no deformations occur during the collision process. They also concluded that the forces beside the contact region reactions are negligible. These assumptions, however, limit the applicability of the mathematical formulation of the instantaneous method since it opposes other types of collisions except for very rigid bodies. Several authors, however, showed the applicability of using the instantaneous method for impact problems involving flexible bodies [18, 19]. They concluded that the effect of these types of collisions on the coefficient of restitution is very little. Furthermore, Keller proposed an integrative process to solve for the impulsive forces based on the coefficient of restitution [7]. Smith, however, demonstrated Newton's work and proposed an algebraic approach to solve the impact problem based on Newton's kinematic definition of the coefficient of restitution [20]. The simplest way of solving the problem is by using the principle of conservation of linear momentum and the kinematic definition of the coefficient of restitution. A kinetic energy balance can be used as well to produce unique solutions for the impact problem. This fundamental approach connects the moments prior to and after the collision and produces unique solutions for the post-collision motion, particularly regarding, the post-collision velocities. This approach requires knowledge about the initial conditions. In addition, knowledge about a physical value of the coefficient of restitution is necessary in order to solve the impact problem [21, 22]. The instantaneous method has always treated impact problems as systems of

particles and unconstrained bodies. However, researchers have extended this assumption to solve impact problems in constrained systems using the impulse momentum approach [23].

The second method for solving impact problems is known as the continuous based method [13], also known as the compliance based method [24]. This approach assumes that the interacting or colliding bodies act in a continuous behavior. In addition, it allows the contact forces to be part of the system's equations of motion. In the continuous based methods, local compliance is considered and the collision period can be divided into two main phases: compression and restitution phases, where the dynamic behavior of the colliding bodies is mainly governed by material properties, configuration, and initial conditions of the colliding objects [3, 5, 9, 16]. When the colliding bodies are in contact, the compression phase starts by converting the initial kinetic energy to elastic potential energy. This phase lasts until the normal relative velocities of the colliding bodies are equal and deformation is at its maximum. Once the compression phase ends, the restitution phase starts and the colliding bodies begin to leave each other while remaining in contact. The restitution phase ends when the colliding bodies are fully separated from each other. During the compression phase, the kinetic energy is transformed into internal energy; in the restitution phase, the maximum elastic potential energy stored is converted into kinetic energy [25]. Note that it is not always the case that the initial kinetic energy is fully recovered at the end of the collision. This is only possible for elastic collisions. One of the most fundamental challenges during the process of collision is the process of energy transfer. In the continuous based method, the energy transfer is characterized by a hysteresis loop on the force

displacement curves [26]. Since the contact forces act upon the system in a continuous manner as a function of the relative displacement and velocity, the energy loss can be evaluated from the relative displacement and the velocities of the colliding bodies [27]. One of the main reasons for the use of continuous based methods is the difficulty of extending the impulse momentum based method for multibody systems. The continuous based method are suitable to generalize for multibody systems and for impacts concerning non-rigid collisions [28]. Non-rigid collisions involve bodies of materials whose composition are flexible or soft. These type of collisions mostly exhibit large deformations, and geometric changes may exist when subjected to external forces. Examples of these problems are mainly seen in the presence of friction where no uniquely possible solutions exist [29, 30]. Kumar and Howard stated that the use of the impulse momentum in the presence of friction may result in inconsistent solutions since it poses difficulties in collisions involving friction [31]. They concluded that in order to avoid ambiguities that might result and to resolve the problem, it is important to consider compliance-based modeling in the dynamic model. One the main features of the continuous based method is the fact that it allows the use of springs and dampers, which makes it possible to investigate the dynamics of collisions in a continuous manner [32]. The first compliant model for the collision between two spheres was developed by Hertz [33]. In his work, he considered the collision between the two spheres to have a perfectly elastic collision. It lies under the assumption that no energy is lost or dissipated during the collision process. In his model, he only incorporated the stiffnesses of the colliding bodies to model the collision process without considering damping. In addition, the relationship between the

contact force and relative displacement is nonlinear. In an extension of Hert'z work, Dubowsky and Freudenstein proposed a linear viscous damping term to the original Hertz contact law [34].

In the continuous analysis based methods for examining direct central impacts, two common contact force models have been used: visco-elastic contact force models and elasto-plastic contact force models. The basic principle of modeling collisions with only linear springs and damper does not yield sufficient conclusions about the dynamic behavior of the collision process [35–37]. As a result, many authors have introduced contact force based models with damping terms. In visco-elastic contact force models, the damping term is incorporated with the Hertz contact force model to represent the energy dissipation during the process of collision [38]. The general form of visco-elastic force models consist of two main terms, elastic, which is conservative, and viscous which, is dissipative [39]. The elastic term of the contact force model is based on Hertzian contact, which is nonlinear, while the dissipative term can be either linear or nonlinear depending on the proposed hypotheses. The dissipative or damping term consists of the relative velocity and damping coefficient. The damping coefficient contains the relative deformation and hysteresis damping factor [40]. Furthermore, the hysteresis damping factor consists of the initial conditions, contact stiffness, and coefficient of restitution. Clearly in such models, there are distinct characteristics differentiating the conservative and dissipative terms. First, the conservative terms includes only the contact stiffness, which is a property depending on the geometry of the colliding bodies. On the other hand, the damping term is associated with the energy dissipation and is directly tied to the coefficient of restitution [6,40,41].

Dissipative parameters such the hysteresis damping factor, which contributes to representing the energy transfer throughout the collision period, are computed based on energy balance [42]. Dissipative terms can also be computed through the equations of motion [43–45]. For visco-elastic force models, it is important to evaluate the damping coefficient to model the energy transfer within a system. It is, however, challenging as the energy loss within a system depends on the geometric configuration, design, and material properties [46]. The coefficient of restitution is used in the damping coefficient term to account for different forms of losses such as internal damping, heat, and wave propagation [47]. Goldsmith introduced the first contact force model in which he considered damping in the contact force model based on the Kelvin-Voight spring-dashpot linear dissipative force model [5]. Khulief and Shabana extended the Kelvin-Voight model and derived unique expressions for the contact stiffness and damping coefficients using energy balance methods [42]. In addition, Hunt and Crossley proposed a linear viscous damping term and introduced a new constant parameter called the coefficient of damping. The coefficient of damping was derived based on the kinematic impact law, initial conditions, and material properties [40]. Hunt and Crossley assumed that the energy dissipation process is achieved by material damping and energy is dissipated in the form of heat. Furthermore, Lankarani and Nikravesh introduced a linear visco-elastic contact force model and assumed that the energy loss is due to material damping for low impact velocities [6]. These proposed impact models are accurate to use for nearly elastic collisions, but, for inelastic collisions, the results contain large errors in the dynamic modeling. On the other hand, Lee and Wang proposed a nonlinear viscous damping term

to solve the impact problem [43]. Over the years, several visco-elastic models have been proposed. Many authors introduced nonlinear damping terms in their models [6, 40, 41, 48, 49], while others considered the linear form of damping for energy dissipation in their models [50–52]. Force models with viscous damping terms have several advantages over representing the colliding bodies with springs and damper only. Such models include no discontinues in the contact force during the collision process, especially at the beginning and end of impact [53]. Moreover, representing the colliding bodies using only the elastic Hertz contact force model poses difficulties since it doesn't incorporate any dissipative terms. Generally, visco-elastic contact force models produce good agreements with the experimentally measured outcomes for values of high coefficient of restitution, in nearly elastic impacts. These models, however, become more difficult to apply in the presence of plastic deformation. One of the drawbacks of modeling collisions with viscous damping, for example, is the assumption that all of the energy losses are due to material damping. These assumptions do not obey the actual energy losses produced by collisions.

The second type of contact force models, elasto-plastic contact force models, considers collisions involving plastic deformations. This type of contact force models identifies plastic deformations as the governing source of energy loss. They are based on the elastic Hertz contact force model. A hysteresis loop on the force displacement diagram is used to account for plastic deformations and energy dissipation during the process of collision [54]. Parameters are needed for the evaluation of the plastic deformation or permanent indentation term. These parameters are the maximum compressive force and maximum deformation. The kinetic energy dissipated in elasto-plastic collisions depends

mainly on wave propagation, friction, and plastic deformation [55]. For elasto-plastic collisions, the energy dissipated during the collision process can be observed by relating the work done in deforming the colliding objects [56]. The energy lost during the process of elasto-plastic collision can involve the propagation of elastic waves, but, in fully plastic collisions, these losses are very small or negligible. Lankarani and Nikravesh introduced a contact force model based on the assumption that collisions experience fully plastic impacts [12]. They related their contact force model during the compression phase to the original Hertz contact force model and proposed a contact force model for the variation in the restitution phase, which accounts for plastic deformation. The necessary parameters, such as the maximum compressive force and deformation, were obtained by using energy balance and conservation of linear momentum. In addition, integration of the effective equation of motion was done to achieve the derivation of the final analytical expression of the permanent indentation term. These parameters are functions of initial condition, coefficient of restitution, geometric, and material properties of the colliding bodies. The force model is nonlinear, and the dominant source of energy dissipation is local plasticity at the contact region. Ravani and Stronge introduced a new bilinear contact force model for elasto-plastic collisions [57]. In their model, they related the force during the restitution phase to the energetic coefficient of restitution to account for the variation during restitution. In addition, the contact stiffness during restitution is divided by the energetic coefficient of restitution to account for plastic losses. The expression of the permanent indentation was obtained by relating the energetic coefficient of restitution and maximum compression through the work done in deforming the objects during

both phases of collision: compression and restitution. Ismail and Stronge introduced a new bilinear contact force model which accounts for collisions that exhibit both viscous and plastic effects [58]. A plastic loss factor is introduced in their model to account for the energy dissipation. In addition, a visco-plastic coefficient of restitution is introduced for the collision of very stiff bodies. This coefficient of restitution accounts for collisions that exhibit elasto-plastic and visco-elastic effects. Their model is based on modifications to the Maxwell model to account for the losses caused by both viscous and plastic effects. One of the major advantages of elasto-plastic contact force models is the fact that they are efficient for conditions with high impact velocities or very low values of the coefficient of restitution. On the force displacement diagram, the end conditions state that the force vanishes and displacement is nonzero. The area under the force displacement curve represents the energy lost as a result of the collision. Generally, elasto-plastic contact force models are more efficient to use than visco-elastic based models. They produce consistent results and good agreement with the experimentally measured outcomes such as the post-impact velocities and coefficient of restitution. The fundamental basis of elasto-plastic based models includes reasonable and logical representation of energy dissipation during impacts. In addition, proper use of the coefficient of restitution provides logical means for representing energy losses and gives consistent solutions.

1.2. Coefficient of Restitution

The coefficient of restitution remains the most debatable and arguably, the most important constant that is used in the solution of impact problems [59]. Coefficients such as the coefficient of restitution are important in describing the solution of the final velocities, normal impulses, and kinetic energy of the colliding bodies [17]. In impact mechanics, simple coefficients such as the coefficient of restitution represent the complex behavior and scenarios that occur during collisions [8]. The simplicity of the coefficient of restitution makes it easy to use in relating other parameters for representing the energy dissipation, but the coefficient of restitution requires experimental measurements to accurately model collisions [60]. For the best modeling of energy loss during the process of collisions, the coefficient of restitution is used [16]. The loss of kinetic energy for collisions involving deformations can be caused by energy losses through stress, friction, and the work done on deforming the colliding objects [55]. Other sources of energy dissipation occur in the form of stress waves or wave propagation. These waves are generated at the contact point during impacts and they travel back and forth in the material with finite time and velocity [61]. This phenomena mostly happens in collisions between bodies with dissimilar size and material properties. Another source of energy loss can be in the form of plasticity or plastic deformation. This happens at the contact region where there is permanent indentation or damage left as a result of the collision. Energy loss also occurs in the form of material damping, where energy is lost due to internal damping within the material itself. Furthermore, energy can be lost in different forms such as heat or sound.

In general, energy loss during impacts can be either due to local collision properties or vibrations. The loss due to local deformations is permanent, while the vibrational energy loss is partially recovered [59]. The coefficient of restitution is used to express energy loss due to impacts. For perfectly elastic collisions, the coefficient of restitution is $e = 1$. For perfectly plastic collisions, the coefficient of restitution is $e = 0$. Therefore, the coefficient of restitution is limited between $0 \leq e \leq 1$. Perfectly elastic collisions indicate that the energy is fully recovered at the end of impact. Perfectly plastic collisions, however, indicate that the maximum amount of energy is lost as a result of collision. Moreover, for inelastic collision ($0 < e < 1$), the energy at the end of the impact is partially recovered. The three fundamental definitions in describing the coefficient of restitution are the Newtonian (kinematic) [14], Poisson's (kinetic or impulsive) [62], and Stronge's (energetic) definitions of the coefficient of restitution [63].

Generally, the coefficient of restitution depends in nature on many parameters such as material properties, geometric configuration of the colliding bodies, initial velocities, period of collision, and friction [5]. The coefficient of restitution can be defined for objects of any shape as the negation of the normal velocity ratio before and after impact [64]. Hunt and Corssley stated that the coefficient of restitution between two rigid bodies colliding in one dimensional impact and in pure translation as the ratio of their relative speeds before and after the impact [40]. In addition, Newton's kinematic definition of the coefficient of restitution relates the ratio of the relative normal velocities before and after impact, which he claimed to be dependent on the material properties of which the colliding bodies are made [14]. Poisson introduced the

kinetic definition of the coefficient of restitution and defined it as the ratio of the restitution to the compression normal impulses [62]. Stronge, however, defined his energetic definition of the coefficient of restitution as the square root of the negative ratio of the energy released in the restitution phases to the energy absorbed in compression during the collision period [63]. Therefore, it is simply defined as the square root of the negative ratio of the work done during restitution to the work done in compression.

In addition, Poisson studied the possible scenarios that may arise during impacts in the presence of friction. Poisson and Morin showed that for frictional impacts, one can relate the normal and tangential components of the contact force by using Columbs's friction model [65]. Routh introduced a graphical method based on the kinetic definition of coefficient of restitution to deal with impact problems with friction [66]. In his work, he studied and solved the case of frictional impacts, where velocity reversal takes place. In addition, velocity reversal happens in frictional impacts, when the direction of the slip motion of the colliding bodies changes direction. Wang and Mason used the Routh graphical method to solve for the impact problem with friction [3]. Whittaker expanded Newton's work to take into account frictional effects [15]. His method accounts for slippage in cases when the coefficient of friction is less than the ratio of the normal and tangential impulses. In addition, his method provides an algebraic solution by combining the kinematic and kinetic definitions of the coefficient of restitution. The algebraic solution provides an easy solution for the post-impact velocities. The drawback of his method is the fact that his solution is inconsistent for the case of velocity reversal when the slip motion changes direction. Kane and Levinson

have showed that in the presence of tangential effects during collisions, the coefficient of restitution produces inconsistent results [21]. In addition, they showed that Whittaker's method results in errors in the presence of friction. Brach developed an algebraic solution for the impact problem in the presence of friction [16]. His solution takes into account velocity reversal during the collision period [17]. Furthermore, his method corrects the energy paradox resulting from the change of direction during slip motion. Keller introduced a method for impact problems with friction using Poisson's definition of the coefficient of restitution [7]. In his method, he provided a correction based on the kinetic impact law such that energy does not increase. Keller addressed the energy paradox in frictional impacts that results only when the velocity reverses direction during slip motion. He stated that the magnitude of the tangential impulse is equal to the coefficient of friction times the normal impulse, and that this is only valid when the direction of slip motion remains unchanged and velocity doesn't reverse direction. His method requires the integration of the equations of motion for obtaining the full solution. Stronge introduced the energetic definition of the coefficient of restitution [63]. In his work, he considered friction impacts. In addition, he concluded that the use of Newton's impact law will provide inconsistency since it only accounts for the normal components of velocity. Moreover, his method corrects the inconsistencies in Poisson's definition of the coefficient of restitution in the presence of friction.

1.3. Impacts with Cylinders

Over the years, researchers have investigated the classical impact problem: the collision between two balls. This classical problem has been extended for linear chains of balls and multibody systems. Researchers have extended the ball problem to investigate different shapes and geometries, such as rocking blocks and cylinders. Stoianovici and Hurmuzlu studied the collision of cylindrical bars on external surfaces [67]. One very interesting observation is the significant variation in the kinematic coefficient of restitution that occurs as a result of varying the inclination angle. As a result, a discretized rigid body model of the cylinder is proposed to explain the physical behavior and variation. The variation in the coefficient of restitution was tied to two main factors: internal vibrations and multiple impacts. Hurmuzlu developed a new method to accurately predict the post-impact velocity for the collision of cylindrical bars on massive external surfaces [59]. The proposed method accounts for the local and global energy losses that occur as result of the collision. The proposed method generalizes the concept of the coefficient of restitution such that it can be used widely in different applications. In addition, a revised and energetically based coefficient of restitution is used, which takes into account the local and vibrational energy losses. The proposed method is validated with numerous sets of experiments.

Several authors have investigated the ball-cylinder collision problem. Auerbach investigated the relevance of colliding balls to colliding rods [68]. He stated that collision of balls is the same as colliding rods if the balls' and rods' radii and lengths are the same. Freschi *et al.* introduced a detailed study on the compression waves and kinetic energy losses for collisions involving balls

and cylinders with different lengths [69]. In their study, they investigated the fractional loss of kinetic energy and coefficient of restitution as a function of the rod's length using the principles of conservation of momentum and energy balance. Their work concluded that the fractional loss of kinetic energy increases as length and the coefficient of restitution decreases. Hu *et al.* studied the collision between a ball and an elastic rod [70]. They used the boundary approach and incorporated the elastic Hertz contact force model to represent the longitudinal waves in rods. Their work suggests combining both elastic and rigid body dynamics for longitudinal impacts into two timescale modes. The first is for the short term behavior, which includes for the wave phenomena, and the other is for the long term behavior after impact. Schiehlen *et al.* studied the collision between aluminum balls and cylinders using a finite element approach [71]. They investigated the coefficient of restitution to represent the energy loss and evaluated it numerically to include wave propagation. They stated that for repeated impacts, plastic deformation reaches a finite value and does not spread further; the remainder of energy loss on cylindrical bodies is in the form of waves. Schiehlen and Seifried studied the collision of balls impacting cylinders and half circular plates [72]. They approached the problem using the wave equation and elastic Hertz contact force model. In another contribution, Seifried *et al.* studied the collision of balls and half circular plates using the finite element approach [73]. Belyaev *et al.* studied the longitudinal impacts on a thin rod by a body and studied wave propagation using the finite element method and the elastic Hertz contact force model [74]. YuFeng and DeChao analyzed the collision of a particle colliding with a rod attached to a spring [75]. They stated that both the wave equation

and elastic Hertz contact force model produce the same results. They concluded that these approaches can be extended to beams, plates, and complex structures. Wang *et al.* investigated the collision of elastic bars and beams on massless springs [76]. In their analysis, they approached the solution to the problem by deriving the wave equations for the cases of constrained and free motion. In addition, they investigated the effect of the coefficient of restitution for this type of collision. Their analysis concluded that the coefficient of restitution is only dependent on the stiffness ratio and independent of the incident velocity. Yigit *et al.* studied the dynamics of radially rotating beams with impacts [53, 77]. They introduced a model based on the momentum balance and kinematic coefficient of restitution to investigate the applicability of using rigid body motion. Experimental and numerical work concluded that using rigid body analysis enables the prediction of the pre- and post-collision motion and the effect of the geometric configuration of the dynamic system on the coefficient of restitution is small for most impact situations. Gau and Shabana developed a solution procedure for the propagation of elastic waves in translating and rotating beams that undergo large displacements [78]. They formulated the equations of motion based on the principle of virtual work. The impact induced waves are analyzed using the generalized impulse momentum, which is expressed in terms of different parameters including the coefficient of restitution and Jacobian matrix of the kinematic constraints. In addition, they evaluated the applicability of their solution numerically using different values for the coefficient of restitution.

1.4. Multibody Impacts

Multibody dynamics is the study of systems composed of many bodies [79]. It can be also defined as systems with multiple bodies in which their interaction is governed by external forces, geometric, and kinematic constraints [79–81]. The interaction between the colliding bodies cause changes in the system’s behavior including courteous and rapid changes in velocities and acceleration. Multibody impacts are collections of bodies interconnected by forces [80]. Multibody impact is also a field which deals with the modeling and analysis of systems that can exhibit large deformations when subjected to collisions [82]. In these collisions, the colliding bodies experience rigid body motion, elasto-plastic deformations, and in some cases rotations. These types of collisions exist in many engineering applications such as robotics [83], biomechanics [84], railway design [85], space systems [86], automobiles [87], composite granular medium [88], and multi link manipulators [89].

This class of problems, however, is complex in nature. The selection of appropriate parameters and dynamic modeling is required to achieve good results [90–92]. In multibody impacts, nonlinearities and discontinuities may occur as a result of intermittent collisions [93]. Studying the geometric, kinematic, and dynamics structures of multibody systems can be highly complex due to the fact that these systems of connected bodies exhibit complex behaviors when subjected to collisions, which requires complex mathematical modeling and computational procedures [81]. Over the past few decades, researchers have been trying to extend the impact problem from single to multiple impacts and produce consistent solutions to accurately predict the post-impact velocities. As a result, the two main methods in approaching the solution to impact

problems, impulse momentum methods and compliance based methods, have been investigated and extended to multibody impacts. Experimental verification of certain parameters is necessary to obtain and to validate the proposed solution. These parameter include the coefficient of restitution between the colliding pairs and pre- and post-impact velocities.

Using the impulse momentum based methods for multibody impact problems, several authors have proposed solution procedures. The most fundamental solution procedure considers the impulse momentum and coefficient of restitution laws. Ceanga and Hurmuzlu were the first in obtaining uniquely and energetically consistent solutions for the post-impact velocities of balls in a linear chain [24]. They used the impulse momentum method for triplets of balls and introduced a new constant parameter called the impulse correlation ratio. The impulse correlation ratio relates the impulses in the chain. This constant parameter depends on the sequence, mass distribution, geometric and material properties. They incorporated the energetic coefficient of restitution to produce energetically consistent solutions. Analytically and energetically consistent solutions for the post-impact velocities were derived for the case of three balls. The proposed hypothesis was generalized for the N-ball problem. Furthermore, they conducted a large set of experiments to validate the solution for the three, four, five, and six ball impacts. Their generalized solution accounts for the intermittent collision phenomena, in which multiple impacts occur at a single contact point.

Walkiewicz and Newby proposed a solution method for the three ball problem which satisfies the conservation of momentum and energy principles [94]. The conclusion drawn from their work is that there are infinite

solutions for this class of problems. Johnson proposed a solution procedure based on subsequent impacts under the assumption of distinct collisions [95]. Han and Gilmore proposed algorithmic procedures to solve the multibody problem involving multiple collisions [96]. Their proposed solution, however, resulted in sets of post-impact velocities that are only valid for the same initial conditions. The three ball problem was also considered by Brogliato [97]. He stated that the impulse momentum approach does provide enough information to achieve a unique solution for the post-impact velocities. Therefore, for this class of problems, the compliance based approach has been considered to solve the non-uniqueness issues in predicting the post-impact velocities.

The second solution method considers compliance based methods, where the colliding bodies are connected to each other with local compliance. Newby investigated the three ball problem by adding springs and conducted parametric analysis to investigate the effect on the post-impact velocities [98]. Two conclusions were drawn from his analysis. First, it is possible to determine the desired stiffness ratio from the velocity outcome of the colliding bodies. Second, in other cases, no such determination is possible. Hinch and Jean studied the case of a long line of stationary balls subjected to impact on one end by another ball [99]. They considered the elastic Hertz contact force model. In addition, they investigated both cases of linear and nonlinear contact during the collision process. Cholet extended the analysis of three ball problem and used the method of convex analysis to solve the multiple impact problem [100]. His analysis was based on Moreau's sweeping process [101]. He was able to produce analytical solutions for the post-collision velocities. The main disadvantage of his work is that his solution is based on nonlinear parameters

that are difficult to predict from experiments. Stronge, however, proposed a solution method for the three ball problem using local compliance at the contact points considering elasto-plastic collisions [102]. In his approach, he introduced the stiffness gradient, which is associated with the local compliance between the second and the third balls and represents the gradient of the local wave speed. This local wave speed depends on the local compliance and masses. The stiffness gradient determines the phase relation between the reactions at the contacts [103]. Experimental verification of the stiffness gradient has been conducted [104, 105]. In a similar contribution by Stronge for the multiple impact problem, he introduced stiffness and mass gradients [106]. In addition, he considered both spherical and cylindrical contacts. He concluded that for multibody collisions, reaction forces which are time dependent can be replaced by reaction impulses for certain values of the proposed parameters. Gharib *et al.* solved the elastic multiple impact problem for linear chain of steel balls using the elastic Hertz and impulse momentum with the impulse correlation ratio hypothesis [107]. In addition, they showed that both methods produce similar results for the post-impact velocities for elastic collisions. They calculated the impulse correlation ratio from the post-impact velocities of the first ball by using the elastic Hertz method. The obtained impulse correlation ratio was used to calculate the post-impact velocity for three, four, and five balls. They also developed a shock absorption mechanism by trapping small balls between the larger balls in the chain, which resulted in high energy absorption. They carried a set of experiments to validate the theoretical results. Liu *et al.* proposed a new method that can handle multibody collisions in multibody systems based on the nonlinear Hertz contact model [108, 109].

The method is designed to predict the post-impact velocities. In this model, however, a distribution law is proposed, in which it relates the energy dispersion by mapping the time scale into the impulsive scale. This distribution law is associated with the Darboux-Keller approach, where the normal impulse is treated as an independent variable. The distribution law is designed to handle mono and bi stiffness models. Their method states that the kinetic energy during impacts is associated with the relative contact stiffness and the relative potential energy.

1.5. Impacts of Kinematic Chains

The class of impact problems focused on particle kinematic chains has been studied by many researcher in the field of robotics. The origin of this class of problems dates back to Newton [14]. This special class of impact problems exists in many engineering applications such as walking machines and space structures [110]. In addition, particle kinematic chains impact problems consider multilink mechanisms and robotic manipulators [111]. The impact problem of particle kinematic chains plays a major role in the stabilization of bipedal gait [112]. This class of problems is highly nonlinear and requires the inclusion the incorporation of the nonlinear effects [113]. Three approaches can be used for the solution of this class of problems. The first approach is the rigid body approach, where rigidity is assumed at any point in the chain [114]. The second approach considers local springs and dampers at every contact point [115]. The third approach incorporates continuum mechanics equations for the entire systems [97]. The solution to this class of problems, however, requires information about the coefficient of restitution and coefficient of friction [116].

Chang and Hurmuzlu studied the rigid body collision of planar kinematic chains with rough and flat surfaces [111]. In their work, they considered a three link kinematic chain with one end resting on the ground and the other end impacting. They proposed a methodology to obtain the exact outcome of the velocities. The methodology accounts for different impact scenarios during the collision event including: velocity reversals, normal impulses, and velocities at contact points in the presence multiple impacts. They concluded that the frictional impulse and horizontal velocity are the governing factors of the slippage direction of the resting end. Moreover, they concluded that the velocity reversal may affect the outcome of the solution and the post-impact velocities. Marghitu and Hurmuzlu analyzed the planar ground impact problem of the open kinematic chain [1]. They developed two unique solution procedures in differential and algebraic forms for the ground impact problem. In addition, the differential form is used to produce three unique sets of solutions using the kinematic, kinetic, and energetic definitions of the coefficient of restitution. The algebraic form solution was formulated to obtain solutions based on the kinematic coefficient of restitution. In another contribution, Marghitu and Hurmuzlu studied the chain impact problem with multiple contact points with an emphasis on three dimensional analysis [116]. In their work, planar and spatial impacts of the three link kinematic chain outcomes are studied and compared using differential and algebraic approaches. Particular emphasis is given the relation between the pre- and post-impact energies, slippage, rebound velocities at the contact points, as well as differences between planar (2D) and three-dimensional (3D) solutions. Tavakoli *et al.* studied a two mass system with multiple contact points [117]. In their model, they solved the

ground impact problem with an emphasis on impulse momentum, the impulse correlation ratio, and energetic coefficient of restitution in order to solve for the post-impact velocities. In addition, they solved the impact problem for the cases of sliding and bouncing on flat and inclined surfaces subjected to friction. They studied the impulse correlation ratio as a function of the link's length. Experimental study showed that the impulse correlation ratio decreases as the length increases. In addition, as the inclined surface's angle of inclination increased, the impulse correlation ratio decreased. Tavakoli and Hurmuzlu presented a study and results of three generations of the locomotion of a family tree of dynamical systems [118]. In addition, they analyzed the impact of single, two, and three mass mechanisms. Furthermore, they developed active control schemes for each system. Hurmuzlu developed an approach to describe the objective function of a planar five link bipedal locomotion model [110]. In his model, the motion of the biped was characterized in terms of the progression speed, step length, maximum step height, and knee bias. Furthermore, he developed a general approach based on discrete mapping to analyze the stability of bipedal locomotion [113]. Hurmuzlu and Moskowitz studied the double inverted pendulum bipedal locomotion system [112, 119, 120]. In addition, they developed a nonlinear model for the system. They showed that the system achieved stability. They concluded that periodic impact with the ground plays an important role in the stabilization of the locomotive bipedal system.

1.6. Structure of the Dissertation

In chapter one, we introduce a literature review covering topics presented in this dissertation. In chapter two, we solve the Ball-Ball and Ball-Cylinder impact problems with emphasis on the coefficient of restitution. We also investigate variation in the Ball-Ball and Ball-Cylinder coefficients of restitution and we propose a discretization method for predicting the Ball-Cylinder coefficient of restitution based on the Ball-Ball coefficient of restitution. Our simulations show that one needs to segment softer material more than harder ones. We validate our proposed method by conducting sets of experiments using different materials, including steel, wood, and rubber, and we establish a relationship between the stiffness ratio and the number of segments of the softer material. In chapter three, we solve the multiple impact problem of ball and cylinder connected in linear chains. We consider the three, four, and five-body problem, and propose a discretization method based on the segmentation of the softer material to predict the post-impact velocities of the colliding bodies. In this chapter, we use the relationship we built in chapter two to determine the required number of segments needed for each of the colliding bodies to produce post-impact velocities with the greatest agreements with the experimental results, and we validate the proposed method by conducting numerous sets of experiments. In chapter four, we solve the rigid body collision problem of particle based planar kinematic chains with multiple contacts with external surfaces. We use the linear and angular momentum principles with a set of complementary equations to solve the impact problem. In addition, we use the energetic definition of the coefficient of restitution to model the impact event, finding critical configurations such that the contact

mass has zero normal velocity and normal impulse. We achieve the solution by solving for the normal velocity and impulse of the contact mass as a function of the normal impulse of the impact mass. For the three-mass system, we consider the impact on inclined and different level surfaces, and we also derive the general solution of the five-mass system. We find their critical configurations and conduct sets of experiments for the three-mass system on a flat and inclined surfaces to verify the theoretical solution. In chapter five, we present conclusions of the accomplished work.

Chapter 2

On Planar Impacts of Cylinders and Balls

2.1. Introduction

In mechanics, an impact is a collision between two or more bodies in which the colliding bodies exert a large force on each other over a short period of time [16]. Forces created by collisions are exerted and removed in a very short interval of time and initiate stress waves which travel away from the region of contact [5]. Velocities experience jump discontinuities as a result of the impact event [110, 113]. The two approaches to the solution to impact problems are instantaneous and continuous analyses [6].

In the instantaneous approach, the impact interval is divided into two stages: compression and restitution. Then, a coefficient of restitution (COR) is defined as the ratio of the post and pre-impact normal velocities, normal impulses, or the work done during the compression and restitution phases, depending on the particular restitution model [7, 62, 63]. These models provide a framework for determining the post-impact and contact velocities [121]. Subsequently, linear and angular momentum equations are used to calculate the post-impact velocities. This classical approach is typically used for direct central impacts [21, 23, 24, 122–124].

Continuous analysis requires the use of Newton's second law of motion, where the contact forces are involved in the system's equations of motion.

This is also referred to as the compliance-based method [24]. The simplest way of modeling this problem is by connecting the impacting bodies with a linear spring and damper, which is known as the Kelvin-Voigt model [5].

Hurmuzlu developed an energy-based discrete model for the collision of bars with external surfaces [59]. This proposed method accounts for impact-induced vibrations of the impacting rigid bars. Similarly, Stoianovici and Hurmuzlu studied the collision of steel bars with external surfaces. They discovered unusual variation of the COR as a result of changing the pre-impact inclination angle [67]. Wang *et al.* investigated the collision of elastic bars and beams on massless springs [76]. In their analysis, they approached the solution to the problem by deriving the wave equations for the cases of constrained and free motion. In addition, they investigated the effect of the COR on this type of collision. Their analysis concluded that the COR is only dependent on the collision stiffness ratio and is independent of the incident velocity. Auerbach investigated the relevance of colliding balls to colliding rods [68]. He stated that collision of balls is same as colliding rods if the ball's and rod's radii and lengths are the same. There have been several studies proposed to address the effect of energy dissipation in collision problems (see [125] and references within). Freschi *et al.* introduced a detailed study on compression waves and kinetic energy losses in collisions involving balls and cylinders with different lengths [69]. In their study, they investigated the fractional loss of kinetic energy and the COR as a function of the rod's length using the principles of conservation of momentum and energy balance equations. Hu *et al.* studied the collision between a ball and an elastic rod [70]. They used the boundary approach and incorporated the elastic Hertz contact force model to represent

the longitudinal waves in rods. In addition, Schiehlen *et al.* studied the collision between balls, cylinders, and long bars [71]. They investigated the COR to represent the energy loss and evaluated it numerically to include wave propagation. Their numerical simulation analysis concluded that the COR is dependent on the yield stress of the colliding bodies. Khalid *et al.* showed that the ball-ball and ball-cylinder COR for the colliding pairs of the same materials are not necessarily equal [126].

In this study, we conduct a set of Ball-Ball (B-B) and Ball-Cylinder (B-C) collision experiments with pairs of identical or different materials. We use three types of materials: steel, wood, and rubber. In addition, we estimate the corresponding COR using the experimental data for all collision pairs. Unexpectedly, we discover that the B-B and B-C COR of same pairs are not necessarily equal. Moreover, one would expect that the COR would be only related to the local compliance. However, in the B-C collisions this is not the case. To investigate the cause of the COR variations between B-B and B-C, we propose a discretization method. We employ this method in three different impact models including; rigid body, bimodal linear, and bimodal Hertz. At the contacting segments, we use the B-B COR to calculate the B-C COR for the same material. We find that segmenting the softer material results in better prediction of the B-C COR.

2.2. Experimental Setup

In our work, we focus on direct central impact balls and cylinders. For that purpose, we build a frame that produces direct central impacts for the B-B and B-C experiments (see Figs. 2.1-2.2).

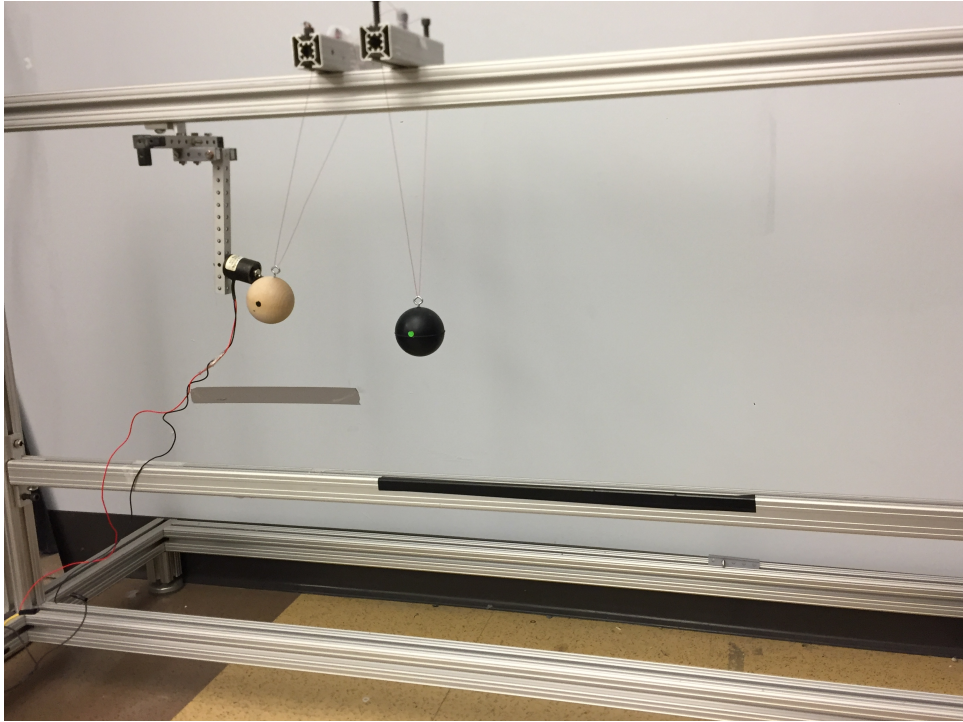


Figure 2.1: B-B collision experimental setup

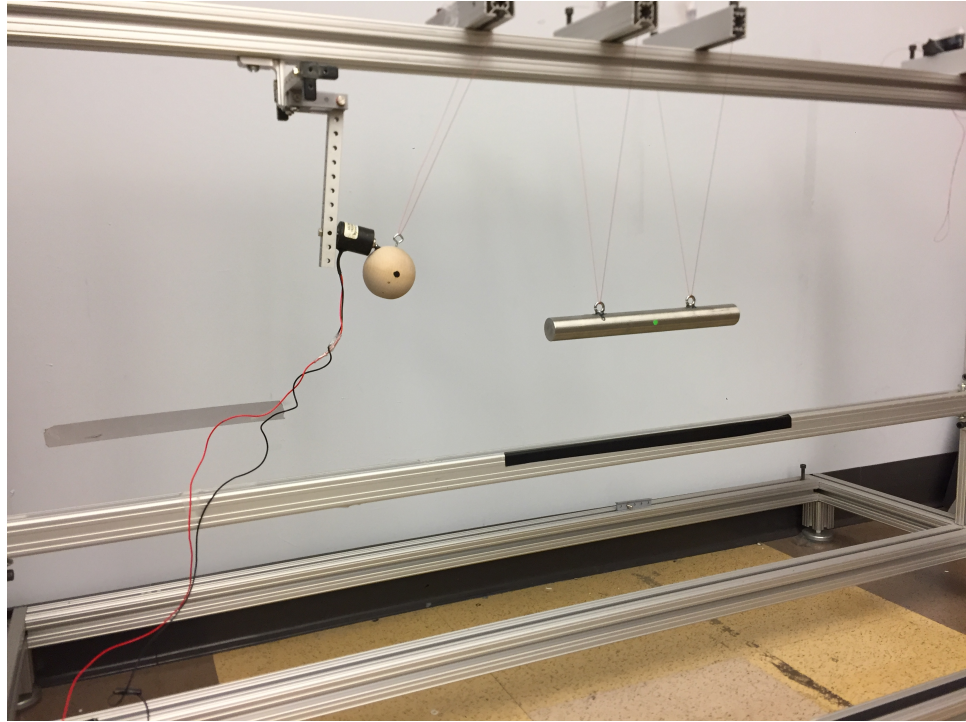


Figure 2.2: B-C collision experimental setup

As seen in Figs. 2.1-2.2, the colliding bodies are suspended by adjustable strings that are attached to the adjustable upper rail of the frame. This provides a proper adjustment of the bodies to achieve a direct central impact on the horizontal plane. The wires are connected in a v-formation, and the height of the cables is carefully selected to avoid unwanted wobbling and energy losses. Each experiment is initiated by dropping the ball from an initial height while the other body is resting in its lowest position. The release height is adjusted to achieve different pre-impact velocities. The release mechanism consists of an electromagnet that can release the ball with a turnable switch. Reflective markers for position tracking are placed at the center of mass for each of the colliding bodies. A high speed Sony camera with capability of 960

frames per second is positioned on a tripod. The tripod is aligned with the center of mass of the bodies and is placed sufficiently close to achieve high video resolution and to reduce visual distortion.

The captured videos are transferred to a personal computer for video processing and digitization. The video analysis and digitization is performed by first capturing the positions of the colliding bodies in each video frame. Subsequently, the captured position data are used to determine pre- and post-impact velocities by numerical differentiation of the position data. The position data is first smoothed by applying filtering in order to cancel any noise present.

Mainly, three types of materials have been selected for the experimental study for balls and cylinders. These materials include: steel (S), wood (W), and rubber (R). All balls have the same diameter size. The cylinders consist of two diameter sizes (C1 and C2) per material and the same length for all materials per diameter size. Table 2.1 shows the masses and geometric values of the balls and cylinders.

Table 2.1: Masses and geometric values

Balls	Mass (Kg)	Radius (m)
S	0.544	0.0254
W	0.045	0.0254
R	0.097	0.0254
Cylinders	Mass (Kg)	Length (m)
S1	0.968	0.241
W1	0.084	0.241
R1	0.187	0.241
S2	3.865	0.24
W2	0.285	0.24
R2	0.699	0.24

After obtaining the pre- and post-impact velocities, one can measure the kinematic COR by taking the negative of the relative velocity ratio before and after the impact. Table 2.2 summarizes the average experimentally measured COR values for all B-B (e_L) and B-C (\bar{e}_G) collision experiments.

Table 2.2: Experimental COR values

Type	B-B		
	S	W	R
S	0.92 ± 0.05	0.67 ± 0.071	0.70 ± 0.073
W	0.63 ± 0.059	0.78 ± 0.041	0.69 ± 0.031
R	0.68 ± 0.024	0.68 ± 0.067	0.74 ± 0.047
Type	B-C1		
	S	W	R
S	0.9 ± 0.047	0.59 ± 0.039	0.6 ± 0.086
W	0.62 ± 0.061	0.72 ± 0.046	0.56 ± 0.039
R	0.61 ± 0.039	0.57 ± 0.054	0.67 ± 0.054
Type	B-C2		
	S	W	R
S	0.82 ± 0.047	0.59 ± 0.067	0.64 ± 0.07
W	0.6 ± 0.027	0.77 ± 0.039	0.52 ± 0.025
R	0.62 ± 0.026	0.63 ± 0.073	0.69 ± 0.038

Conducting a theoretical study necessitates the estimation of the contact stiffness values of the colliding bodies. In order to achieve the measurements of the stiffness values of each ball and cylinder, a compression testing machine is used. We used the Instron 5967 material testing machine to perform the stiffness analysis testing. We conducted multiple loading-unloading compression cycles. The output raw data consists of displacement and force measurements. Subsequently, multiple force-displacement plots are obtained for each material and configuration. Then, an averaged stiffness is found by averaging the slope of the force displacement curve. After plotting the force-displacement data, we obtain the corresponding curve fit equations. In addition, we use two curve

fit equations to obtain the linear and Hertzian stiffness values.

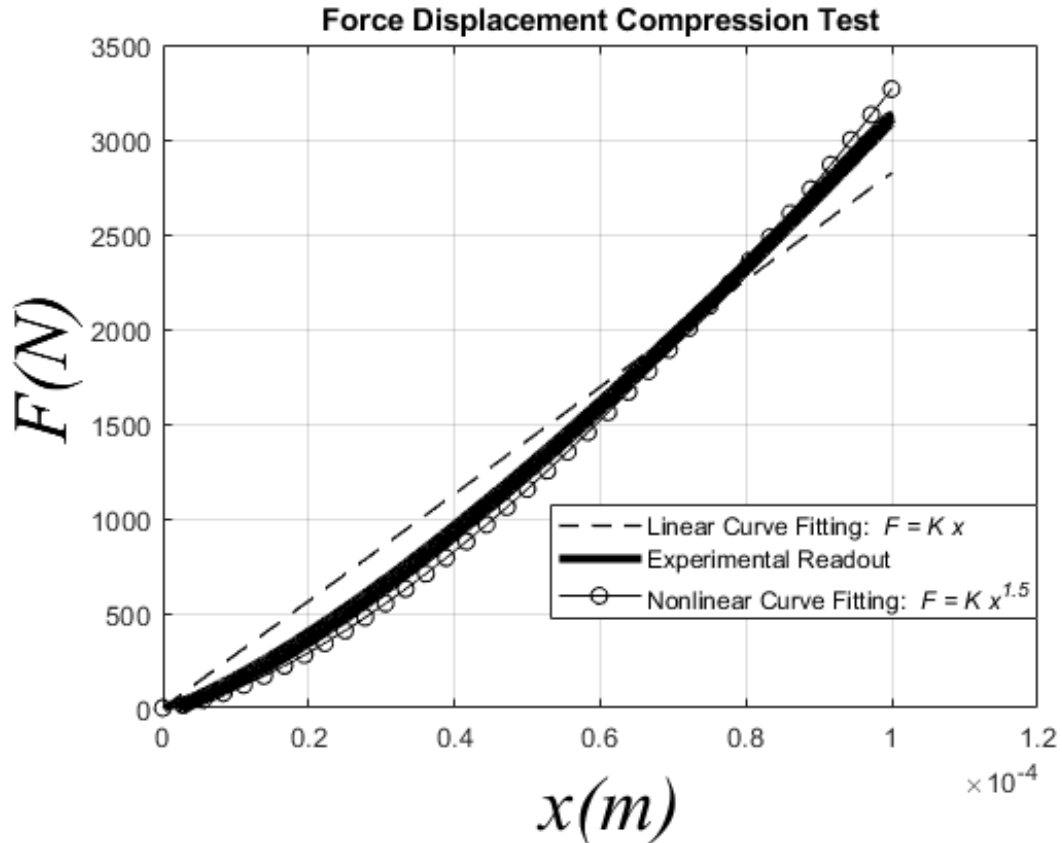


Figure 2.3: Experimental Contact Stiffness Testing

Table 2.3 summarizes the experimentally measured stiffness values for all balls and cylinders.

Table 2.3: Experimental stiffness values

Type	Linear Stiffness ($\frac{N}{m}$)	Nonlinear Stiffness ($\frac{N}{m^{1.5}}$)
S	3.7655×10^7	4.3335×10^9
W	6.948×10^5	3.642×10^8
R	2.5735×10^4	9.5105×10^5
S1	5.3445×10^7	6.157×10^9
W1	1.05×10^7	5.321×10^9
R1	7.8365×10^4	4.043×10^6
S2	3.7×10^8	4.27×10^{10}
W2	3.145×10^7	1.592×10^{10}
R2	5.438×10^5	2.8×10^7

2.3. Problem Description

The objective of this chapter is to investigate the relation between Ball-Ball and Ball-Cylinder collisions. One would assume that for colliding objects of the same materials, the COR would remain the same regardless of the geometry of the colliding objects. However, our experiments revealed that this is not the case (Table 2.2). We discretized the colliding masses in the form of masses with connected springs. In addition, the contact is modeled using three different models: rigid body, bimodal linear, and bimodal Hertz.

2.4. Generalized Equations of Motion

Figure 2.4 represents the general B-C discrete model. Here, the ball and cylinder are divided into j_1 and j_2 equal segments, respectively. Each internal segment in the ball and cylinder is connected with linear internal springs (K^i).

At the contacting segments, we define the external contact springs of the ball (K_b^e) and cylinder (K_c^e) to model the contacting force (\vec{F}_c). The x -coordinates of the center of mass of each segment are defined as x_i .

The masses of each segment of the ball and cylinder are defined as:

$$m_i = \begin{cases} \frac{m_b}{j_1} & 1 \leq i \leq j_1 \\ \frac{m_c}{j_2} & j_1 + 1 \leq i \leq N \end{cases} \quad (2.1)$$

where, m_b and m_c are the total masses of the ball and cylinder, respectively.

The total number of segments is $N = j_1 + j_2$.

The stiffnesses of the internal springs of the ball and cylinder are given by:

$$K_b^i = K_b(j_1 + 1) \quad (2.2)$$

$$K_c^i = K_c(j_2 + 1) \quad (2.3)$$

where, K_b and K_c are the overall stiffnesses of the ball and cylinder, respectively.

The relative displacement (δ_i) of each internal spring of the ball and cylinder is defined as:

$$\delta_i = \begin{cases} x_{i-1} - x_i + \frac{2R_b}{j_1} & 1 < i \leq j_1 \\ x_{i-1} - x_i + \frac{L_c}{j_2} & j_1 + 1 < i \leq N \end{cases} \quad (2.4)$$

where, R_b and L_c are the radius of the ball and the length of the cylinder, respectively.

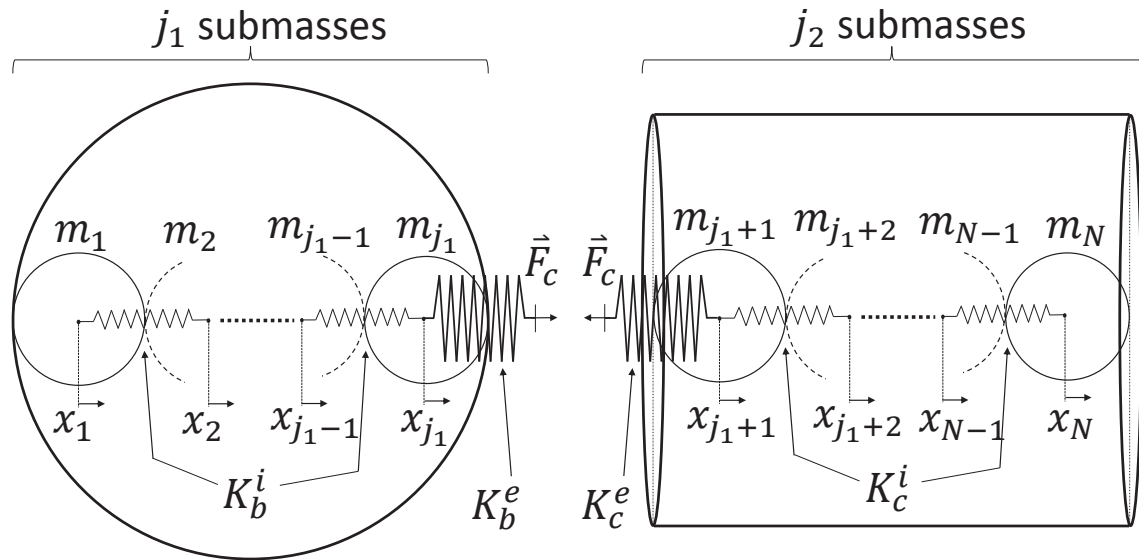


Figure 2.4: General discrete B-C model

The equations of motion of each segment are defined as:

$$m_i \ddot{x}_i + K^i (\delta_{i+1} - \delta_i) = 0 \quad (2.5)$$

The velocity of the center of mass of the ball and the cylinder can be expressed as:

$$\dot{x}_b^+ = \frac{\sum_{i=1}^{j_1} \dot{x}_i^+}{j_1} \quad (2.6)$$

$$\dot{x}_c^+ = \frac{\sum_{i=j_1+1}^N \dot{x}_i^+}{j_2} \quad (2.7)$$

where, \dot{x}_i^+ is the post-impact velocity of each segment. The equivalent mathematical expression for the experimental B-C COR is defined as:

$$e_G = -\frac{\dot{x}_b^+ - \dot{x}_c^+}{\dot{x}_b^- - \dot{x}_c^-} \quad (2.8)$$

where, \dot{x}_b^- and \dot{x}_c^- are the initial pre-impact velocities of the ball and cylinder.

2.4.1. Rigid Body Method

A classical approach for modeling impacts between two bodies can be performed by using the rigid body analysis. In this approach, colliding bodies are assumed to be rigid. One can relate the pre- and post-impact velocities by using the principle of conservation of linear momentum and the COR. By using the conservation of linear momentum at the contacting segments j_1 and $j_1 + 1$, we have the following:

$$m_{j_1} \Delta \dot{x}_{j_1} = m_{j_1+1} \Delta \dot{x}_{j_1+1} \quad (2.9)$$

where, $\Delta \dot{x}_{j_1}$ and $\Delta \dot{x}_{j_1+1}$ are the changes in velocities. The changes in velocities of j_1 and $j_1 + 1$ can be expressed as:

$$\Delta \dot{x}_{j_1} = \dot{x}_{j_1}^+ - \dot{x}_{j_1}^- \quad (2.10)$$

$$\Delta \dot{x}_{j_1+1} = \dot{x}_{j_1+1}^+ - \dot{x}_{j_1+1}^- \quad (2.11)$$

The local COR is defined as:

$$e_L = - \frac{\dot{x}_{j_1}^+ - \dot{x}_{j_1+1}^+}{\dot{x}_{j_1}^- - \dot{x}_{j_1+1}^-} \quad (2.12)$$

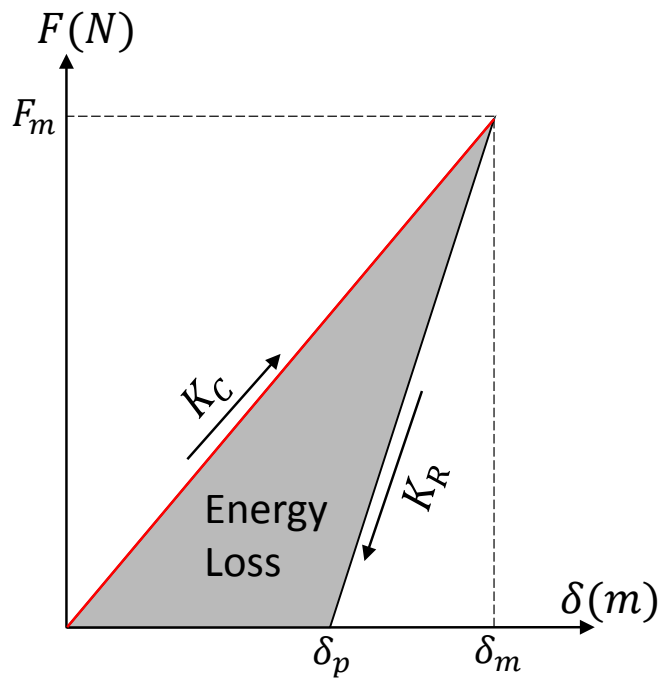
Hence, by using Eqns. (2.9) and (2.12) we obtain the following post-impact velocities for the segments j_1 and $j_1 + 1$:

$$\dot{x}_{j_1}^+ = \frac{1}{m_{j_1} + m_{j_1+1}} [(m_{j_1} - e_L m_{j_1+1}) \dot{x}_{j_1}^- + (1 + e_L) m_{j_1+1} \dot{x}_{j_1+1}^-] \quad (2.13)$$

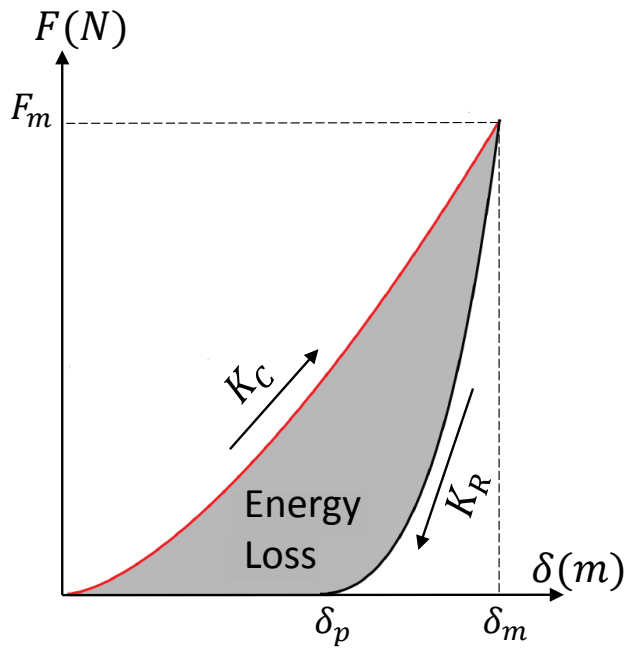
$$\dot{x}_{j_1+1}^+ = \frac{1}{m_{j_1} + m_{j_1+1}} [(m_{j_1+1} - e_L m_{j_1}) \dot{x}_{j_1+1}^- + (1 + e_L) m_{j_1} \dot{x}_{j_1}^-] \quad (2.14)$$

2.4.2. Bimodal Contact Force Model

We use a spring-based contact force model that is modified to incorporate energy dissipation, called the bimodal force model [58, 63, 109, 127]. Figure 2.5 shows the force displacement curves for the bilinear and nonlinear force models. The energy loss is given by the net work done in deforming the objects in the compression and restitution phases, which are shown as the shaded areas under the force displacement curves. From Fig. 2.5, δ , δ_p , K_C , and K_R are the relative displacement, permanent indentation, and collision stiffnesses during the compression and restitution phases, respectively. In addition, at the maximum compression, δ_m and F_m are the maximum displacement and contact force, respectively.



(a) Bilinear Force Model



(b) Nonlinear Force Model

Figure 2.5: Force Displacement Curves

The contact force between the segments j_1 and j_1+1 during the compression and restitution phases is defined as:

$$\vec{F}_c = \begin{cases} K_C(\delta)^n & \text{Compression Phase} \\ K_R(\delta - \delta_p)^n & \text{Restitution Phase} \end{cases} \quad (2.15)$$

During the collision event, the relative contact displacement at the contacting segments can be expressed as:

$$\delta = x_{j_1} - x_{j_1+1} + \frac{R_b}{j_1} + \frac{L_c}{2j_2} \quad (2.16)$$

The collision stiffnesses during both phases of contact are described as:

$$\frac{1}{K_C} = \frac{1}{K_b^e} + \frac{1}{K_c^e} \Rightarrow K_C = \frac{K_b^e K_c^e}{K_b^e + K_c^e} \quad (2.17)$$

$$K_R = \frac{K_C}{e_L^{2n}} \quad (2.18)$$

The maximum contact force can be obtained from Eqn. (2.15):

$$F_m = K_C(\delta_m)^n \quad (2.19)$$

$$F_m = K_R(\delta_m - \delta_p)^n \quad (2.20)$$

From Eqns. (2.19) and (2.20), the permanent indentation can be found as:

$$\delta_p = \delta_m \left(1 - \left(\frac{K_C}{K_R} \right)^{\frac{1}{n}} \right) \quad (2.21)$$

The work done during the compression and restitution phases can be obtained by integrating the contact force over the corresponding collision period as follows:

$$W_C = \int_0^{\delta_m} K_C \delta^n d\delta = \frac{K_C \delta_m^{n+1}}{n+1} \quad (2.22)$$

$$W_R = \int_{\delta_m}^{\delta_p} K_R (\delta - \delta_p)^n d\delta = \frac{-K_R (\delta_m - \delta_p)^{n+1}}{n+1} \quad (2.23)$$

The local energy loss during the impact can be expressed as:

$$E_l = W_C + W_R \quad (2.24)$$

When $n = 1$, we have the bilinear force model, whereas when $n = 1.5$, the force model is called the bimodal Hertzian model. Furthermore, at the contacting segments j_1 and $j_1 + 1$, we incorporate the contact force in Eqn. (2.15) to the right hand side of the corresponding equations of motion in Eqn. (2.5). Once the contact force is incorporated into the system's equations of motions, the post-impact velocities of each segment are found by performing the numerical integration. For the external spring at the contact point, we incorporate the linear stiffness for the bimodal linear and the nonlinear stiffness for the bimodal Hertz models.

2.5. Numerical Simulation and Results

We categorize the B-C collision experiments into three categories: collision experiments of the same material, Hard-Soft different materials (H-S), and Soft-Hard different materials (S-H). Here, hard is defined as material with a higher stiffness than the soft material. For example, SW1 falls under the H-S category, while the WS1 is included in the S-H category. Next, we analyze the impact dynamics of all possible combinations of j_1 and j_2 , where each varies from 1 to 10 for a total of 100 cases. Then, for each iteration we compute the theoretical e_G and compare it with the experimentally measured \bar{e}_G . The percentage error (PE) between e_G and \bar{e}_G can be calculated as:

$$PE = \left| \frac{\bar{e}_G - e_G}{\bar{e}_G} \right| \times 100 \quad (2.25)$$

Based on the theoretical prediction we choose the best (the one that produces the lowest percentage error) model in estimating \bar{e}_G . Figure 2.6 depicts the average percentage error of all three categories for all models. As one can see, the bimodal Hertz has the lowest average percentage errors compared to other models. The average percentage error for the bimodal Hertz and for all categories is approximately 9%.

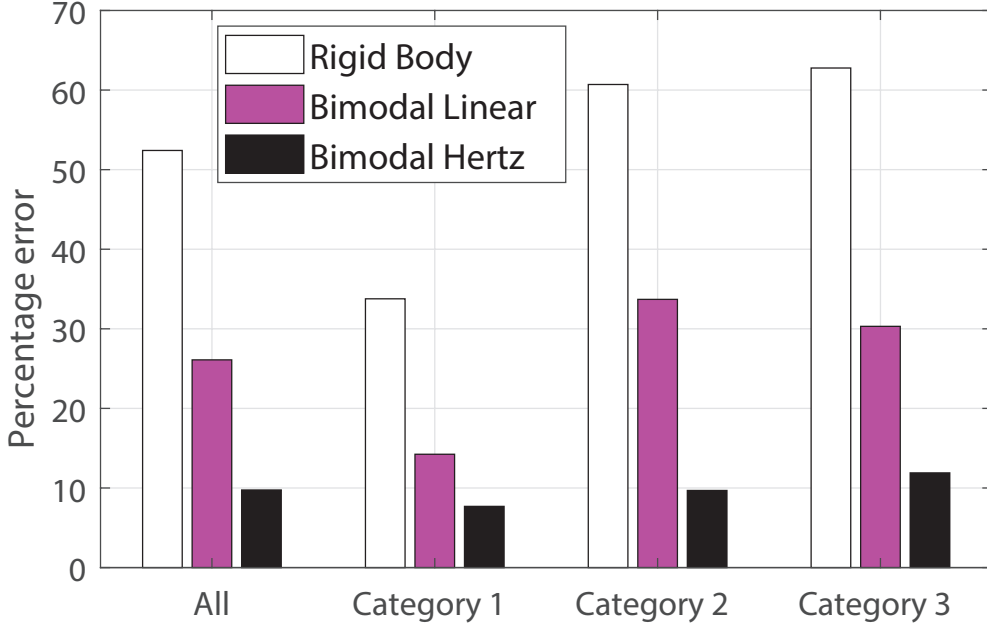


Figure 2.6: Average percentage error for all categories

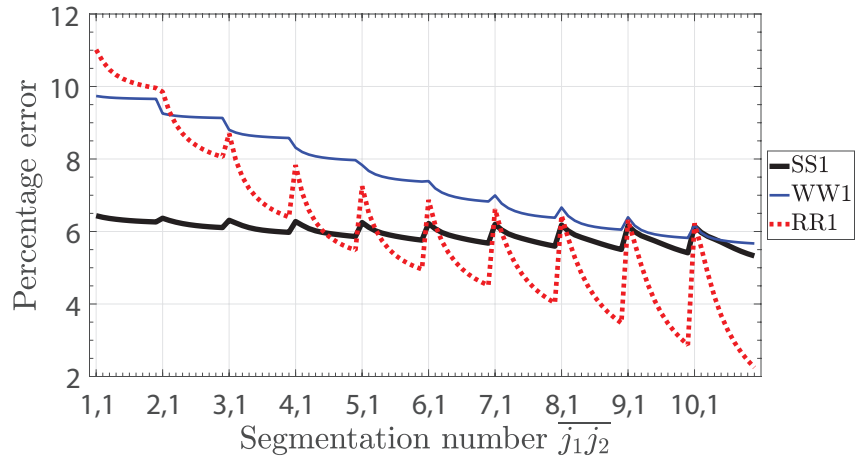
Based on the results obtained from Fig. 2.6, we choose the bimodal Hertz model to answer the following questions:

- The effect of the number of segments on the COR prediction
- The dependency of the COR prediction on the stiffness

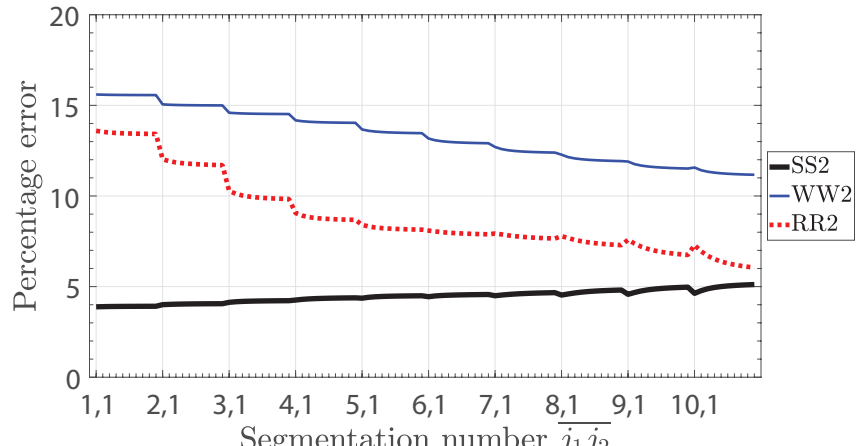
Figures 2.7-2.9 depict the percentage error of all B-C collisions and for each category as a function of segmentations. The segmentation number $\overline{j_1 j_2}$ on the horizontal axis is composed of j_1 and j_2 segments. Accordingly, each number on the horizontal axis corresponds to a specific j_1 and j_2 values. For example, $\overline{j_1 j_2} = 21$ means that $j_1 = 2$ and $j_2 = 1$. As one can see, the periodic behavior depicted in the figure occurs because of the specific arrangements on the horizontal axis. For each 10 segments, j_1 is fixed while j_2 is varied from

1 to 10. Figures 2.7a-2.7b depict the percentage error for the first category of the B-C collisions. For this category, by increasing the number of j_1 and j_2 segments the percentage error decreases. One can see that by increasing j_1 the percentage error drops more.

For the second category in Figs. 2.8a-2.8b, the percentage error decreases as we increase j_2 segments, while the percentage error is nearly unchanged as j_1 increases. In addition, by increasing j_1 and j_2 the percentage error encounters a repeated pattern. Hence, j_1 can be chosen as equal to one and then j_2 can be varied to obtain the lowest percentage error. This also means that we do not need to segment the ball. For the third category in Figs. 2.9a-2.9b increasing j_1 causes reduction in the percentage error, while increasing j_2 has almost no effect.



(a) Category 1: B-C1



(b) Category 1: B-C2

Figure 2.7: Percentage error of category 1 B-C collisions

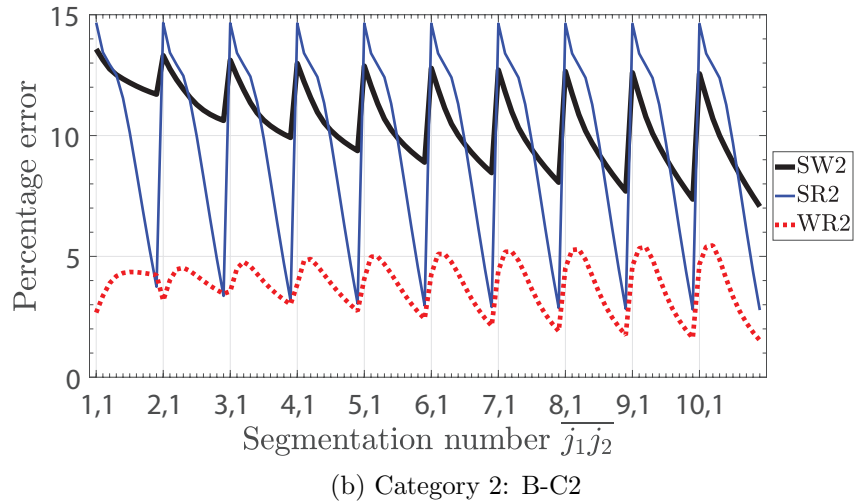
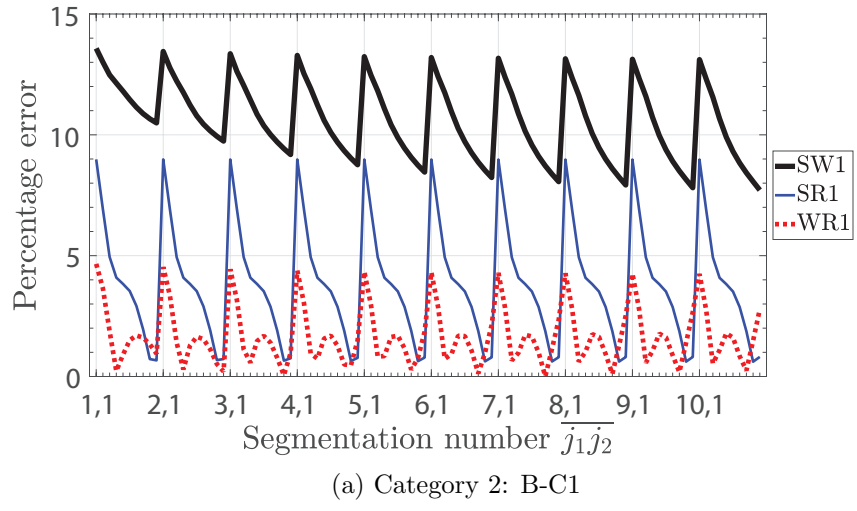
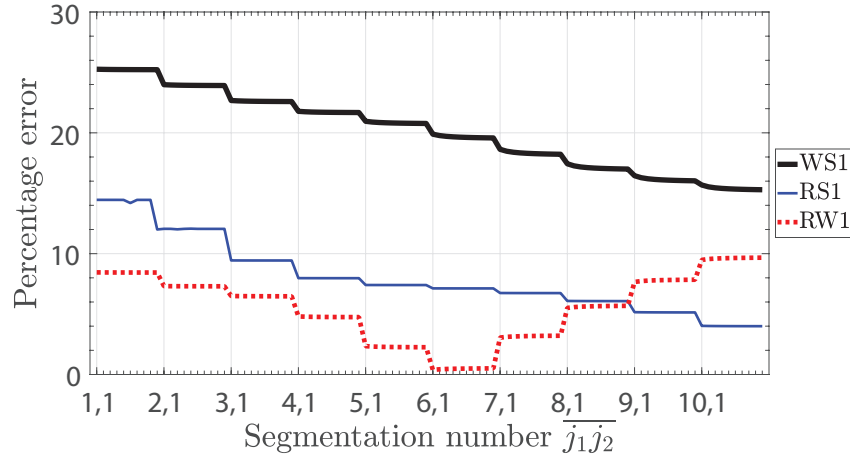
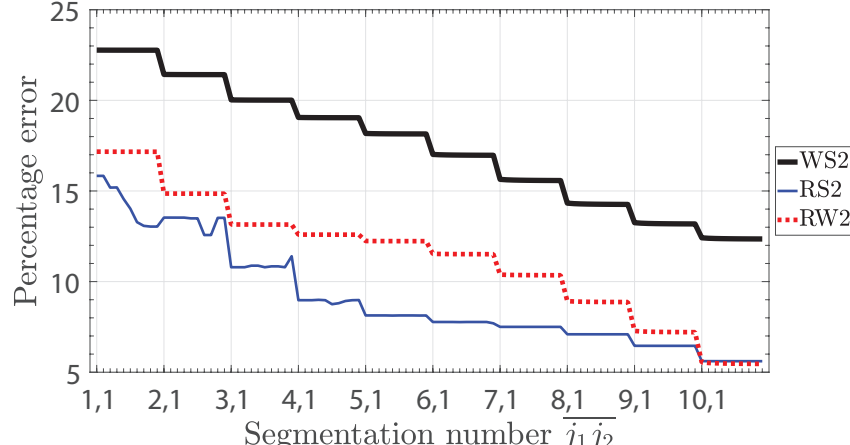


Figure 2.8: Percentage error of category 2 B-C collisions



(a) Category 3: B-C1



(b) Category 3: B-C2

Figure 2.9: Percentage error of category 3 B-C collisions

Figure 2.10 depicts the overall average percentage error of all B-C collisions for each category. Based on the result obtained in Fig. 2.10, one can see that segmenting the softer material results in a good approximation of the B-C \bar{e}_G . Increasing the number of segments results in larger collision stiffness, which translates into a larger contact force. Figure 2.11 depicts a numerical example

of the force displacement profile, where the enclosed area under the curves represents the local energy loss at the contacting segments.

Since there is no bending and we are dealing with direct central impacts, our numerical simulation for all B-C collisions showed that the contribution of the vibrational energy loss to the B-C COR is negligible.

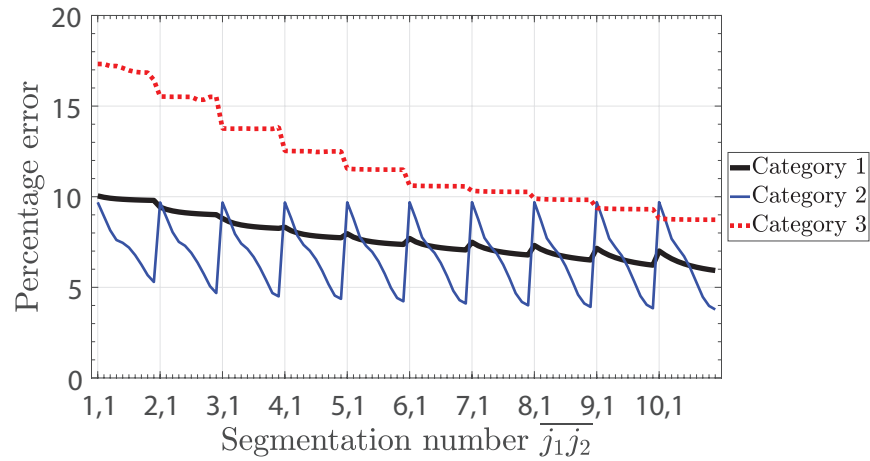


Figure 2.10: Average percentage error for all categories

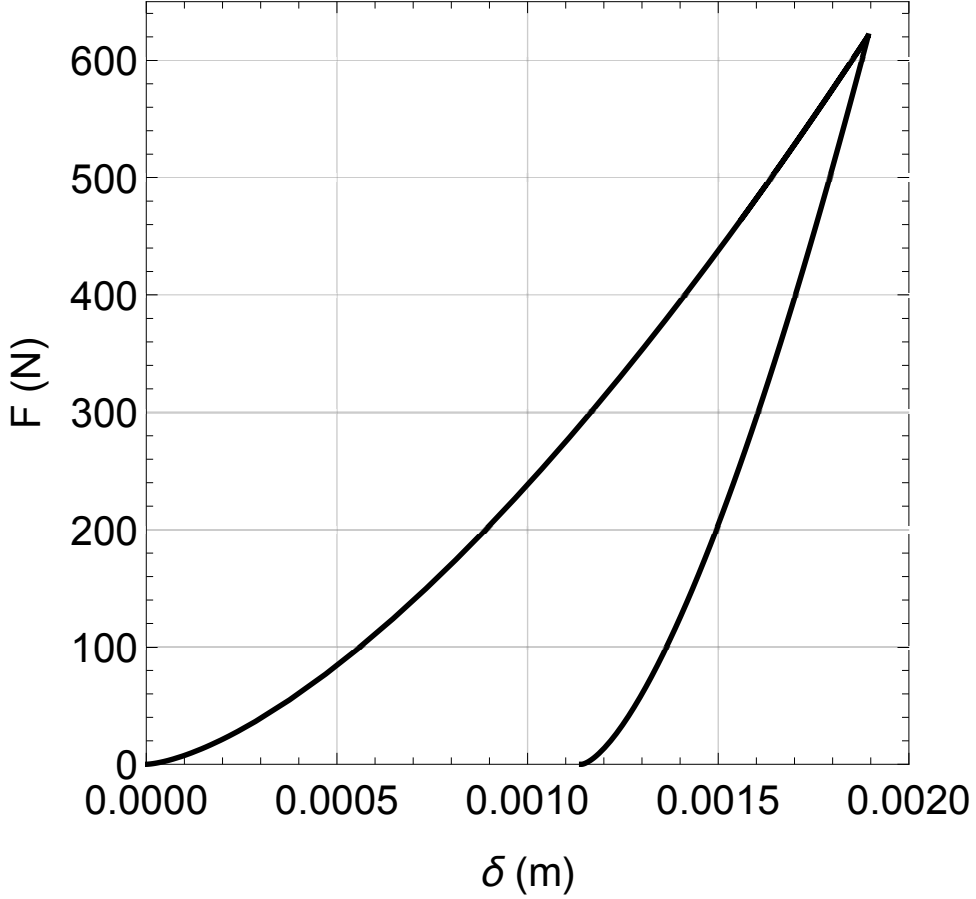


Figure 2.11: Numerical force displacement profile

Our objective is to find the minimum average percentage error (APE_m) of the B-C COR for each category. We conduct numerical simulation runs for all collision pairs, where j_S is varied from 1 to 50 and j_H is varied from 1 to 10. For each iteration of j_H , we find the average percentage error (APE) of all six combinations in each category as follows:

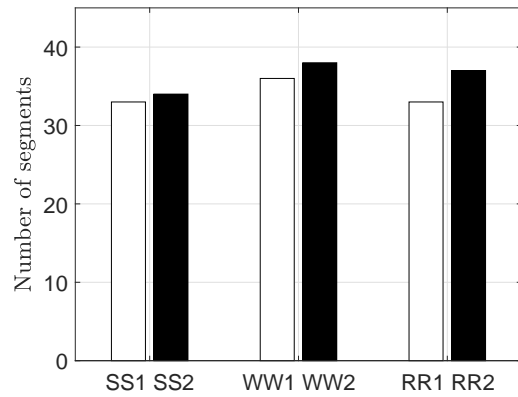
$$APE_i = \frac{\sum_{n=1}^{6 \times 50} PE_n}{6 \times 50}; \quad i = 1, \dots, 10 \quad (2.26)$$

Then, we identify j_H that corresponds to the minimum value of the average

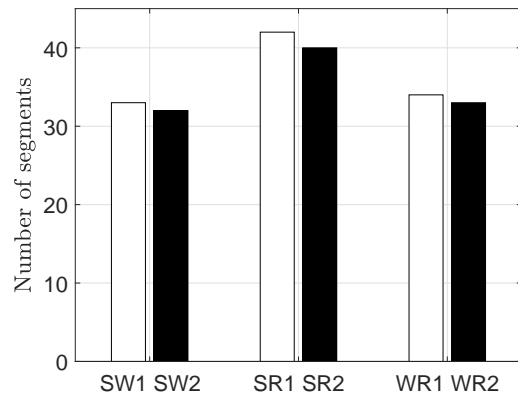
percentage error. Now, we define:

$$APE_m = \min\{APE_i\}_{i=1,\dots,10} \quad (2.27)$$

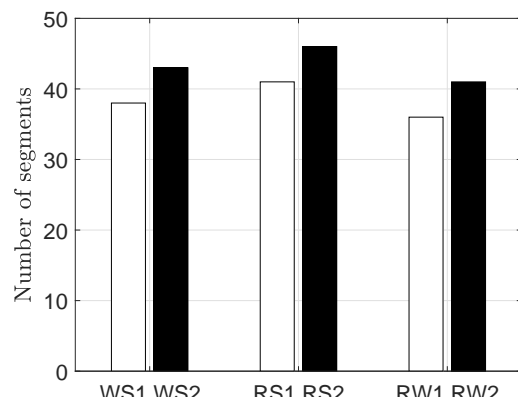
After that, we choose the j_S value that corresponds to the lowest average percentage error. Figure 2.12 depicts the number of segments of the softer material (j_S) producing the lowest average percentage error in estimating the B-C COR. These number of segments represent a saturation point beyond which increasing segmentation does not affect the percentage error. Following these steps, the number of the segments of the harder material is found to be $j_H = 4$ for the first category, $j_H = 6$ for the second category, and $j_H = 4$ for the third category. Figure 2.12a depicts the number of segments of the softer material for the first category. As one can be seen from Figs. 2.12a,2.12c more segments are needed for the larger cylinder sizes. For the second category, however, for each collision pair the softer material requires slightly more segments in order to achieve good approximation of \bar{e}_G . Table 2.4 shows the APE_m for the corresponding number of segments shown in Fig. 2.12. As one can see, the APE_m is 2.028%, 3.1%, and 1.31% for the first, second, and third categories, respectively.



(a) Category 1



(b) Category 2



(c) Category 3

Figure 2.12: Number of segments corresponding to APE_m

Table 2.4: Minimum average percentage error of each category

	Category 1	Category 2	Category 3		
SS1	3.9	SW1	6	WS1	1.59
SS2	3.88	SW2	6.8	WS2	0.21
WW1	0.08	SR1	2.2	RS1	2.72
WW2	4.2	SR2	1.13	RS2	1.29
RR1	0.03	WR1	0.97	RW1	0.38
RR2	0.08	WR2	1.5	RW2	1.68
Average	2.028	Average	3.1	Average	1.31

We have observed that in order to achieve good estimations of the B-C COR, one needs to focus on the segmentation of the softer material. Based on the results we observed in Fig. 2.12, we seek to build a relationship between the number of the segments of the softer material and the stiffness ratio of the corresponding collision pair. For that reason, we define the stiffness ratio r_K as follows:

$$r_K = \frac{K_S^i}{K_H^i} \times 100 \quad (2.28)$$

where, K_S^i and K_H^i are the internal stiffnesses of the soft and hard materials, respectively.

We plot the number of segments of each collision pair shown in Fig. 2.12 as compared to the corresponding stiffness ratio r_K . Figure 2.13 shows the number of segments of the softer material versus the stiffness ratio r_K for all collision pairs. An empirical curve fit of the data (Regression value $R = 0.89$) is shown as the solid curve. The corresponding curve fit equation is found to be as follows:

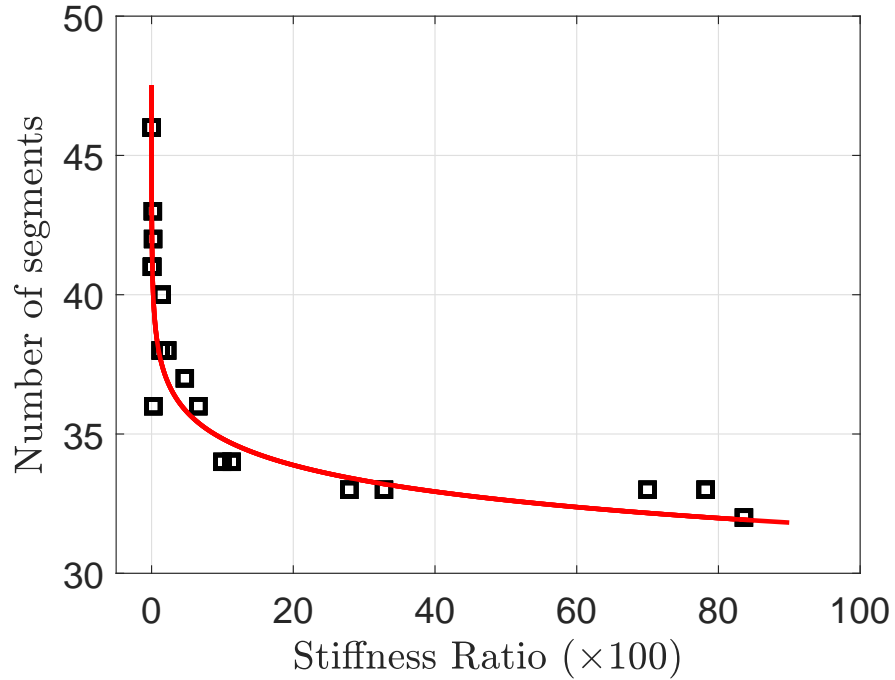


Figure 2.13: Number of segment of the softer material and stiffness ratio

$$j_S = a (r_K)^b + c \quad (2.29)$$

$$a = 2089$$

$$b = -0.00006584$$

$$c = -2051$$

We obtain a relationship that shows the dependence of the number of segments of the softer material for all collision pairs versus the stiffness ratio r_K . Furthermore, we can see that the number of segments of the softer material decreases as the stiffness ratio increases.

2.6. Verification of Results

For verification purposes, we conduct two additional sets of collision experiments that covers all categories. Based on the stiffness ratio and the curve fit Eqn. (2.29), we can determine how many segments we need for the softer material to achieve a good approximation of the B-C COR. We use small steel and wood balls with the masses and geometric properties shown in Table 2.5. Here, S_s and W_s indicate small steel and small wood balls, respectively.

Table 2.5: Masses and geometric values of the small balls

Balls	Mass (Kg)	Radius (m)
S_s	0.07	0.0127
W_s	0.006	0.0127

Since the experimental testing requires a standard procedure as observed in the experimental study, we performed stiffness analysis testing to obtain the stiffness values shown in Table 2.6. Then, we conduct the B-B collision experiments for $S_s S_s$ and $S_s W_s$ and found their corresponding local COR e_L .

Table 2.6: Experimental stiffness values

Type	Linear Stiffness ($\frac{N}{m}$)	Nonlinear Stiffness ($\frac{N}{m^{1.5}}$)
S_s	2.825×10^7	3.27×10^9

The stiffness ratios for the $S_s S_1$ and $S_s W_1$ are 52.85 and 37.16, respectively. Now, since we have the r_K values we use the curve fit relationship in Eqn. (2.29) to find the number of segments of the softer material j_S that are needed to

estimate the B-C COR. The number of segments are needed for S_sS1 is $j_S = 32$ and for S_sW1 is $j_S = 33$. We choose $j_S = 32$ and $j_H = 4$ for S_sS1 in the S-H category and $j_S = 33$ and $j_H = 6$ for S_sW1 in the H-S category and run the numerical simulation to calculate the theoretical e_G . Choosing these segmentation values, the theoretical e_G is 0.847 and 0.53 for S_sS1 and S_sW1 , respectively.

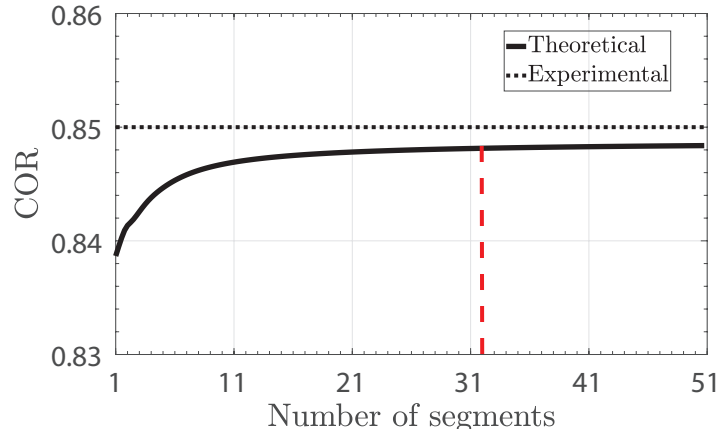
In addition, we conduct the B-C collision experiments for the S_sS1 and S_sW1 and find the corresponding \bar{e}_G values. The B-B and B-C COR values are listed in Table 2.7. The percentage error between the theoretical and experimental B-C COR are 0.24% and 4.2% for S_sS_s and S_sW_s , respectively.

Table 2.7: Experimental COR values with the small balls

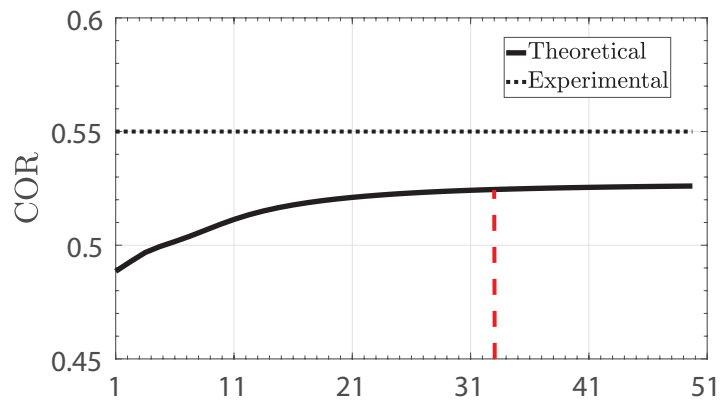
Type	B-B
S_sS_s	0.91 ± 0.065
S_sW_s	0.65 ± 0.036
Type B-C1	
S_sS1	0.85 ± 0.01
S_sW1	0.55 ± 0.037

To further verify our methodology, we confirm whether the number of segments given by Eqn. (2.29) are indeed error saturation points for the two cases we considered. Figure 2.14 depicts the theoretical prediction of the B-C COR as a function of the number of segments of the softer material. For the S_sS1 case, Fig. 2.14a shows the B-C COR prediction as we vary the number of segments of the softer material (solid curve). Here, the dashed horizontal line is the experimental B-C COR. The vertical dashed line is the j_S found by using

Eqn. (2.29). As one can see, that the theoretical B-C COR saturated in the neighborhood of $j_S = 32$ as expected. Similarly, Fig. 2.14b depicts the S_sW1 collision case. As one expects, the theoretical prediction curve flattens out at approximately $j_S = 33$.



(a) S_sS1



(b) S_sW1

Figure 2.14: COR versus the number of segments of the softer material

Chapter 3

Planar Impacts in Hybrid Chains of Cylinders and Balls

3.1. Introduction

Multibody dynamics is the study of systems consisting of multiple bodies [79]. It can be understood as systems with multiple bodies where their interaction is governed by external forces, geometric and kinematic constraints [79–81]. When the bodies are in contact, the system of interconnected bodies experiences changes in velocities and accelerations. As a result of the collision event, the velocities of the colliding bodies experience jump discontinuities [110,113]. Multibody impacts exist in a variety of engineering applications including robotics [83], biomechanics [84], and railway design [85]. Developing analytical solutions to predict the post collision velocities of the colliding bodies in multibody systems possess difficulties and unanswered questions [24,116].

The first approach of solving the multiple impact problem is based on the use of the impulse momentum method and the coefficient of restitution (COR) [14]. Han and Gilmore proposed an algorithmic procedures to solve the multibody problem involving multiple collisions [96]. The three ball problem was considered by Brogliato [125]. He recommended using the local compliance at the impacting bodies. Ermolin and Kazakov proposed an enhanced method for multiple collision problems based on the impulse momentum method [128]. In addition, the method allowed inelastic collisions with energy loss. Fur-

thermore, their work demonstrated the cases of two and three dimensional impacts. Ceanga and Hurmuzlu used the impulse momentum method to solve the multiple impact problem [24]. They proposed a new constant called the impulse correlation ratio, which relates the impulses in the chain. This phenomena depends on the sequence, mass distribution, geometric and material properties. A closed form solution of the maximum compression impulses is obtained by solving the momentum equations. They conducted a large set of collision experiments of three, four, five, and six balls impacts. Walkiewicz and Newby solved the multiple impact problem of three balls [94]. Their solution was based on the conservation of momentum and energy principles.

The second approach is based on the compliance methods, where springs are added at the contact points of the interacting bodies. Newby also investigated the three ball problem by adding springs and conducted parametric analysis to investigate the effect on the post-impact velocities [98]. Liu *et al.* proposed a new method that can handle multibody collisions in multibody systems based on the nonlinear Hertz contact model [108, 129]. The method is designed to predict the post-impact velocities of the multiple impact problem. They used a distribution law which relates the energy dispersion by mapping the time scale into the impulsive scale. Stronge studied the chain reaction impact problem of a linear chain of three balls [102]. In his work, he used the bilinear compliant contact force model with plastic deformation. In addition, he defined the local wave speed, which depended on the local contact stiffness and the mass of the adjacent bodies.

Several authors considered the collision problem with cylinder. Hurmuzlu developed an energy based discretization method for the collision of bars on

external surfaces [59]. The proposed solution allowed accurate prediction of the post-impact velocity of the impacting bar. Stoianovici and Hurmuzlu studied the collision of rigid bars on external surfaces [67]. They discovered unusual variation in the COR as a result of changing the pre-inclination angle. Auerbach studied the ball and rod collision problem [68]. In his work, he concluded that colliding balls is same as colliding rods if the balls and rods radii are the same. Belyaev *et al.* studied the longitudinal impacts on a thin rod by a body and studied wave propagation using finite element method and elastic Hertz contact force model [74]. YuFeng and DeChao analyzed the collision of a particle colliding a rod attached to a spring [75]. They stated that both the wave equation and elastic Hertz contact force model produced the same results. Wang *et al.* investigated the collision of elastic bars and beams on massless springs [76]. They studied the effect of the coefficient of restitution for this type of collisions. Their analysis concluded that the coefficient of restitution is only dependent on the stiffness ratio and independent of the incident velocity.

In this chapter, we solve the multiple impact problem of Balls (B) and Cylinders (C). We consider three, four, and five body impact problems. We use different diameter sizes of the balls and cylinders. Furthermore, three different types of materials are used including: steel, wood, and rubber. We conduct the Ball-Ball (B-B) collision experiments of all collision pairs of the same and different type of materials and obtain their corresponding COR values. Then, we conduct the multiple impact collision experiments and obtain their pre- and post-impact velocities. We propose a discretization method and utilize the bimodal Hertz contact force model at the contacting segments. At the contacting segments, we employ the experimental B-B COR values to ac-

curately predict the post-impact velocities of the multiple impact problem. In our previous work, we found that by segmenting the softer material results in a good prediction of post-impact velocities. Here, softer is defined as material with lower stiffness than the hard material. In addition, we obtained a relationship between the stiffness ratio and the number of segments of the softer material for Ball-Cylinder (B-C) collisions. In the present study, we use this relationship to calculate the number of segments of the colliding bodies in the chain such that we obtain the greatest agreement of the post-impact velocities.

3.2. Experimental Setup

In this study, we focus on direct central impact of balls and cylinders. For that purpose, we built a frame that produces direct central impacts for the collision experiments (see Figs. 3.1-3.3).

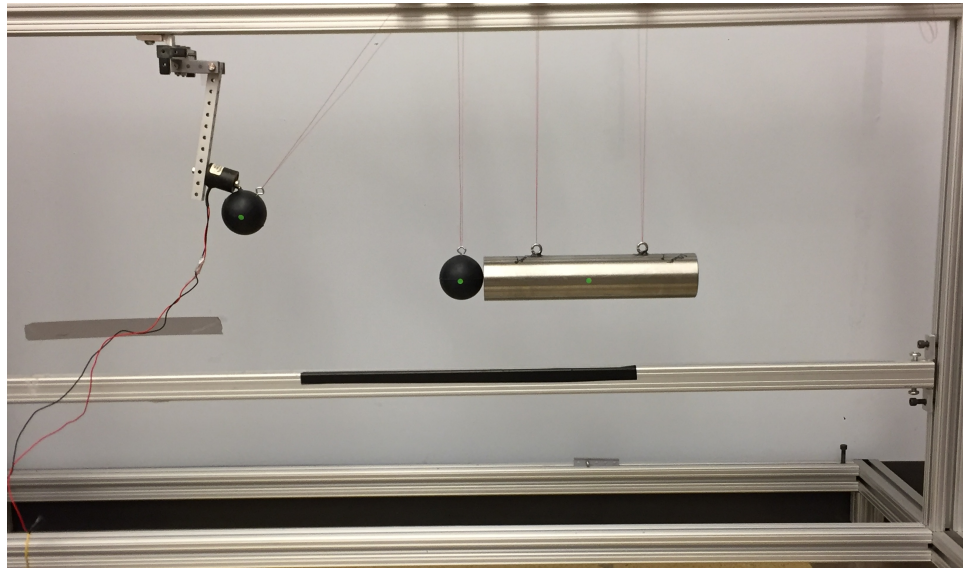


Figure 3.1: Three-body collision experimental setup

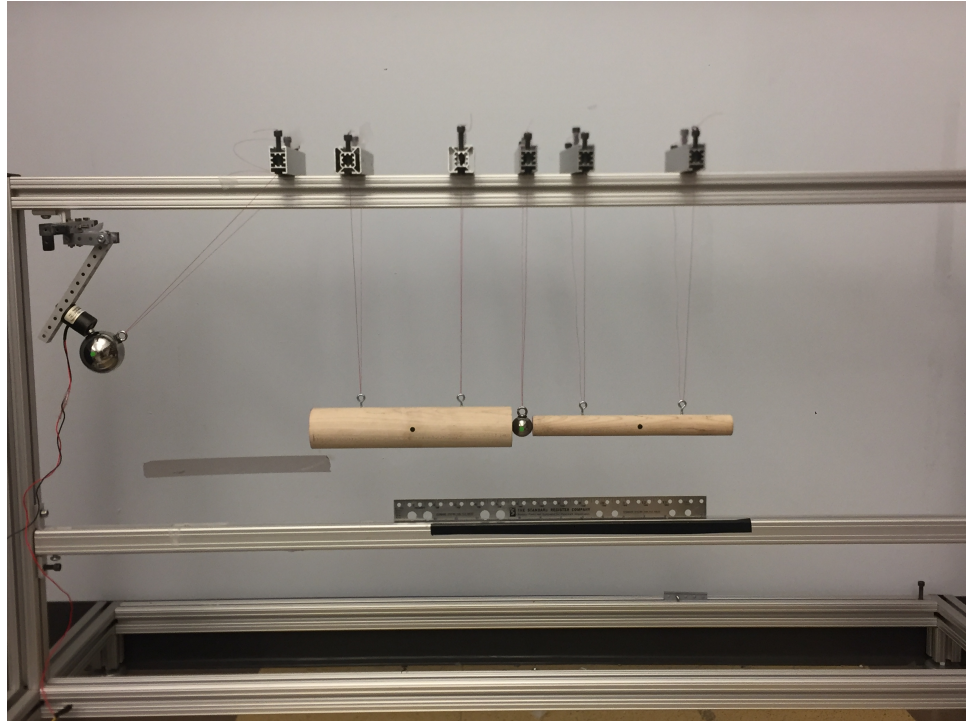


Figure 3.2: Four-body collision experimental setup



Figure 3.3: Five-body collision experimental setup

As seen in Figs. 3.1-3.3 the colliding bodies are suspended by adjustable strings that are attached to the adjustable upper rail of the frame. This provides a proper adjustment of the bodies to achieve a direct central impact on the horizontal plane. In addition, the wires are connected in v-formation, and the height of the cables is carefully selected to avoid unwanted wobbling and energy losses. Each experiment is initiated by dropping the ball from an initial height while the other body is resting in its lowest position. The release height is adjusted to achieve different pre-impact velocities. The release mechanism consists of an electromagnet that can release the ball with a turnable switch. Reflective markers are placed at the center of mass of each of the colliding bodies for position tracking. A high speed Sony camera with 960 frames per second capability is positioned on a tripod. The tripod is aligned with the center of mass of the bodies. In addition, it is placed sufficiently close to achieve better video resolution and to reduce visual distortion.

The captured videos are transferred to a personal computer for video processing and digitization. The video analysis and digitization is performed by first capturing the positions of the colliding bodies in each video frame. Subsequently, the captured position data are used to determine pre- and post-impact velocities by numerical differentiation of the position data. The position data is first smoothed by applying filtering in order to cancel any noise present.

Mainly, three types of materials have been selected for the experimental study for balls and cylinders. These materials include: steel (S), wood (W), and rubber (R). All balls used consist of multiple diameter sizes. The cylinders consist of two diameter sizes per material and the same length for all materials. The cylinder diameters are 0.0254 m and 0.0508 m . Table 3.1 shows the masses

and geometric values of the balls and cylinders. Note that the subscripts indicate the diameter size and the superscript indicates whether its a ball (b) or a cylinder (c).

Table 3.1: Masses and geometric values

Balls	Mass (Kg)	Radius (m)
S_1^b	0.07	0.0127
S_2^b	0.544	0.0254
W_1^b	0.01	0.01587
W_2^b	0.027	0.0222
W_3^b	0.045	0.0254
R_1^b	0.012	0.0127
R_2^b	0.097	0.0254
Cylinders	Mass (Kg)	Length (m)
S_1^c	0.968	0.241
W_1^c	0.084	0.241
R_1^c	0.187	0.241
S_2^c	3.865	0.24
W_2^c	0.285	0.24
R_2^c	0.699	0.24

After obtaining the pre- and post-impact velocities of the B-B collision experiments, one can measure the kinematic coefficient of restitution by taking the negative of the relative velocity ratio before and after the impact. Table 3.2 summarizes the average experimentally measured COR values for all B-B (\bar{e}) collision experiments.

Table 3.2: Experimental B-B COR values

Type	B-B		
	S_2^b	W_3^b	R_2^b
S_2^b	0.92 ± 0.05	0.67 ± 0.071	0.70 ± 0.073
W_3^b	0.63 ± 0.059	0.78 ± 0.041	0.69 ± 0.031
R_2^b	0.68 ± 0.024	0.68 ± 0.067	0.74 ± 0.047

Conducting theoretical study necessitates the estimation of the stiffness values of the colliding bodies. In order to achieve the measurements of the stiffness values of each ball and cylinder, a compression testing machine is used. We use the Instron 5967 material testing machine to perform the stiffness analysis testing. We conduct multiple loading-unloading compression cycles. The output raw data consist of displacement and force measurements. Subsequently, multiple force-displacement plots are obtained for each material and configuration. Then, an averaged stiffness is found by averaging the slope of the force displacement curve. After plotting the force-displacement data, we obtain the corresponding curve fit equations. In addition, we use two curve fit equations to obtain the linear and Hertzian stiffness values. Table 3.3 summarizes the experimentally measured stiffness values for all balls and cylinders.

Table 3.3: Experimental stiffness values

Type	Linear Stiffness ($\frac{N}{m}$)	Nonlinear Stiffness ($\frac{N}{m^{1.5}}$)
S_1^b	2.825×10^7	3.27×10^9
S_2^b	3.7655×10^7	4.3335×10^9
W_1^b	4.33×10^5	2.176×10^8
W_2^b	4.4×10^5	2.339×10^8
W_3^b	6.948×10^5	3.642×10^8
R_1^b	1.4645×10^4	5.4×10^5
R_2^b	2.5735×10^4	9.5105×10^5
S_1^c	5.3445×10^7	6.157×10^9
W_1^c	1.05×10^7	5.321×10^9
R_1^c	7.8365×10^4	4.043×10^6
S_2^c	3.7×10^8	4.27×10^{10}
W_2^c	3.145×10^7	1.592×10^{10}
R_2^c	5.438×10^5	2.8×10^7

3.3. Problem Description

The main objective of the present study is to investigate the multiple impact problem of balls and cylinder and investigate the post-impact outcomes of the colliding objects. We develop a mechanism to calculate the post-impact velocities of the multiple impact problem in a chain of balls and cylinders. The dynamics of the collision event of the balls and cylinders are represented by a discretization method. We employ the B-B COR to model the collision event at the contacting segments. In addition, we use the bimodal Hertz contact force model with plastic deformation. Then, we calculate the post-impact ve-

locities of all collision pairs and compare the theoretical prediction with the experimentally measured results.

3.3.1. Generalized B-B-C

We consider the generalized three-body Ball-Ball-Cylinder (B-B-C) model shown in Fig. 3.4. First, let's assume that the two balls are of the same material and size. Hence, they have the same radius and geometric properties. Here, the two balls and cylinder are divided into j_1 , j_2 , and j_3 equal segments, respectively. Each internal segment in the balls and cylinder is connected with linear internal springs (K^i). At the two contacting regions, the external non-linear collision stiffnesses of the balls (K_b^e) and cylinder (K_c^e) are incorporated. The external collision stiffnesses are used to model the contact forces between the two balls (\vec{F}_{c1}), and ball and cylinder (\vec{F}_{c2}), respectively. The segment's center of mass coordinates are defined as x_i .

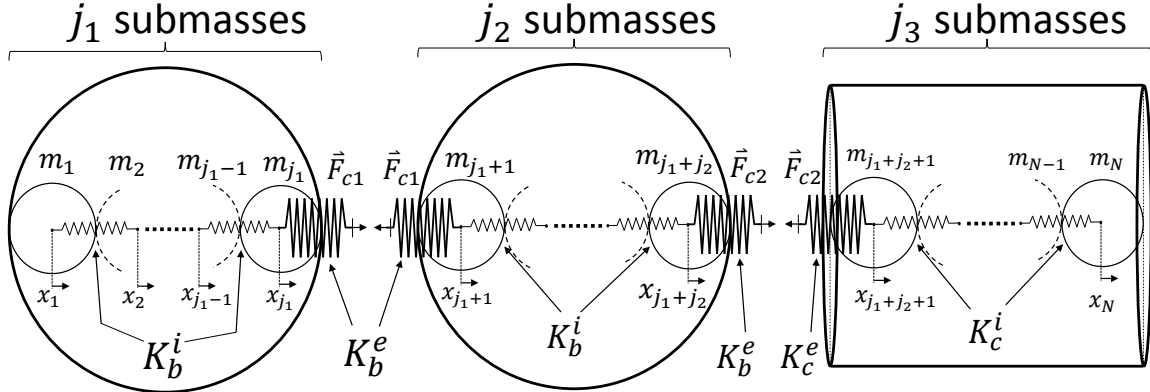


Figure 3.4: General discrete B-B-C model

The masses of the balls and cylinder of each segment are defined as:

$$m_i = \begin{cases} \frac{m_b}{j_1} & 1 \leq i \leq j_1 \\ \frac{m_b}{j_2} & j_1 + 1 \leq i \leq j_1 + j_2 \\ \frac{m_c}{j_3} & j_1 + j_2 + 1 \leq i \leq N \end{cases} \quad (3.1)$$

where, m_b and m_c are the total masses of the balls and cylinder, respectively.

The total number of segments is $N = j_1 + j_2 + j_3$.

The segments of each of the colliding bodies are connected together with their respective internal springs. We define the stiffnesses of the internal springs of the balls and cylinder as follow:

$$K_{b,1}^i = K_b(j_1 + 1) \quad (3.2)$$

$$K_{b,2}^i = K_b(j_2 + 1) \quad (3.3)$$

$$K_{c,3}^i = K_c(j_3 + 1) \quad (3.4)$$

where, K_b and K_c are the overall linear stiffnesses of the balls and cylinder, respectively. We define the relative displacement (δ_i) of each internal spring

of the balls and cylinder as:

$$\delta_i = \begin{cases} x_{i-1} - x_i + \frac{2R_b}{j_1} & 1 < i \leq j_1 \\ x_{i-1} - x_i + \frac{2R_b}{j_2} & j_1 + 1 < i \leq j_1 + j_2 \\ x_{i-1} - x_i + \frac{L_c}{j_3} & j_1 + j_2 + 1 < i \leq N \end{cases} \quad (3.5)$$

The generalized form of the second order differential equation of each segment can be written as follows:

$$m_i \ddot{x}_i + K^i (\delta_{i+1} - \delta_i) = 0 \quad (3.6)$$

At the onset of the collision the initial velocities of the balls and cylinder are as follow:

$$\dot{x}_i^- = \begin{cases} \dot{x}_{b,1}^- & 1 \leq i \leq j_1 \\ 0 & j_1 + 1 \leq i \leq j_1 + j_2 \\ 0 & j_1 + j_2 + 1 \leq i \leq N \end{cases} \quad (3.7)$$

where, $x_{b,1}^-$ is the pre-impact velocity of the striking ball, while the ball in the middle and cylinder are resting.

Now, at the end of the collision event, the center of mass post-impact velocities of each body can be computed as follow:

$$\dot{x}_{b,1}^+ = \frac{\sum_{i=1}^{j_1} \dot{x}_i^+}{j_1} \quad (3.8)$$

$$\dot{x}_{b,2}^+ = \frac{\sum_{i=j_1+1}^{j_1+j_2} \dot{x}_i^+}{j_2} \quad (3.9)$$

$$\dot{x}_{c,3}^+ = \frac{\sum_{i=j_1+j_2+1}^N \dot{x}_i^+}{j_3} \quad (3.10)$$

where, \dot{x}_i^+ is the post-impact velocity of each segment. Note, that the second index in the subscript indicates the arrangement in the chain.

We use the Hertz contact force model with plastic deformation to solve the multiple impact problem [33, 58, 108, 109, 127]. In addition, we incorporate the B-B COR (\bar{e}) to represent the energy dissipation between each colliding pair. Figure 3.5 depicts the force displacement curves of the Hertz contact force model with plastic deformations. The energy losses are given by the net work done in deforming the objects in the compression and restitution phases, which are shown as the two enclosed areas under the force displacement curves. From Fig. 3.5, δ , δ_p , K_C , and K_R are the relative displacement, permanent indentation, and collision stiffnesses during the compression and restitution phases, respectively. In addition, at the maximum compression δ_m and F_m are the maximum displacement and contact force, respectively.

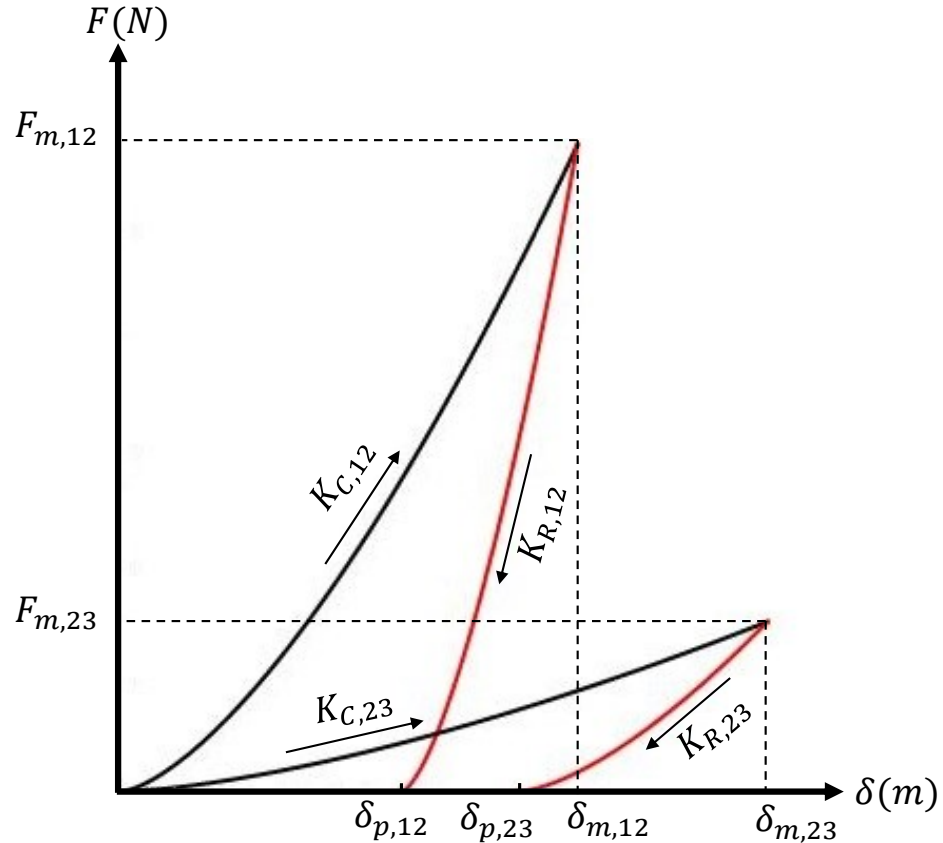


Figure 3.5: B-B-C force displacement curves

The contact forces \vec{F}_{c1} and \vec{F}_{c2} during the compression and restitution phases are defined as:

$$\vec{F}_{c1} = \begin{cases} K_{C,12}(\delta_{c,12})^n & \text{Compression Phase} \\ K_{R,12}(\delta_{c,12} - \delta_{p,12})^n & \text{Restitution Phase} \end{cases} \quad (3.11)$$

$$\vec{F}_{c2} = \begin{cases} K_{C,23}(\delta_{c,23})^n & \text{Compression Phase} \\ K_{R,23}(\delta_{c,23} - \delta_{p,23})^n & \text{Restitution Phase} \end{cases} \quad (3.12)$$

During the collision event, the relative contact displacements at the contacting segments are expressed as:

$$\delta_{c,12} = x_{j_1} - x_{j_1+1} + \frac{R_b}{j_1} + \frac{R_b}{j_2} \quad (3.13)$$

$$\delta_{c,23} = x_{j_1+j_2} - x_{j_1+j_2+1} + \frac{R_b}{j_2} + \frac{L_c}{2j_3} \quad (3.14)$$

The collision stiffnesses during the compression phase at the contacting segments are expressed as:

$$K_{C,12} = \frac{K_b^e K_b^e}{K_b^e + K_b^e} \quad (3.15)$$

$$K_{C,23} = \frac{K_b^e K_c^e}{K_b^e + K_c^e} \quad (3.16)$$

In order to relate the collision stiffnesses variation during the restitution phase, one needs to use the energetic definition of COR at the contacting segments [63]. The energetic CORs at the contacting segments are defined as:

$$\bar{e}_{12}^2 = -\frac{W_{R,12}}{W_{C,12}} \quad (3.17)$$

$$\bar{e}_{23}^2 = -\frac{W_{R,23}}{W_{C,23}} \quad (3.18)$$

where, W_C and W_R are the work done during the compression and restitution phases, respectively. Now for the first contacting segments, the work done

during both phases of contact is expressed as:

$$W_{C,12} = \int_0^{\delta_{m,12}} K_{C,12} \delta_{c,12}^n d\delta_{c,12} = \frac{K_{C,12} \delta_{m,12}^{n+1}}{n+1} \quad (3.19)$$

$$W_{R,12} = \int_{\delta_{m,12}}^{\delta_{p,12}} K_{R,12} (\delta_{c,12} - \delta_{p,12})^n d\delta_{c,12} = \frac{-K_{R,12} (\delta_{m,12} - \delta_{p,12})^{n+1}}{n+1} \quad (3.20)$$

Substituting Eqns. (3.19), (3.20) into Eqn. (3.17) yields the collision stiffness variation during the restitution phase as follows:

$$K_{R,12} = \frac{K_{C,12}}{\bar{e}_{12}^{2n}} \quad (3.21)$$

The maximum contact force can be obtained from Eqn. (3.11) as follows:

$$F_{m,12} = K_{C,12} (\delta_{m,12})^n \quad (3.22)$$

$$F_{m,12} = K_{R,12} (\delta_{m,12} - \delta_{p,12})^n \quad (3.23)$$

From Eqns. (3.22) and (3.23), the permanent indentation can be found as:

$$\delta_{p,12} = \delta_{m,12} \left(1 - \left(\frac{K_{C,12}}{K_{R,12}} \right)^{\frac{1}{n}} \right) \quad (3.24)$$

Following the same procedure for the second contacting segments, the restitution collision stiffness and permanent indentation are expressed as:

$$K_{R,23} = \frac{K_{C,23}}{\bar{e}_{23}^{2n}} \quad (3.25)$$

$$\delta_{p,23} = \delta_{m,23} \left(1 - \left(\frac{K_{C,23}}{K_{R,23}} \right)^{\frac{1}{n}} \right) \quad (3.26)$$

The local energy losses can be expressed as:

$$E_{l,12} = W_{C,12} + W_{R,12} \quad (3.27)$$

$$E_{l,23} = W_{C,23} + W_{R,23} \quad (3.28)$$

Note, the same procedure is applied for the four and five-body problems.

3.3.2. Segmentation Process

In our previous work, we considered Ball-Cylinder (B-C) impacts of the same and different types of materials. We used the largest size diameter of the balls and all diameter sizes of the cylinders (see Table 3.1). We conducted all collision pairs of the same and different types of materials. We developed a discretization method to calculate the B-C COR based on the B-B COR of the same pair. We categorized our B-C collision experiments into three categories including collision experiments of the same material, Hard-Soft different materials (H-S), and Soft-Hard different materials (S-H). Here, soft is defined as material with lower stiffness than the hard material. Our simulation runs showed that segmenting the softer material resulted in a good prediction of the B-C COR. We obtained the minimum average percentage error (APE_m) of the

B-C COR. We chose the number of segments of the softer material that corresponded to the APE_m . These number of segments represented a saturation point beyond which increasing segmentation does not affect the percentage error. The number of the segments of the harder material was found to be $j_H = 4$ for the S-H and $j_H = 6$ for the H-S collisions. Then, we found a relationship between the stiffness ratio (r_K) and the number of segments of the softer material. The stiffness ratio is defined as follows:

$$r_K = \frac{K_S^i}{K_H^i} \times 100 \quad (3.29)$$

where, K_S^i and K_H^i are the internal stiffnesses of the soft and hard materials, respectively.

Then, we plotted the number of segments of each collision pair versus the corresponding stiffness ratio. Figure 3.6 shows the number of segments of the softer material versus the stiffness ratio for all collision pairs. An empirical curve fit of the data (Regression value $R = 0.89$) was found, which is shown as the solid curve. The curve fit equation was found to be as follows:

$$j_S = a (r_K)^b + c \quad (3.30)$$

$$a = 2089$$

$$b = -0.00006584$$

$$c = -2051$$

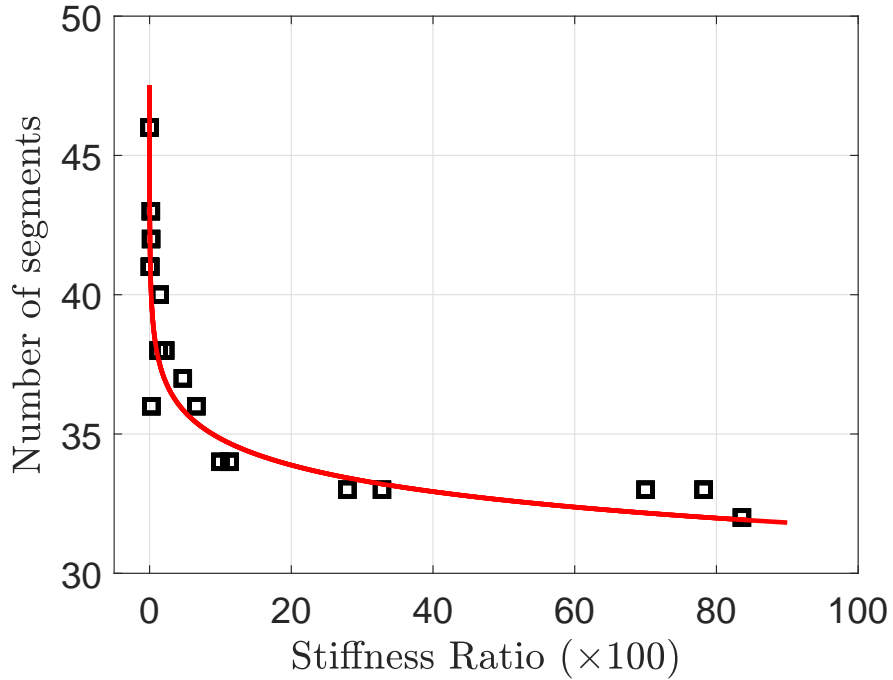


Figure 3.6: Stiffness ratio versus the number of segments

Here, we use this relationship between each B-C pair in the chain to estimate the post-impact velocities. One can follow these steps to find the number of segments of each of the colliding bodies in the chain:

1. For a given chain, look at balls and cylinders that are in contact and treat them as individual sets.
2. For each set, compute the stiffness ratio r_K and calculate the number of segments of the softer material in the set based on Eqn. (3.30).
3. If the set is H-S, then $j_H = 6$, otherwise, $j_H = 4$.
4. If there is more than one candidate of j_S , choose the maximum value of j_S .

- For the case of two balls in contact with each other and only one of them is in contact with the cylinder, the number of segments of the two balls are equal.

Let's consider the example of five-body chain combination of B-C-C-B-B shown in Fig. 3.7. Here, we have two different sets. For the first set, $j_1 = 6$ and $r_{K_1} = 1.44$. By using Eqn. (3.30), the number of segments for $j_2 = 38$. Similarly, for the second set, $j_4 = 4$ and $r_{K_2} = 11.3$, which gives $j_3 = 37$. In addition, the number of segments of j_5 equal to j_4 .

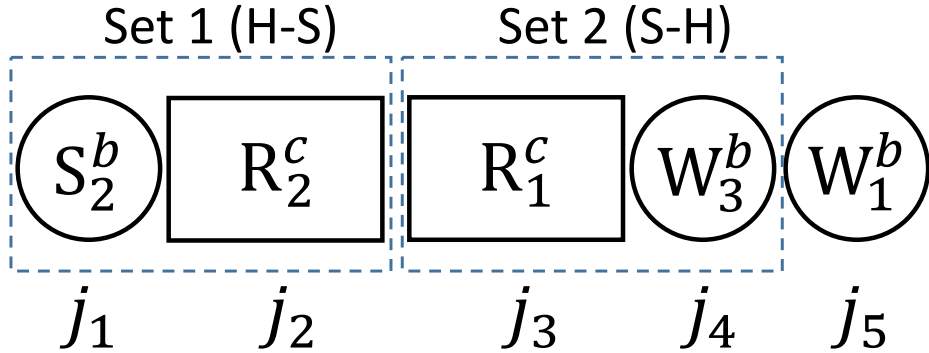


Figure 3.7: Example of five-body chain combination

3.4. Numerical Simulation and Results

In this section, we analyze the theoretical post-impact outcome results of three, four, and five-body collisions. In addition, for each collision set, we use the corresponding experimental B-B COR and pre-impact velocities. Also, we follow the segmentation procedure explained earlier to determine the number of segments of each of the colliding bodies. Then, we compare the experimental post-impact velocities with the theoretically computed ones.

First, we define percentage error of the post-impact velocity of each body (PE_i) and the corresponding average percentage error (APE) as follow:

$$PE_i = \left| \frac{\dot{x}_i^+ - \dot{x}_i^+}{\dot{x}_i^+} \right| \times 100; \quad i = 1, \dots, k \quad (3.31)$$

$$APE = \frac{\sum_{i=1}^k PE_i}{k} \quad (3.32)$$

where, \dot{x}_i^+ and $\dot{\bar{x}}_i^+$ are the theoretical and experimental post-impact velocities of each body, respectively.

For the three-body collisions, we use the largest diameter of the same pair of balls and both diameter sizes of the cylinders. Furthermore, the arrangements in the chain are B-B-C and B-C-B forms. Table 3.4 summarizes the APE of all B-B-C collisions. Here, the average of the APE of the first, second, and third groups are 4.2%, 3.7%, and 2.2%, respectively.

Table 3.4: Three-body (B-B-C) post-impact velocities

Three-body	v_1^-	v_1^+	v_2^+	v_3^+	APE
$S_2^b S_2^b S_1^c$	0.0325	-0.004	0.0006	0.0219	5.28
$S_2^b S_2^b S_2^c$	0.0411	-0.022	-0.0024	0.0091	1.25
$W_3^b W_3^b W_1^c$	0.0478	-0.002	0.0018	0.028	4.57
$W_3^b W_3^b W_2^c$	0.0455	-0.013	0.0011	0.0095	3.59
$R_2^b R_2^b R_1^c$	0.042	0.0005	0.006	0.0185	2.93
$R_2^b R_2^b R_2^c$	0.0507	-0.0091	0.0025	0.0083	7.36
$S_2^b S_2^b W_1^c$	0.0256	0.0009	0.019	0.0315	5.67
$S_2^b S_2^b W_2^c$	0.0298	0.0003	0.051	0.0274	0.64
$S_2^b S_2^b R_1^c$	0.0268	0.0021	0.0164	0.029	6.10
$S_2^b S_2^b R_2^c$	0.0262	0.0017	0.0032	0.0182	4.65
$W_3^b W_3^b R_1^c$	0.0362	-0.004	0.003	0.0111	3.36
$W_3^b W_3^b R_2^c$	0.0616	-0.018	0.0006	0.0053	1.75
$W_3^b W_3^b S_1^c$	0.0512	-0.014	0.0013	0.0028	2.01
$W_3^b W_3^b S_2^c$	0.0431	-0.017	0.0019	0.0007	2.5
$R_2^b R_2^b S_1^c$	0.0634	-0.015	0.0038	0.0073	1.71
$R_2^b R_2^b S_2^c$	0.055	-0.017	-0.002	0.0017	2.19
$R_2^b R_2^b W_1^c$	0.0355	0.0046	0.0098	0.0247	0.76
$R_2^b R_2^b W_2^c$	0.0527	-0.003	0.0047	0.0188	4.05

Table 3.5 shows the APE of all B-C-B collisions. The average APE of each of the three groups are 3.63%, 4.87%, and 1.94%.

Table 3.5: Three-body (B-C-B) post-impact velocities

Three-body	v_1^-	v_1^+	v_2^+	v_3^+	APE
$S_2^b S_1^c S_2^b$	0.0534	-0.0105	0.0123	0.0426	2.96
$S_2^b S_2^c S_2^b$	0.0821	-0.0496	0.0137	0.0278	4.57
$W_3^b W_1^c W_3^b$	0.0508	-0.0047	0.0117	0.0339	5.58
$W_3^b W_2^c W_3^b$	0.0629	-0.0288	0.0112	0.0214	4.02
$R_2^b R_1^c R_2^b$	0.0864	-0.0066	0.0235	0.0496	1.49
$R_2^b R_2^c R_2^b$	0.0319	-0.043	0.0156	0.0297	3.17
$S_2^b W_1^c S_2^b$	0.0298	0.01318	0.0133	0.0162	4.13
$S_2^b W_2^c S_2^b$	0.0608	0.01279	0.0245	0.0329	4.03
$S_2^b R_1^c S_2^b$	0.0564	0.01426	0.0202	0.0333	6.69
$S_2^b R_2^c S_2^b$	0.0619	0.00595	0.0142	0.0393	4.16
$W_3^b R_1^c W_3^b$	0.0896	-0.0195	0.0186	0.0309	5.35
$W_3^b R_2^c W_3^b$	0.0866	-0.0425	0.0079	0.0109	4.87
$W_3^b S_1^c W_3^b$	0.0746	-0.0308	0.0047	0.0069	1.17
$W_3^b S_2^c W_3^b$	0.0791	-0.0378	0.0013	0.0019	2.23
$R_2^b S_1^c R_2^b$	0.0529	-0.0212	0.0073	0.0103	1.24
$R_2^b S_2^c R_2^b$	0.133	-0.0716	0.0051	0.0072	2.01
$R_2^b W_1^c R_2^b$	0.0824	0.01076	0.0210	0.0511	2.86
$R_2^b W_2^c R_2^b$	0.0643	-0.0112	0.0171	0.027	2.13

For the four-body collisions in Table 3.6, we use multiple sizes of the balls and cylinders. The arrangements in the chain are in the form of B-C-B-C. The average APE of all collision combinations is approximately 4.81%.

Table 3.6: Four-body post-impact velocities

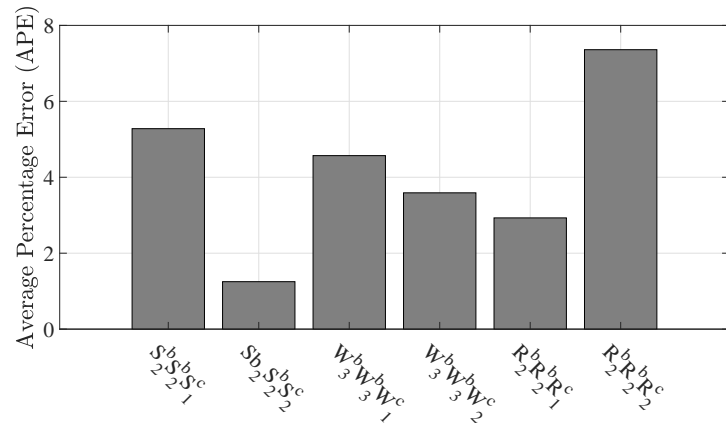
Four-body	v_1^-	v_1^+	v_2^+	v_3^+	v_4^+	APE
$S_2^b R_2^c S_1^b R_1^c$	0.0954	0.0103	0.03427	0.0499	0.0729	7
$W_3^b R_2^c W_1^b R_1^c$	0.0268	-0.05718	0.00366	0.00518	0.01331	7.1
$W_3^b W_2^c W_1^b W_1^c$	0.201	-0.08607	0.0236	0.02944	0.05795	1.44
$R_2^b R_2^c R_1^b R_1^c$	0.199	-0.0936	0.0273	0.0383	0.04716	3.79
$S_2^b W_2^c S_1^b W_1^c$	0.0887	0.0248	0.0292	0.062	0.06915	5.15
$S_2^b S_2^c S_1^b S_1^c$	0.0897	-0.051	0.0149	0.0199	0.0333	4.63
$W_3^b R_2^c S_1^b R_1^c$	0.174	-0.0764	0.01234	0.0131	0.0224	4.54

Finally, the five-body problem consists of different combinations of the arrangements in the chain. Thus, all cylinders and balls diameter sizes are used. Table 3.7 depict the five-body collision combinations of balls and cylinders. The average APE of all of the five-body collision combinations is approximately 6.17%.

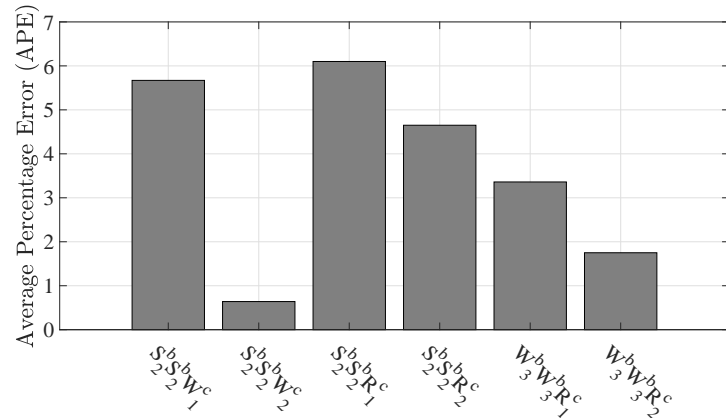
Table 3.7: Five-body post-impact velocities

Five-body	v_1^-	v_1^+	v_2^+	v_3^+	v_4^+	v_5^+	APE
$S_2^b R_2^c R_1^c W_3^b W_1^b$	0.05967	0.006348	0.02486	0.03892	0.05548	0.05795	3.76
$S_2^b W_2^c W_1^c R_2^b R_1^b$	0.07555	0.0317	0.03326	0.0474	0.06236	0.12	5.93
$S_2^b W_2^c W_3^b S_1^b R_1^c$	0.06317	0.02676	0.02614	0.031	0.0325	0.03748	7.8
$W_3^b R_2^c W_2^b R_1^c W_1^b$	0.115	-0.0524	0.00789	0.01276	0.01389	0.0141	7.2

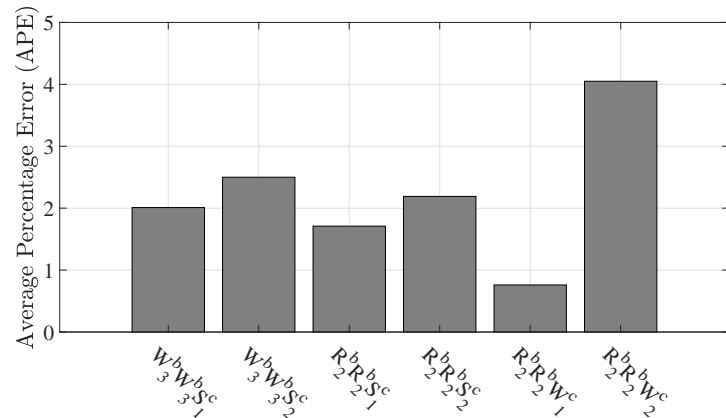
The APE of each collision combination of the three, four, and five-body chains are graphically presented in Figs. 3.8-3.11.



(a) B-B-C

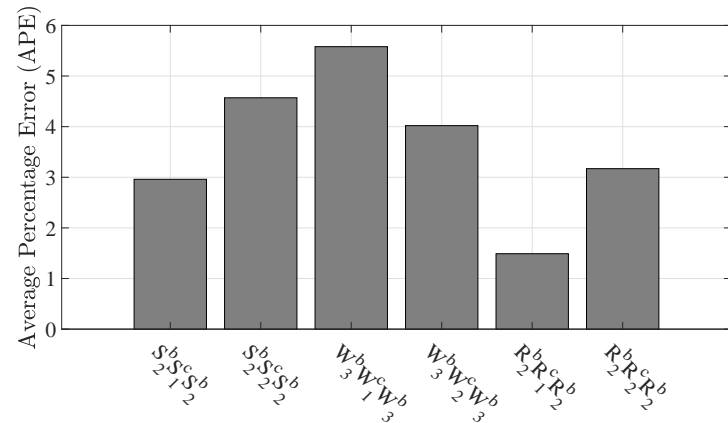


(b) B-B-C

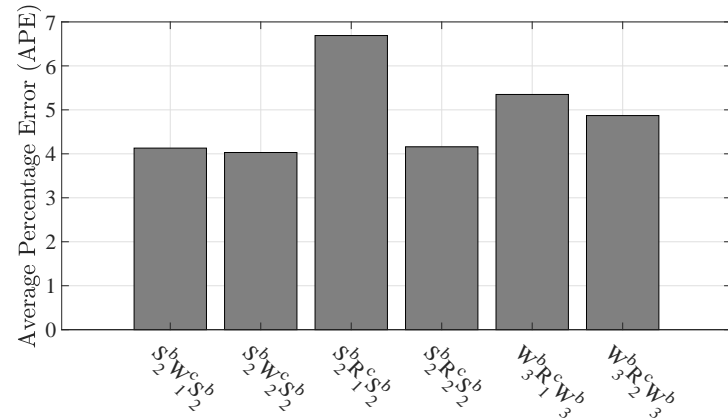


(c) B-B-C

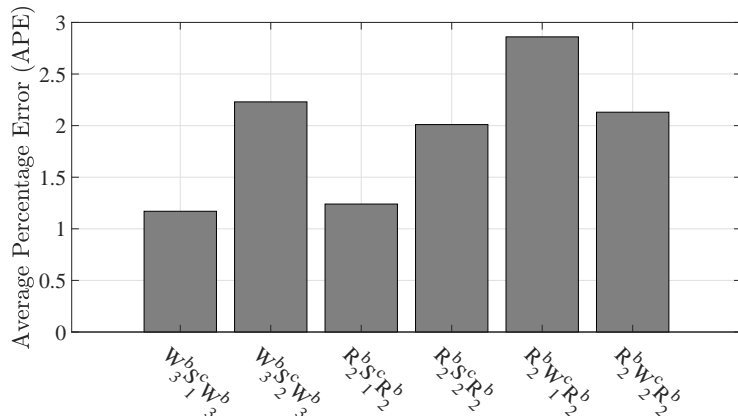
Figure 3.8: Three-body (B-B-C) APE



(a) B-C-B



(b) B-C-B



(c) B-C-B

Figure 3.9: Three-body (B-C-B) APE

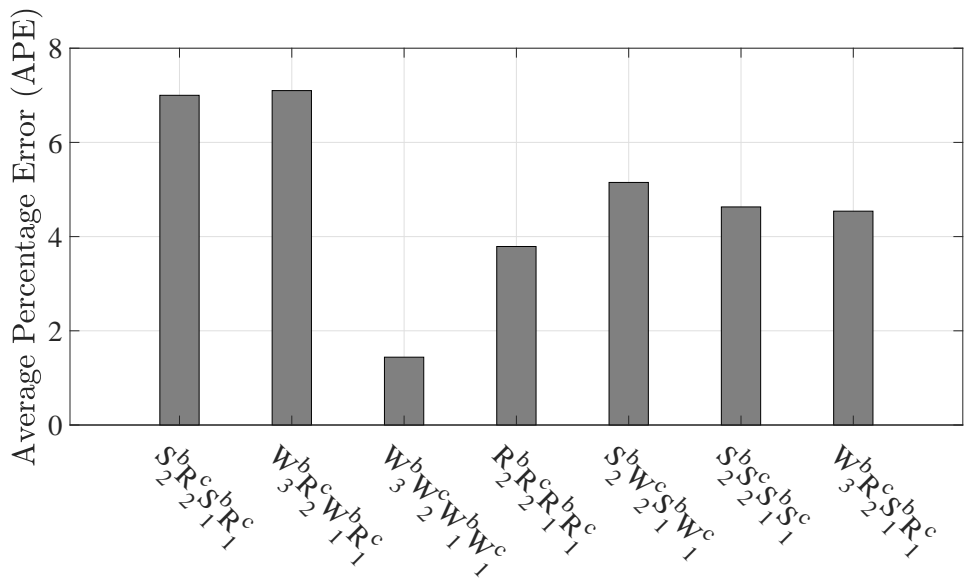


Figure 3.10: Four-body system APE

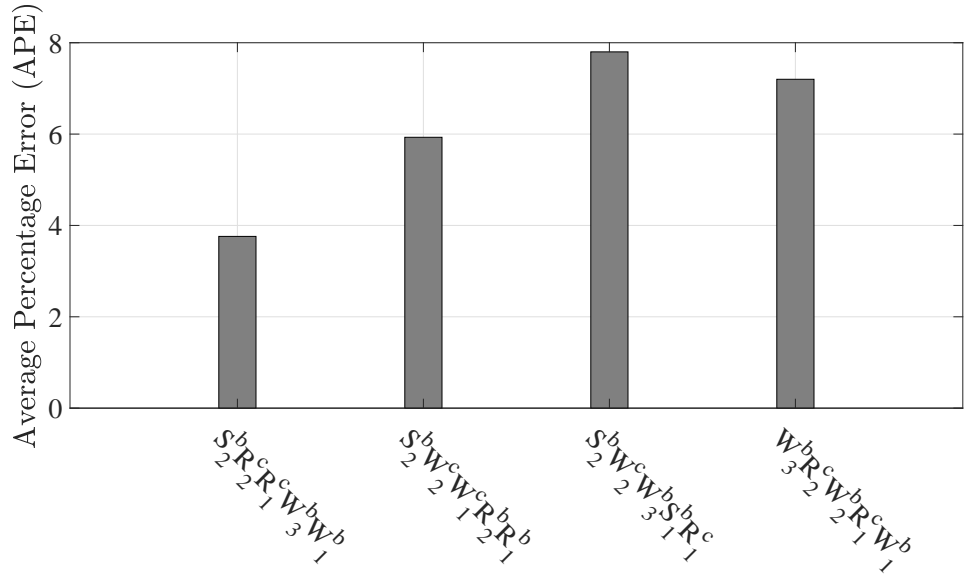


Figure 3.11: Five-body system APE

Chapter 4

On Uniqueness and Existence of Solutions to Multiple-Contact Collisions of Planar-Particle Based Kinematic Chains

4.1. Introduction

The impact problem of linear kinematic chain has been the focus of many researchers in the field of robotics. The importance of this class of impact problems arises in the modeling and simulation of robotic systems such as robotic manipulators and locomotion robots (i.e bipedal mechanisms), to name a few. Three main approaches exist to solve the general impact problem including rigid body [114], the soft laws [115], and the continuum mechanics equations for the entire system [97]. In this chapter, however, we consider the impact as rigid one. Solving rigid body collisions dates back to Newton. Newton stated that the ratio of the relative velocities of two colliding masses before and after the impact has a constant value called the coefficient of restitution. Presently, the coefficient of restitution has different definitions [1, 116].

Kane and Levinson observed that in the presence of friction, Newton's definition fails to satisfy the energy conservation principle [1, 21, 116]. In 1818, Poisson proposed the kinetic definition of the coefficient of restitution. He divided the collision period into two phases: compression and restitution. Thus, the coefficient of restitution is represented by the ratio of the accumulated normal restitution impulse and the normal compression impulse. In 1855, Morin

used Poisson's definition to show that the tangential contact forces at the contact point can be related using Coulomb's friction law. Routh used the same definition to present a new graphical method for solving the 2D inelastic collision problem [3, 130, 131]. Kane used Routh's method to analyze the ground impact of a compound pendulum. As a result, an inconsistency in the energy level was observed [132]. The method can lead to loss of energy even when the coefficient of restitution was unity. Stronge introduced the energetic definition of the coefficient of restitution [63]. He defined the square of the coefficient of restitution as the ratio of the energy released during the restitution phase to the energy absorbed by the deformation during the compression phase.

Multi-body impact problems falls into two categories. The first category is impacts that involve a sequence of contacting masses with simultaneous internal collisions [108, 121, 126, 133–139]. The second category is a kinematic chain with one end striking an external surface while other ends rest on other external surfaces. The second category is often seen in robotic systems. For example, one leg of a bipedal robot encounters an impact due to a heel strike of the swing leg, while the foot of the stance leg rests of the walking surface. Hurmuzlu and Moskowitz studied the role of the ground periodic impacts to achieve the locomotion stability of a bipedal system [112, 119, 120]. Hurmuzlu and Chang developed a methodology to solve the problem of multi-contact points of a planar kinematic chain [111].

Pereria and Nikravesh [27] studied the impact of the compound double pendulum using the kinematic definition of the coefficient of restitution. In addition, they studied the impact dynamics and the dry friction effect of the open and closed loop mechanical systems. Ahmed *et al.* [140] presented the

impact of two kinematic chains with each other. In their research, the Poisson's definition was used to avoid the energy paradox. However these analyses involved only one impact point but no external contact points. Hurmuzlu and Marghitu used all three definitions of the coefficient of restitution to compare the outcomes of ground impact for one end of the chain striking an external surface while other ends rest on other surfaces (n-point impact) in 2D and 3D problems [1, 116]. They compared three approaches for a specific example of a planar three-link kinematic chain with two contact points. Tavakoli *et al.* presented the impact problem of a two-mass system called "Baton" [124]. They studied the effect of the baton's length and the external surface angle on the impulse correlation ratio [117]. Tavakoli and Hurmuzlu presented the locomotion of a family tree of dynamical systems [118, 141]. They studied the two-point impact problem with a single contact for one, two and three-mass systems.

As we discussed above, the n-point impact problem was considered before by Hurmuzlu and his co-workers. Yet, in their work, they have presented a solution but never proved analytically the uniqueness and existence of the possible solutions. In this chapter, we consider the n-point impact problem. Such problems may arise in robotics for multi-legged robots (quadrupeds, hexapods, and spiders) or when one finger of a robotic multi-fingered hand strikes a surface while the other fingers are resting on the other surfaces. We prove analytically the uniqueness and existence of the solution for the n-link general problem.

Thus, the main contribution of this chapter is development of the solution for the n-point impact of a planar rigid particle open chain mechanism with

multiple external surfaces and analytical proof of uniqueness and existence of solutions. In addition, we present precise conditions to detect the *critical configurations* of the chain. When the chain has a critical configuration, the normal velocity and impulse at a contacting end become simultaneously equal to zero.

4.2. Problem Description

The main problem can be described as a general chain that is in contact with multiple surfaces. The impact takes place at one of these contacting points (an impacting mass). Prior to the impact, k masses are in contact with other external surfaces (contacting masses). The relative normal velocities among the contacting masses and the respective external surfaces are zero prior to the impact event. The impact causes the contacting masses to either detach (rebound) from or remain in contact with the respective contact surfaces. Effect of gravity is neglected following the assumption that gravitational forces are much smaller than the ones generated by impact.

Figure 4.1 represents a general particle kinematic chain with multi-contact masses. Here, the overall chain consists of linear branches. Each branch consists of two types of primitive building units: a single-mass with a built-in revolute joint and a massless connection rod. The length of each rod is L_i . As far as the kinematics are concerned, the masses in the chain are either contacting or non-contacting masses. Also, the general chain mechanism may have one or more combinations of contacting and/or non-contacting branches. A non-contacting branch is defined as a sequence of non-contacting masses. While a contacting branch is a sequence of masses that start and/or end with

contacting masses. The general open chain mechanism may have one or more combinations of the contacting and/or non-contacting branches. Based on the chain structure in Fig. 4.1, we define the first contacting-mass on the surface (S_1) as the base mass, the position of this mass is given by (x_1, y_1) . The position of the base mass is chosen as the origin of the reference frame of the chain. The impact is initiated by the last mass in the branch striking an external surface (S_{imp}), called the impacting mass with non-zero velocity. The subscript of each mass in the chain has four components; the first one indicates whether the branch that has the mass is a contacting (c) or a non-contacting branch (nc). Whereas, the second component of the subscript indicates the order of the branch within the chain. The third component indicates whether the mass itself is a contacting (c) or a non-contacting mass (nc). Whereas, the fourth component indicates the position of a particular mass with respect to the first mass in the branch. Thus, the position of any mass in the chain can be described by using the generalized coordinates vector $\{x_1, y_1, \theta_1, \dots, \theta_{n-1}\}^T$. Here, the angles $\{\theta_1, \theta_2, \dots, \theta_{n-1}\}$ are absolute angles measured in the counter-clockwise direction from the positive x-axes.

Hurmuzlu and co-workers proposed a numerical method to solve impact problems of this class [1, 111, 116]. The method is based on enumerating all possible outcomes at a contacting ends and then obtaining all the corresponding mathematical solutions. Once all possible mathematical post impact solutions were obtained, the physically consistent ones were identified by checking the conditions at the contacting ends.

Specifically, at each of the contacting ends, we imposed two possible constraint conditions; the normal velocity V_{i,y_i} was equal to zero, or the normal

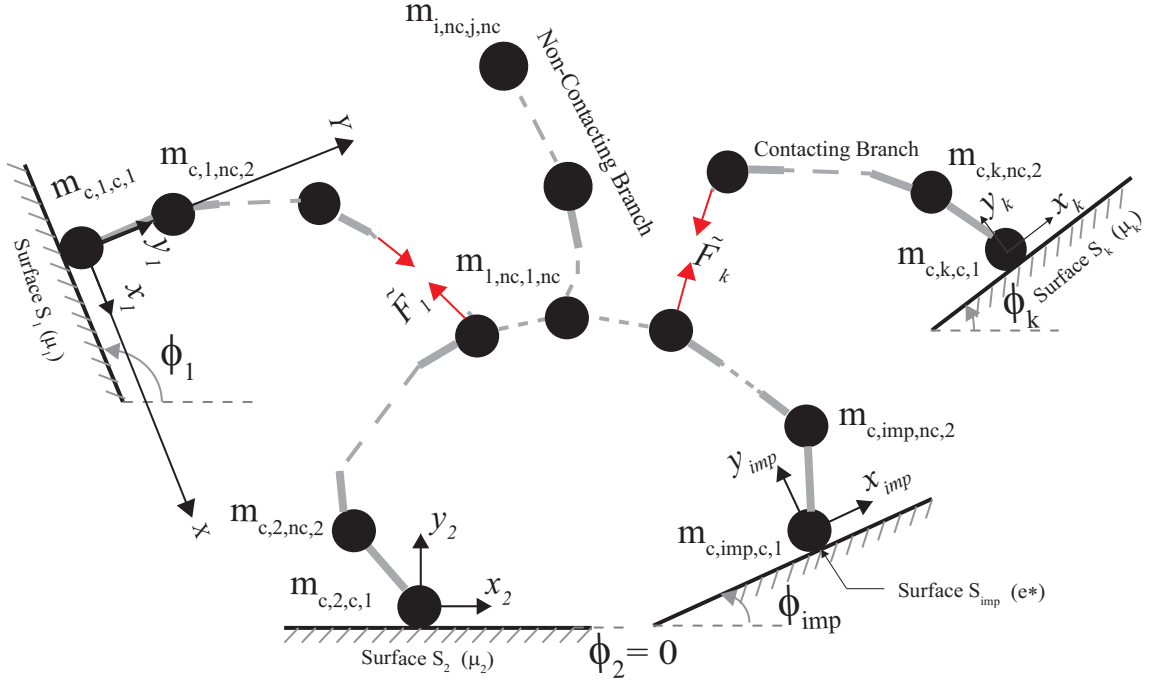


Figure 4.1: Multiple-Contact, Planar, Particle Based Chain

impulse \hat{F}_{i,y_i} was equal to zero. All permutations of such constraints for k ends yields 2^k mathematical solutions. The next step, was to check the feasibility of the resulting solution set. A mathematical solution was feasible if and only if one of the following conditions was true for all contacting ends:

Condition I: if $\hat{F}_{i,y_i} = 0$ is imposed then $V_{i,y_i} \geq 0$

Condition II: if $V_{i,y_i} = 0$ is imposed then $\hat{F}_{i,y_i} \geq 0$

All mathematical solutions that violated both conditions at the contacting ends were eliminated. The main question was whether this process is guaranteed to yield a unique feasible solution. In [1], the uniqueness and existence of the solutions were shown for only few specific examples by using numeri-

cal methods. In the present work, we analytically prove the uniqueness and existence of the solutions for the class of impact problems considered in this chapter.

What follows is the development of equations to prove the existence and uniqueness of the solutions. The summary of the approach is to first express the angular velocities, normal and tangential velocities and impulses at the contacting ends, the tangential velocity and impulse at the impacting point in terms of the normal impulse at the impacting point.

Although it will not be presented in this chapter, one can use the energetic coefficient of restitution to calculate the final value of the normal impacting impulse. This final value of the impulse will be substituted in the relevant equations to obtain the solution to the impact problem.

4.3. Development of the Impact Equations

The classical representation of the dynamics of a robotic mechanism with n revolute joints can be represented as [142]:

$$\mathbf{M}(\mathbf{x})\ddot{\mathbf{x}} + \mathbf{C}(\mathbf{x}, \dot{\mathbf{x}}) + \mathbf{G}(\mathbf{x}) = \begin{bmatrix} 0 \\ 0 \\ \mathbf{T} \end{bmatrix} + \mathbf{D}(\mathbf{x}, \boldsymbol{\phi}) \mathbf{F} \quad (4.1)$$

where, $\mathbf{x} = (x_1, y_1, \theta_1, \dots, \theta_{n-1})^T$ is the $(n+1) \times 1$ dimensional vector of the generalized coordinates, n is the number of masses in the chain, θ_i is the absolute rotation measured in the counter clockwise from the horizontal as shown in Fig. 4.1, $\dot{\mathbf{x}} = (\dot{x}_1, \dot{y}_1, \dot{\theta}_1, \dots, \dot{\theta}_{n-1})^T$ is the $(n+1) \times 1$ dimensional

vector of the generalized velocities, $\dot{\mathbf{x}} = (\ddot{x}_1, \ddot{y}_1, \ddot{\theta}_1, \dots, \ddot{\theta}_{n-1})^T$ is the $(n+1) \times 1$ dimensional vector of the generalized accelerations, $\mathbf{M}(\mathbf{x})$ is the positive definite symmetric $(n+1) \times (n+1)$ mass matrix, $\mathbf{C}(\mathbf{x}, \dot{\mathbf{x}})$ is the $(n+1) \times 1$ the centripetal vector, $\mathbf{G}(\mathbf{x})$ is the $(n+1) \times 1$ vector of gravity terms, \mathbf{T} is the $(n-1) \times 1$ generalized vector of joint moments, $\boldsymbol{\phi} = (\phi_1, \phi_2, \dots, \phi_k, \phi_{\text{imp}})^T$ is the inclination angle vector of surfaces, $\mathbf{D}(\mathbf{x}, \boldsymbol{\phi})$ is the $(n+1) \times 2k$ matrix, and $\mathbf{F} = (F_1^x, F_1^y, \dots, F_{k-1}^x, F_{k-1}^y, F_k^x, F_k^y)^T$ is the $2k \times 1$ vector of contact forces. Here, the superscripts x and y denote the tangential and normal components, respectively.

Solving for the acceleration vector in Eqn. (4.1) yields,

$$\ddot{\mathbf{x}} = \mathbf{M}(\mathbf{x})^{-1} \left\{ -\mathbf{C}(\mathbf{x}, \dot{\mathbf{x}}) - \mathbf{G}(\mathbf{x}) + \begin{bmatrix} 0 \\ 0 \\ \vdots \\ \mathbf{T} \end{bmatrix} + \mathbf{D}(\mathbf{x}, \boldsymbol{\phi})\mathbf{F} \right\} \quad (4.2)$$

On the other hand, the general kinematic expressions for the normal and tangential components of the linear accelerations of the contacting ends of the chain can be written as:

$$\mathbf{a} = \mathbf{H}_1(\mathbf{x}) \ddot{\mathbf{x}} + \mathbf{H}_2(\mathbf{x}, \dot{\mathbf{x}}) \quad (4.3)$$

where, $\mathbf{a} = (a_{1,x}, a_{1,y}, \dots, a_{k-1,x}, a_{k-1,y}, a_{k,x}, a_{k,y})^T$ is the $2k \times 1$ acceleration vector, and two matrices \mathbf{H}_1 and \mathbf{H}_2 are the general forms of the corresponding components of the normal and tangential accelerations [1]. Combining Eqn. (4.2) and Eqn. (4.3) yields,

$$\mathbf{a} = \mathbf{H}_2(\mathbf{x}, \dot{\mathbf{x}}) + \mathbf{H}_1(\mathbf{x}) \mathbf{M}(\mathbf{x})^{-1} \left\{ -\mathbf{C}(\mathbf{x}, \dot{\mathbf{x}}) - \mathbf{G}(\mathbf{x}) + \begin{bmatrix} 0 \\ 0 \\ \mathbf{T} \end{bmatrix} + \mathbf{D}(\mathbf{x}, \boldsymbol{\phi}) \mathbf{F} \right\} \quad (4.4)$$

Proceeding along the lines of Keller's method [1, 7], we eliminate the non-impulsive terms from Eqn. (4.4) (the first term and the first three terms between the braces). Furthermore, assuming that the generalized coordinates do not change during impact, we let the generalized position vector be the constant vector $\bar{\mathbf{x}} = (0, 0, \bar{\theta}_1, \dots, \bar{\theta}_{n-1})^T$. This yields

$$\mathbf{a} = \frac{d\mathbf{V}}{dt} = \mathbf{H}_1(\bar{\mathbf{x}}) \mathbf{M}(\bar{\mathbf{x}})^{-1} \mathbf{D}(\bar{\mathbf{x}}, \boldsymbol{\phi}) \mathbf{F} = \boldsymbol{\Gamma}(\bar{\mathbf{x}}, \boldsymbol{\phi}) \mathbf{F} \quad (4.5)$$

where, \mathbf{V} is the velocity vector of the contacting points of the chain and $\boldsymbol{\Gamma}(\bar{\mathbf{x}}, \boldsymbol{\phi})$ is a constant $2k \times 2k$ matrix that depends on pre-impact positions, masses, rod's lengths, and inclination angles of the contact surfaces. Additional equations can be obtained by considering the relative motions of the contacting ends with respect to their respective surfaces [1].

The impulses at the contact points are given by the following relations:

$$\boldsymbol{\tau} = \begin{bmatrix} \tau_{1,x_1} \\ \tau_{1,y_1} \\ \vdots \\ \tau_{k,x_k} \\ \tau_{k,y_k} \\ \tau_{\text{imp},x_{\text{imp}}} \\ \tau_{\text{imp},y_{\text{imp}}} \end{bmatrix} = \begin{bmatrix} \int_0^t F_{1,x_1} \\ \int_0^t F_{1,y_1} \\ \vdots \\ \int_0^t F_{k,x_k} \\ \int_0^t F_{k,y_k} \\ \int_0^t F_{\text{imp},x_{\text{imp}}} \\ \int_0^t F_{\text{imp},y_{\text{imp}}} \end{bmatrix} = \begin{bmatrix} \hat{F}_{1,x_1} \\ \hat{F}_{1,y_1} \\ \vdots \\ \hat{F}_{k,x_k} \\ \hat{F}_{k,y_k} \\ \hat{F}_{\text{imp},x_{\text{imp}}} \\ \hat{F}_{\text{imp},y_{\text{imp}}} \end{bmatrix} \quad (4.6)$$

Using the last row of the vector in Eqn. (4.6), we let:

$$\frac{d}{dt} = F_{\text{imp},y_{\text{imp}}} \frac{d}{d\eta} \quad (4.7)$$

where, $\eta \equiv \tau_{\text{imp},y_{\text{imp}}}$ is the normal impulse at the impacting point (in order to simplify the notation).

Once the accelerations at the contacting points are defined from Eqn. (4.5), the general form of contact forces and accelerations of the contacting masses in terms of $F_{\text{imp},y_{\text{imp}}}$ can be written as:

$$\begin{bmatrix} \mathbf{F} \\ d\mathbf{V}/dt \end{bmatrix} = \begin{bmatrix} d\boldsymbol{\tau}/dt \\ d\mathbf{V}/dt \end{bmatrix} = F_{\text{imp},y_{\text{imp}}} \begin{bmatrix} \Psi_1(\bar{\mathbf{x}}, \phi) \\ \Psi_2(\bar{\mathbf{x}}, \phi) \end{bmatrix} \quad (4.8)$$

We should note that the vectors Ψ_1 and Ψ_2 do not depend on η (please

see [1]). Dividing Eqn. (4.8) by $F_{\text{imp},y_{\text{imp}}}$ and using Eqn. (4.7) yields,

$$\begin{bmatrix} d\boldsymbol{\tau}/d\eta \\ d\mathbf{V}/d\eta \end{bmatrix} = \begin{bmatrix} \Psi_1(\bar{\mathbf{x}}, \phi) \\ \Psi_2(\bar{\mathbf{x}}, \phi) \end{bmatrix} \quad (4.9)$$

We integrate Eqn. (4.9) to get :

$$\boldsymbol{\tau}(\eta) = \Psi_1(\bar{\mathbf{x}}, \phi)(\eta - \eta_0) + \boldsymbol{\tau}_0 \quad (4.10)$$

$$\mathbf{V}(\eta) = \Psi_2(\bar{\mathbf{x}}, \phi)(\eta - \eta_0) + \mathbf{V}_0 \quad (4.11)$$

where, η_0 , \mathbf{V}_0 , and $\boldsymbol{\tau}_0$ represent the respective initial conditions. These equations express the normal impulses and velocities at the contacting ends in the terms of the normal impulse at impacting end (η). Yet, the uniqueness and existence of the solution have never been proven in [1], this is given in follow.

4.4. Normal Impulse and Normal Velocity Relationship of the Contacting Mass

In general, the post collision outcome at a contacting mass can be obtained as a function of the impacting impulse. In this chapter, we use linear and angular momentum equations to analytically derive the relationships among normal velocities and normal impulses at contacting points. As a result, by solving the linear and angular momentum equations, we can write the outcome of any contacting mass (m_i) in terms of the impacting impulse and the impulses that may arise from the contribution of the other contacting masses in the chain. Equations (4.12) and (4.13) show the general form of the normal velocities and

normal impulses of the contacting masses, respectively.

$$\mathbf{V}_y(\eta) = \begin{bmatrix} V_{1,y_1}(\eta) \\ \vdots \\ V_k(y_k) \end{bmatrix} = \begin{bmatrix} \alpha_1 \\ \vdots \\ \alpha_k \end{bmatrix} \eta + \begin{bmatrix} 0 & \gamma_{1,2} & \cdot & \cdot & \cdot & \gamma_{1,k} \\ \gamma_{2,1} & 0 & \cdot & \cdot & \cdot & \gamma_{2,k} \\ \cdot & \cdot & 0 & \cdot & \cdot & \cdot \\ \cdot & \cdot & \cdot & 0 & \cdot & \gamma_{k-1,k} \\ \gamma_{k,1} & \cdot & \cdot & \gamma_{k,k-1} & 0 & \cdot \\ \cdot & \cdot & \cdot & \cdot & \cdot & \cdot \end{bmatrix} \begin{bmatrix} \hat{F}_{1,y_1}(\eta) \\ \vdots \\ \hat{F}_{k,y_k}(\eta) \end{bmatrix} \quad (4.12)$$

$$\hat{\mathbf{F}}_y(\eta) = \begin{bmatrix} \hat{F}_{1,y_1}(\eta) \\ \vdots \\ \hat{F}_{k,y_k}(\eta) \end{bmatrix} = \begin{bmatrix} \beta_1 \\ \vdots \\ \beta_k \end{bmatrix} \eta + \begin{bmatrix} 0 & \xi_{1,2} & \cdot & \cdot & \cdot & \xi_{1,k} \\ \xi_{2,1} & 0 & \cdot & \cdot & \cdot & \xi_{2,k} \\ \cdot & \cdot & 0 & \cdot & \cdot & \cdot \\ \cdot & \cdot & \cdot & 0 & \cdot & \xi_{k-1,k} \\ \xi_{k,1} & \cdot & \cdot & \xi_{k,k-1} & 0 & \cdot \\ \cdot & \cdot & \cdot & \cdot & \cdot & \cdot \end{bmatrix} \begin{bmatrix} \tilde{F}_{1,y_1}(\eta) \\ \vdots \\ \tilde{F}_{k,y_k}(\eta) \end{bmatrix} \quad (4.13)$$

where, the components of $\boldsymbol{\alpha}$ and $\boldsymbol{\beta}$ are vectors, $\boldsymbol{\xi}$ and $\boldsymbol{\gamma}$ are functions of the generalized coordinates x, y , the masses m_i , the link lengths L_i , and the surfaces inclination angles ϕ_i and coefficient of friction μ . Also, k is the number of the contacting masses in the chain. As a result, $\boldsymbol{\alpha}$ and $\boldsymbol{\beta}$ vectors, and $\boldsymbol{\xi}$ and $\boldsymbol{\gamma}$ matrices. An impulse (\tilde{F}_k) shown in Fig. 4.1 represents the contribution of the impacting mass, which is in contact with the surface S_{imp} to the impulse of the contacting mass m_k . In fact, the general relationship between the two

vectors in Eqns. (4.12) and (4.13) can be written as:

$$\langle \hat{\mathbf{F}}_{\mathbf{y}}(\eta), \mathbf{V}_{\mathbf{y}}(\eta) \rangle = 0, \quad \hat{\mathbf{F}}_{\mathbf{y}}(\eta), \mathbf{V}_{\mathbf{y}}(\eta) \geq 0 \quad (4.14)$$

where, $\langle \cdot, \cdot \rangle$ is the "dot product" between the two vectors. This is a complementarity relation between normal impulse and normal velocity vectors in η domain.

Now, for a linear chain mechanism, where no branches exist (the case of multiple branches will be presented later in Theorem 2 below). This is the simplest impact problem of a linear chain, which one contacting and one impacting mass (only one closed-segment). Then for this case, Eqns. (4.12) and (4.13) reduce to:

$$V_{i,y_i}(\eta) = \alpha_i \eta \quad (4.15)$$

$$\hat{F}_{i,y_i}(\eta) = \beta_i \eta \quad (4.16)$$

Theorem 4.1. *Let C_o be a sub-chain (closed segment) in a general linear chain mechanism. Where, C_o starts with a contacting mass (m_k) and ends with an impacting mass (m_{imp}). Then, the solution of the multi-contact problem always exists and the contacting mass outcome is either a positive normal velocity or a positive normal impulse. The critical configurations are certain geometric configurations where the impulse of the impacting mass (m_{imp}) is not transmitted to the contacting mass (m_k). At the critical configuration both of the contacting mass outcomes $\hat{F}_{i,y_i}(\eta)$ and $V_{i,y_i}(\eta)$ are equal to zero. Critical configuration happens when:*

1. *For any $\theta_i - \theta_{i+1} = \pi/2$, where $k \leq i < imp$. In the other words, the*

angle between two connecting rods becomes $\pi/2$.

2. If $\sin(\theta_k - \phi_k) = 0$, where θ_k is the angle between the contacting mass m_k and the next mass m_{k+1} .

At the critical configurations, the contribution of the impact impulse to the normal contact quantities vanishes. Moreover, after the critical configuration the outcome of the contacting mass is changed. If the mass has a positive normal post impact velocity ($\alpha_i > 0$) before the critical configuration, then this will be changed to a positive normal impulse ($\beta_i > 0$) and vice versa is correct.

Proof. Figure 4.2 shows a section of n-link chain. The theorem can be proved by following the next steps:

1. The solution of the system always exists since the mass matrix M is always invertible. As a result, the solution of the problem depends on the contacting conditions.
2. Since the dot product of the vectors $\hat{\mathbf{F}}_y(\eta)$ and $\mathbf{V}_y(\eta)$ is always zero, then the outcome of any contacting mass can be either a positive normal impulse or positive normal velocity.
3. The linear momentum equation in the y-direction for the entire closed chain (see Fig. 4.2) can be written as:

$$\hat{F}_{1,y}(\eta) + \eta \cos(\phi_{\text{imp}}) = m_1 V_{1,y}(\eta) + \sum_{i=1}^{\text{imp}-1} m_{i+1} L \Delta \dot{\theta}_i \cos(\theta_i) \quad (4.17)$$

where, $\Delta \dot{\theta}_i = \dot{\theta}_i^+ - \dot{\theta}_i^-$. We can use the angular momentum equation to write $\Delta \dot{\theta}_i$. From the kinematic relationship, we can write the velocity of

each mass as a function of the velocities of the previous masses. Then, the velocity (v_{i+1}) of any mass (m_{i+1}) is given by:

$$v_{i+1} = \left(v_{i,x} - L \sin(\theta_i) \Delta\dot{\theta}_i \right) \hat{i} + \left(v_{i,y} + L \cos(\theta_i) \Delta\dot{\theta}_i \right) \hat{j} \quad (4.18)$$

where, \hat{i} , \hat{j} and \hat{k} are the unit vectors in x , y and z directions, respectively.

Then, we can write the angular momentum of the partitioned sub-chain in Fig. 4.2 about the mass m_{i+2} , where the first two terms are the angular momentum of the contribution impulses on mass m_i , the second two terms are the angular momentum of mass m_i and the third two terms are the angular momentum of mass m_{i+1} about mass m_{i+2} :

$$\begin{aligned} & \tilde{f}_{i,x}(\eta) L(\sin(\theta_i) + \sin(\theta_{i+1})) + \tilde{f}_{i,x} L(\cos(\theta_i) + \cos(\theta_{i+1})) + \\ & m_i L(v_{i,x}(\sin(\theta_i) + \sin(\theta_{i+1})) + v_{i,y}(\cos(\theta_i) + \cos(\theta_{i+1}))) + \\ & m_{i+1} L(v_{i,x} \sin(\theta_{i+1}) + v_{i,y} \cos(\theta_{i+1})) + \\ & m_{i+1} L^2 \Delta\dot{\theta}_i (\sin(\theta_i) \sin(\theta_{i+1}) + \cos(\theta_i) \cos(\theta_{i+1})) = 0 \end{aligned} \quad (4.19)$$

where, $\tilde{f}_i(\eta)$ is the internal impulse reaction at joint i . Using the following trigonometric identity:

$$\cos(a) \cos(b) + \sin(a) \sin(b) = \cos(a - b) \quad (4.20)$$

As we know the reaction impulses $(\tilde{f}_{i,x}, \tilde{f}_{i,y})$ are functions of the normal impulse at the impacting end (η), we can write $\Delta\dot{\theta}_i$ as

$$\begin{aligned}\Delta\dot{\theta}_i &= \frac{f(m_i, L, V_{1,y}(\eta), V_{1,x}(\eta), \eta)}{\sin(\theta_{i+1}) \sin(\theta_i) + \cos(\theta_{i+1}) \cos(\theta_i)} \\ &= \frac{f(m_i, L, V_{1,y}(\eta), V_{1,x}(\eta), \eta)}{\cos(\theta_{i+1} - \theta_i)}\end{aligned}\quad (4.21)$$

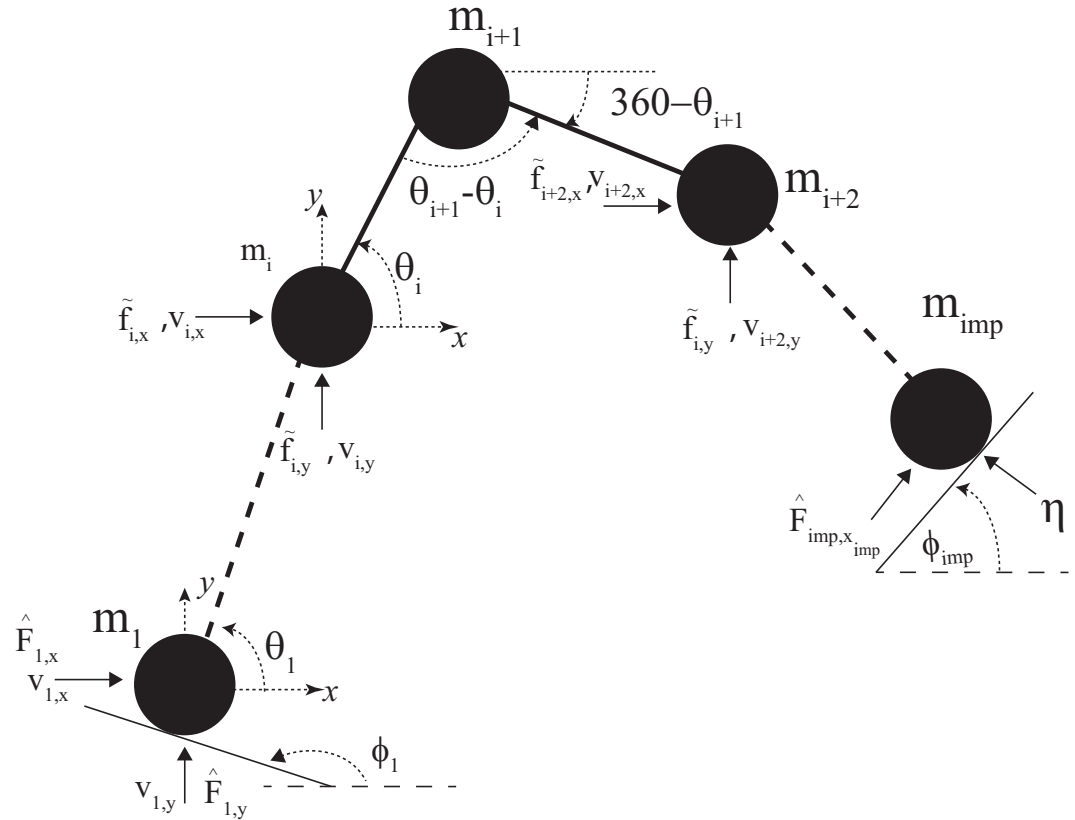


Figure 4.2: A Section of the Linear Chain

4. The tangential velocity ($V_{1,x}(\eta)$) of the contacting mass m_1 can be writ-

ten by taking the moment of the impulse $\hat{F}_1(\eta)$ and $m_1 V_{1,y}(\eta)$ about the next mass:

$$V_{1,x}(\eta) = \frac{f_1(m_1, \hat{F}_1(\eta), V_{1,y}(\eta))}{\sin(\theta_1 - \phi_1)} \quad (4.22)$$

By substituting Eqns. (4.21) and (4.22) into Eqn. (4.17), then the normal velocity and impulse of the contacting mass can be written as:

$$\begin{aligned} \alpha V_{1,y}(\eta) + \beta \hat{F}_{1,y}(\eta) = \\ \prod_{i=1}^{\text{imp}-1} \sin(\theta_1 - \phi_1) \cos(\theta_{i+1} - \theta_i) f_2(m_i, \phi_1, \phi_{\text{imp}}, L) \eta \end{aligned} \quad (4.23)$$

where, α and $\beta > 0$. Since the chain gets closed at impact points, we assume that $\theta_{\text{imp}} = \theta_{\text{imp}-1}$. At the critical configuration, the right hand side of Eqn. (4.23) equals to zero, then we can rewrite Eqn. (4.23) as:

$$\alpha V_{1,y}(\eta) + \beta \hat{F}_{1,y}(\eta) = 0 \quad (4.24)$$

Then,

$$\alpha V_{1,y}(\eta) = -\beta \hat{F}_{1,y}(\eta) \quad (4.25)$$

The only solution for Eqn. (4.25) is $V_{1,y}(\eta) = \hat{F}_{1,y}(\eta) = 0$. Otherwise, they will have different signs, and this conflicts Eqn. (4.14). As a result, at the critical configuration both of $V_{1,y}(\eta)$ and $\hat{F}_{1,y}(\eta)$ are equal to zero.

□

The theorem shows the critical configurations of a linear chain system

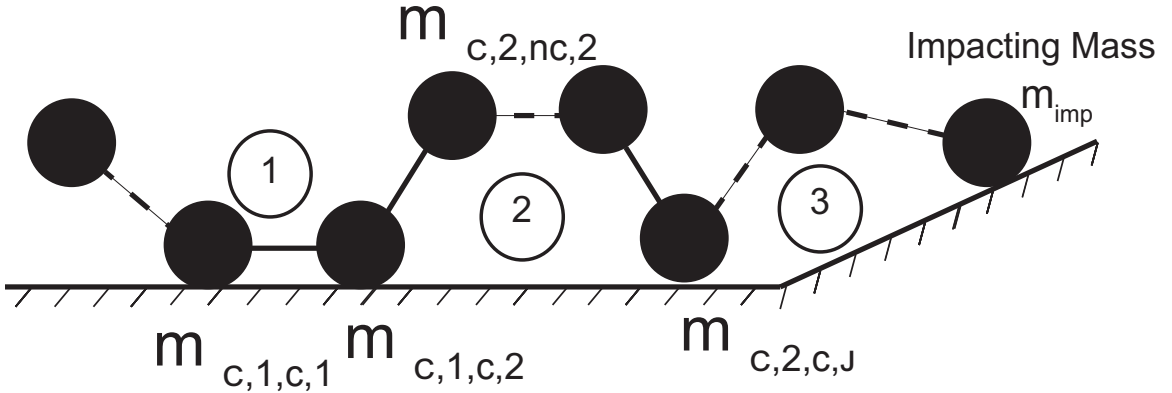


Figure 4.3: General Chain Mechanism

when there are one contacting and one impacting masses. In a general linear chain, the chain may have one or more closed segments with more than one contacting mass. We assume that the impact takes place only at one mass. Consequently, we can apply the theorem at each linear branch in the general linear chain to predict the critical configurations associated with that chain. Figure 4.3 shows a chain with more than one closed segment. Firstly, we start by applying theorem 4.1 for the linear branch that associated with the impacting mass. Based on the notations in theorem 4.1, the sub-chain in Fig. 4.3 is $C_o = \textcircled{3}$. Also, m_k in theorem 4.1 is $m_{c,2,j}$ in Fig. 4.3. We call the critical configuration associated with the linear branch $\textcircled{3}$ the impacting critical configuration. At this point, the impulse at the contacting mass m_k is zero. Moreover, at the impacting critical configuration, the impacting impulse will not be transmitted through the contacting mass m_k to the other contacting mass. If the subchain $\textcircled{3}$ is not at the critical configuration, then the impact impulse may be transmitted through the mass m_k to the other contacting in the chain. In this case, we apply the same theory to the subchain $\textcircled{2}$, and $\textcircled{1}$.

Theorem 4.1 can be extended from a linear chain to a general chain where the chain may have more than two branches at each mass. The general chain can be divided into sub-linear chains (branches), and the critical configuration can be defined for each linear branch. The same procedure, which is used to extend theorem 4.1 to multi-contact case, can be used to extend the theorem for a general chain with multi-contact masses. Theorem 4.2 generalizes theorem 4.1 to a general chain.

Theorem 4.2. *Each contacting mass in a general chain may have one or more critical configurations. At these points, the contacting mass has zero normal impulse and zero normal velocity. These critical configurations can be found by dividing the general chain into linear branches and applying theorem 4.1. Thus, we can find the critical configurations between the impacting mass and any contacting mass in the chain.*

Proof. Theorem 4.1 can be applied for a general chain by using the same procedure that we developed for the multi-contact case in a linear chain. We can apply theorem 4.1 for any linear branch in the main chain. We start with the linear branch that is associated with the impacting mass, branch ① in Fig. 4.4. At the critical configuration of that branch, the impact impulse will not be transferred to any point beyond mass $(m_{c,imp,nc,j})$. We call this critical configuration, the critical impacting point. If we have a positive impulse \tilde{F}_k at mass $(m_{c,imp,nc,j})$ in ①, then we can find the critical configuration for the new linear branch ②. Similarly, we apply theorem 4.1 at the branch ② and we can get the critical configuration for the contacting mass $(m_{c,k,c,1})$. The critical configurations from the impacting point to the critical configuration of

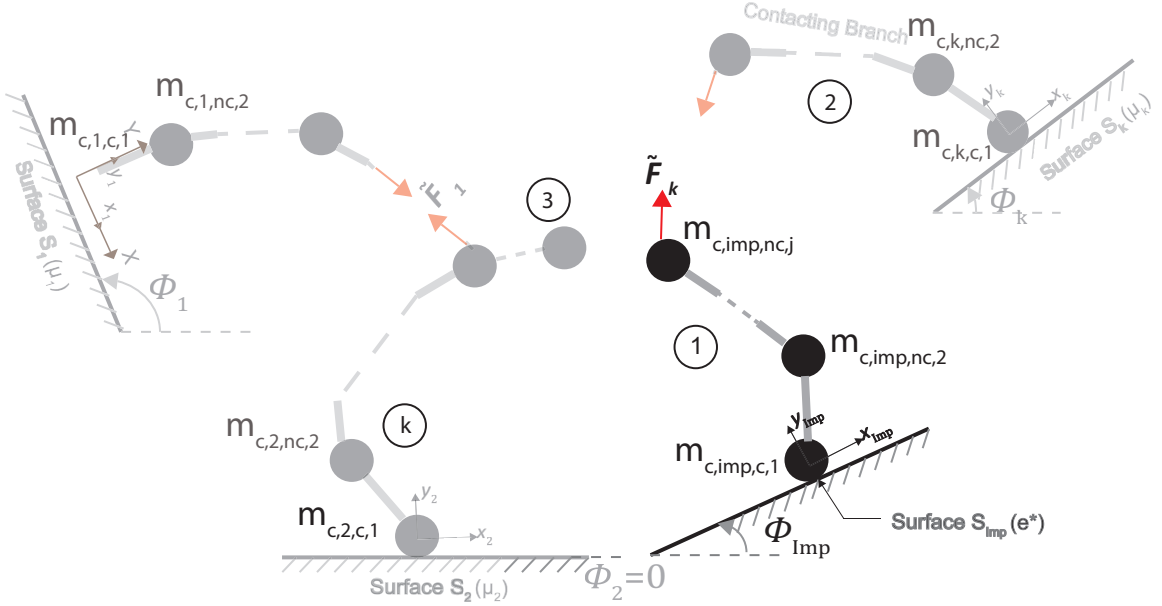


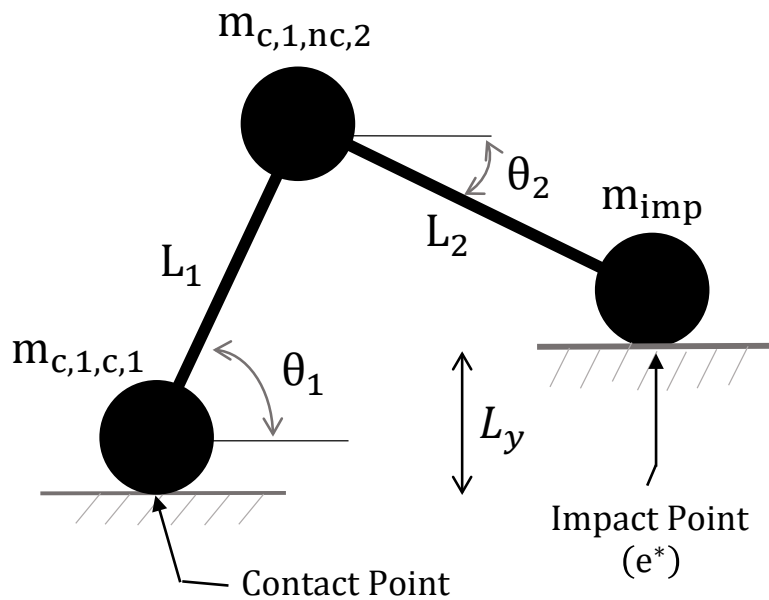
Figure 4.4: General Chain Mechanism with multiple contacting points

branch (2) are the critical configurations of the contacting mass ($m_{c,k,c,1}$). If we have any of them then the impulse of the impacting will have no contribution to the contacting mass ($m_{c,k,c,1}$). The same procedure can be performed to get the critical configurations of the other contacting mass in the chain. \square

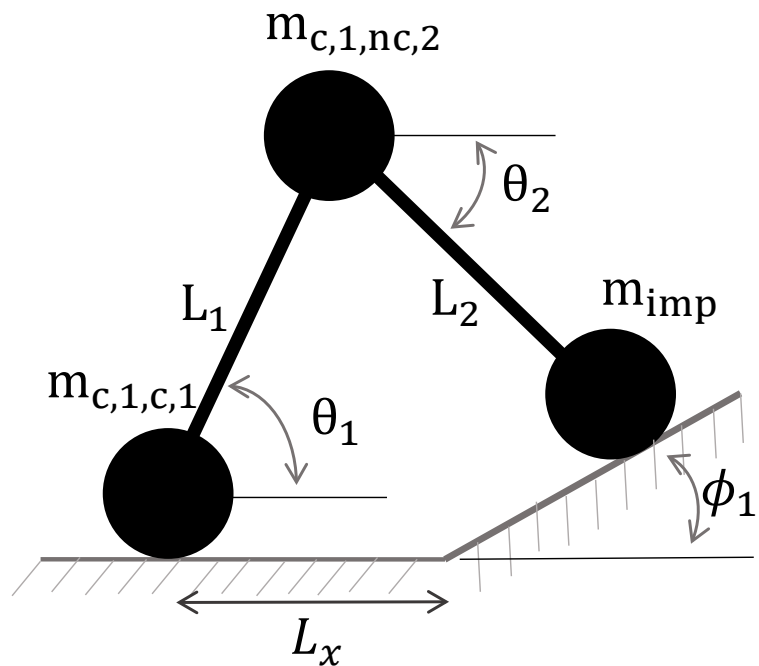
4.4.1. Three-Mass system

The three-mass system is a simplified model of several engineering and robotics systems. The biped robot is a well known example of the three-mass system. In this section, we use the angular and linear momentum principles to depict the critical configuration of the three mass system. In this section, we discuss the impact of the three-mass system with an external surface. First we

start with a flat surface, then we discuss the problem with different external surfaces. Figure 4.5 shows the general case of the three-mass impact with an inclined external surface.



(a) Parallel Level Surfaces.



(b) Inclined Surface.

Figure 4.5: The Three-Masses Chain.

4.4.1.1. Three-Mass System with a Single Flat Surface

The goal of this analysis is to find the critical configuration $\Delta\theta_c$. We can find the critical configuration by solving the linear and angular momentum equations to find the normal contacting impulse as a function of the impacting impulse. The geometric constraint $\theta_2 = -\theta_1$ is used since this is the condition when the impact takes place. In this condition, L_y equals to zero in Fig. 4.5a. The relation between the normal velocity and normal impulse of the contacting mass is:

$$\begin{aligned} \alpha V_{1,y_1}(\eta) + \beta \hat{F}_{1,y_1}(\eta) &= \sin^2(\theta_1) \cos(\theta_1 - \theta_2) f_3(L, m_1, m_2, m_3)\eta \\ &= \sin^2(\theta_1) \cos(2\theta_1) f_3(L, m_1, m_2, m_3)\eta \end{aligned} \quad (4.26)$$

Thus, two kinematic configurations lead to zero normal velocity of the contacting mass :

1. $\theta_1 = 0$ this indicates that $\theta_2 = 0$.
2. $\theta_1 = 45^\circ$ and thus $\theta_2 = -45^\circ$, or in another words $\Delta\theta_c = \theta_1 - \theta_2 = 90^\circ$.

4.4.1.2. Three-Mass System with two Parallel Level Surfaces

When impact takes place and the impacting mass m_3 and the contacting mass m_1 are at different levels, then the geometric constraint of the three-mass system is:

$$\theta_2 = \sin^{-1} \left(\frac{L_1 \sin(\theta_1) - L_y}{L_2} \right) \quad (4.27)$$

where, L_y is the elevation difference between two parallel surfaces shown in Fig. 4.5a.

Thus, we solve the set of the linear and angular momentum equations with the kinematic constraint in Eqn. (4.27) . Given these, the normal velocity of the contacting mass is:

$$\alpha V_{1,y_1}(\eta) + \beta \hat{F}_{1,y_1}(\eta) = f_4(m_1, m_2, m_3, L, L_y) \sin^2(\theta_1) \times \cos\left(\sin^{-1}\left(\sin(\theta_1) - \frac{L_y}{L}\right) - \theta_1\right) \eta \quad (4.28)$$

Generally, the critical configurations arises when the difference between θ_1 and θ_2 ($\Delta\theta_c$) is 90° , or when θ_1 is 0° .

4.4.1.3. Three-Mass System with an Inclined Surface

Figure 4.5b shows the inclined surface case of the impact for the three-mass system. We use the same procedure that we developed in the previous sections with a condition that:

$$\sum_{i=1}^2 L_i \sin(\theta_i) = \tan(\phi_1) \left(\sum_{i=1}^2 L_i \cos(\theta_i) - L_x \right) \quad (4.29)$$

where, L_x is the length from contact mass to the end of the flat surface. Solving the momentum equations with the constraint in Eqn. (4.29) shows coefficient of the impacting impulse always equals to zero when:

1. θ_1 is 0°
2. The difference between the two angles equals to 90° ($\Delta\theta_c = \theta_1 - \theta_2 = 90^\circ$).

In summary, the analytical results agree with theorem 4.1. The contribution of the impacting impulse to the contacting outcome is vanished at the critical configuration.

4.4.2. Five-Mass System

In this section, we consider the five-mass linear closed kinematic chain system on an inclined surface. The complexity of the problem becomes more fundamental as we have one impacting, one contacting, and 3 non-contacting masses. The objective is to theoretically show that for the five-mass system, we can have multiple critical configuration as we have more masses in the chain. Figure 4.6 depicts the five-mass chain on an inclined surface.

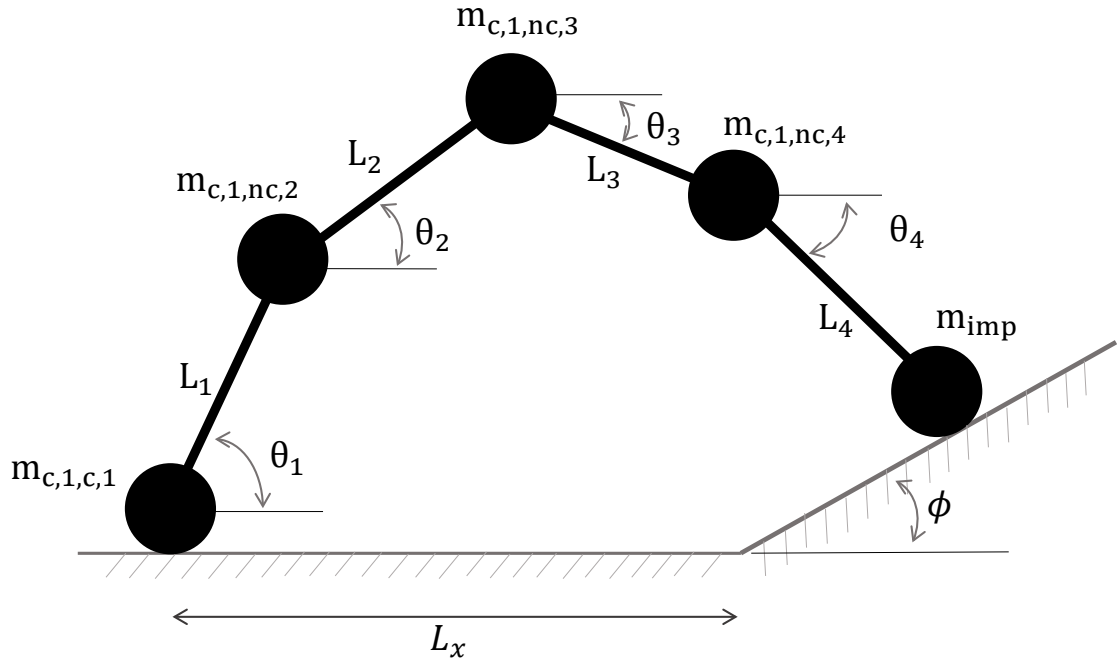


Figure 4.6: The Five-Mass Chain

The geometric constraint equation of the five-mass system is as follow:

$$\sum_{i=1}^4 L_i \sin(\theta_i) = \tan(\phi) \left(\sum_{i=1}^4 L_i \cos(\theta_i) - L_x \right) \quad (4.30)$$

Based on the system configuration in Fig. 4.6 and by using Eqn. (4.23), we have the following:

$$\begin{aligned} \alpha V_{1,y_1}(\eta) + \beta \hat{F}_{1,y_1}(\eta) &= \sin^4(\theta_1) \cos(\theta_2 - \theta_1) \cos(\theta_3 - \theta_2) \cos(\theta_4 - \theta_3) \\ f_5(L, m_1, m_2, m_3, m_4, m_5, \phi)\eta \end{aligned} \quad (4.31)$$

From Eqn. (4.31) the possible critical configurations are enumerated below:

1. θ_1 is 0°
2. The difference between the angles θ_1 , and θ_2 is equal to 90° ($\Delta\theta_{c1} = \theta_1 - \theta_2 = 90^\circ$).
3. The difference between the angles θ_2 , and θ_3 is equal to 90° ($\Delta\theta_{c2} = \theta_2 - \theta_3 = 90^\circ$).
4. The difference between the angles θ_3 , and θ_4 is equal to 90° ($\Delta\theta_{c3} = \theta_3 - \theta_4 = 90^\circ$).

In general, three possible scenarios for the critical configuration can exist. We conclude that at least one of the three conditions has to occur to satisfy the critical configuration solution. However, multiple conditions can happen at the same time as well.

4.5. Experimental Set-up

We design an experimental setup to verify the theoretical outcomes obtained previously in the chapter. Figure 4.7 depicts a photograph of the experimental setup. We built a three-mass kinematic chain with two connecting rods of equal lengths. The three masses are the contacting, impacting, and connecting joint masses, respectively. The connecting mass is designed such that it forms a revolute joint connection. In addition, every rod moves independently from one another and we assume that friction is negligible. The joint is boxed in a metal housing with known dimensions. The top of the metallic housing contains four parallel, adjacent, and equally spaces holes. Four metallic hooks are installed into each of the four holes to provide proper suspension of the chain. The frame design includes a horizontal variable bar with two adjustable rails. For every pair of parallel hooks a string is suspended and passed from one end of one of the upper rails through the parallel hooks, then suspended at the other end of the upper rail. The same scheme is applied to the other upper rail, and the two parallel hooks. The suspension mechanism provides useful means of accomplishing successful planar collision and to minimize wobbling during the experiments. The release mechanism of the impacting mass consist of an electro-magnet with a closing switch to provide consistent drops throughout the experiments.

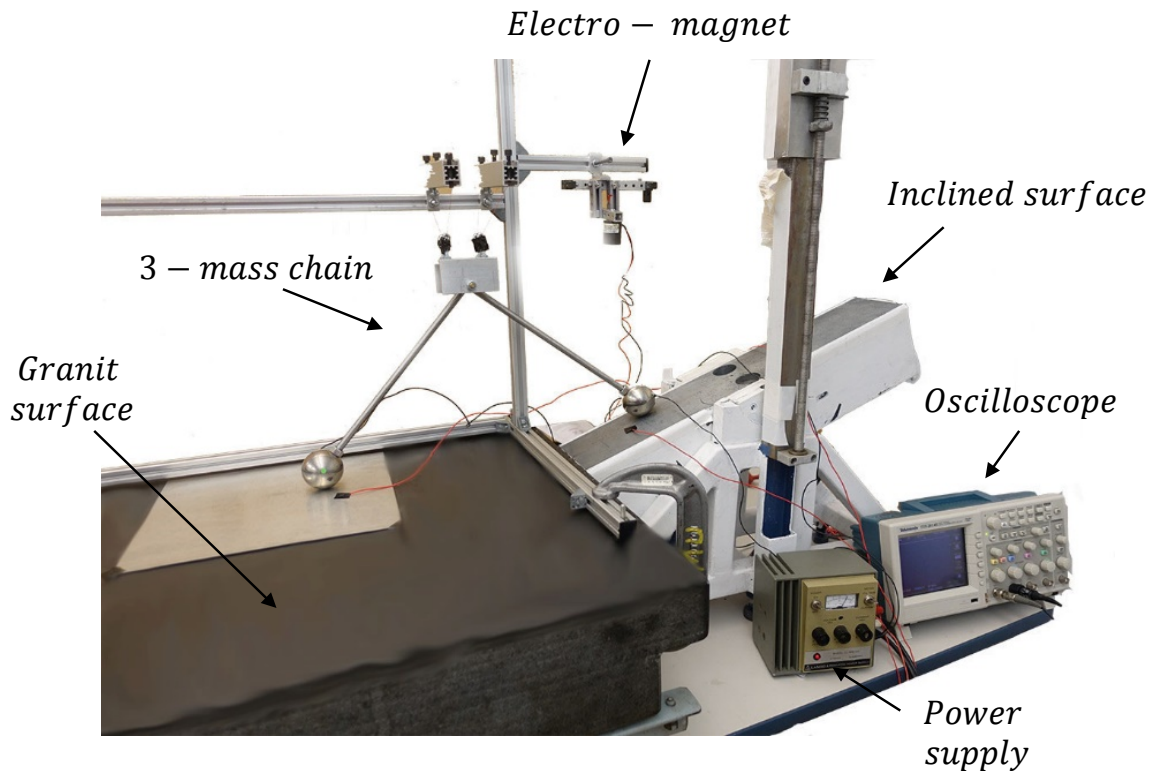


Figure 4.7: Experimental Setup

The detection of the detachment and non-detachment from the surface of contact is accomplished by designing two separate electrical circuits. One for the contacting and another for the impacting mass. We use an oscilloscope, power source, and signal cables to acquire and record the electrical signals. Furthermore, when a mass is in contact with the respecting surface the circuit is closed. Otherwise, when the contact is severed, the circuit will be open. Consequently, separation event of either mass will be observed as a sudden voltage drop.

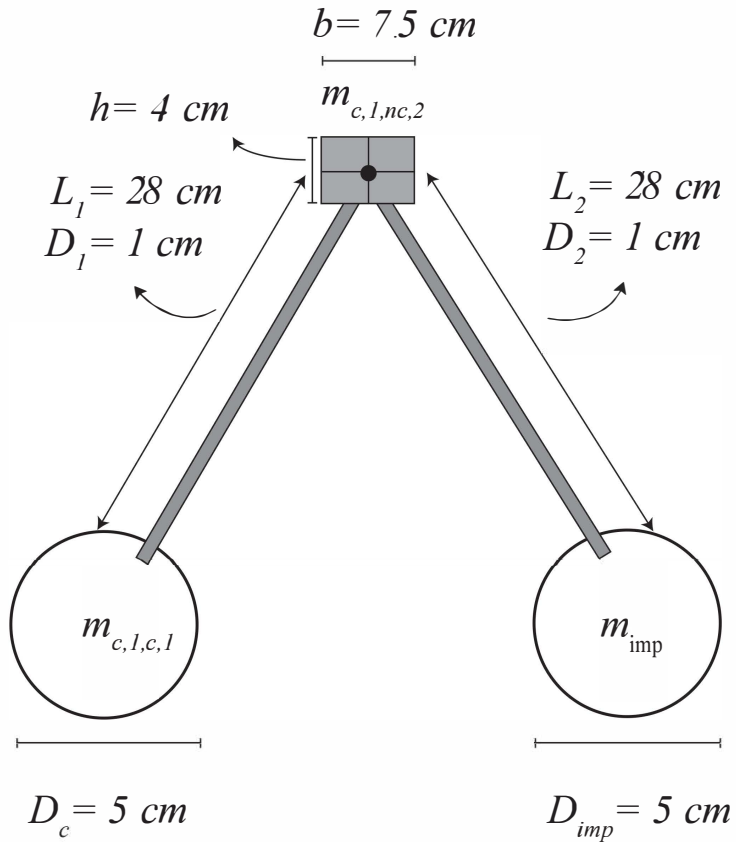


Figure 4.8: Geometric properties of the three mass chain

Figure 4.8 depicts the geometric properties of the three mass kinematic chain. The contacting and impacting masses have a diameter of 5 cm and mass of 544 grams . Each rod has a length of 28 cm from the pin joint to the outer surface of the contact and impact masses. The diameter of each rod is 1 cm . The contact and impact masses are drilled and tapped for connection with the rods. The housing box of the non contacting mass is designed with a length of 7.5 cm , and the height and width are 4 cm each.

4.6. Experimental Verification

In this section, we present the outcomes of the experimental study. The first set of collision experiments considers impacts on a flat surface where the contacting, and impacting masses lie on a single flat surface. The second set consists of collision experiments on a plane with a variable inclination angle. For the collision experiments on an inclined plane, the contacting mass lies on the flat surface, while the impacting mass strikes the inclined plane. We experimentally show the detachment of the contact mass from the surface of contact for different drop angles. For the first set of the collision experiments on a flat surface, Figure 4.9 depicts the theoretical, and experimental prediction of the detachment/non-detachment of the contact mass for all $\Delta\theta$. The theoretical and experimental critical configurations are $\Delta\theta_c^t$ and $\Delta\theta_c^e$ respectively (see Fig. 4.9).

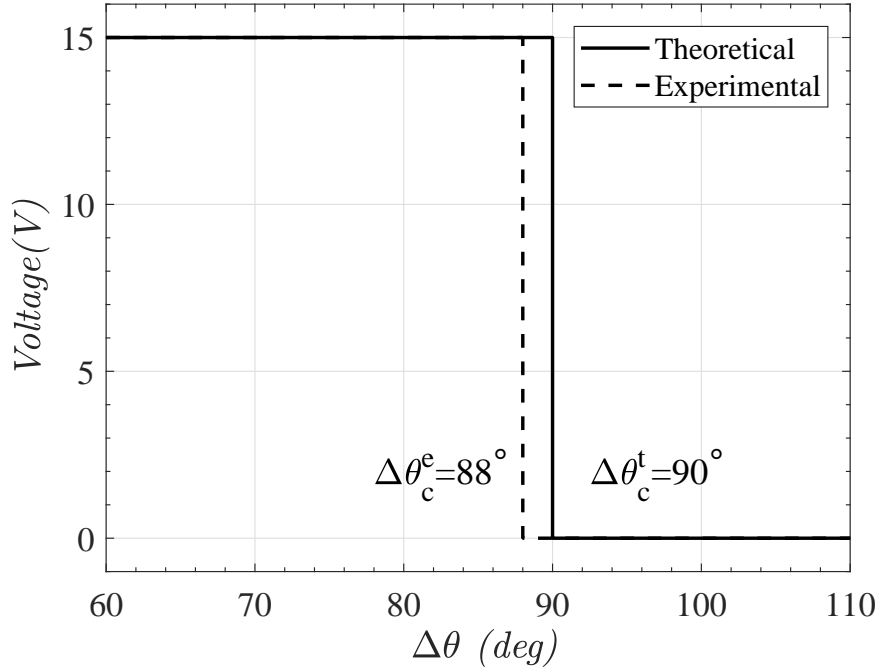


Figure 4.9: Flat surface experimental and theoretical prediction of the detachment of the contact mass

The theoretical prediction for the flat surface collisions shows that the critical configuration, which separates the detachment from non-detachment regions is at $\Delta\theta_c^t = 90^\circ$. For the collision experiments with different drop angles it can be shown that the critical configuration is reached approximately at $\Delta\theta_c^e = 88^\circ$, where the difference from the theoretical prediction is equal to 2° . The detachment of the contact mass is experimentally verified by the electrical circuit such that prior to impact the circuit is closed. When the contact mass detaches from the contact surface the electrical circuit opens, and voltage suddenly drops. This provides means to properly and accurately detect the detachment of the contact mass for all $\Delta\theta$.

Figure 4.10 depicts two cases of the flat surface collision experiments. Fig-

ure 4.10a shows the detachment case for the 70° drop angle. One can see the detachment of the contact mass as the voltage drops at the end of the collision event. On the other hand, when the critical configuration is reached, the contact mass doesn't rebound from the surface (see Fig. 4.10b).

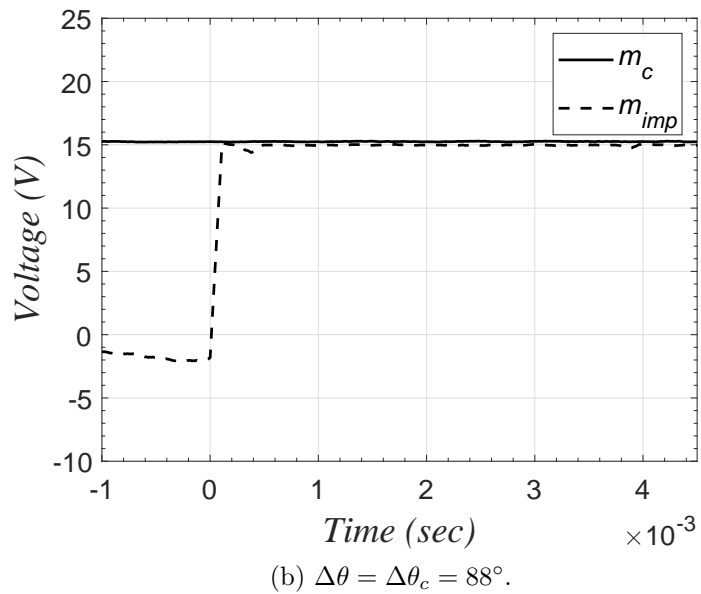
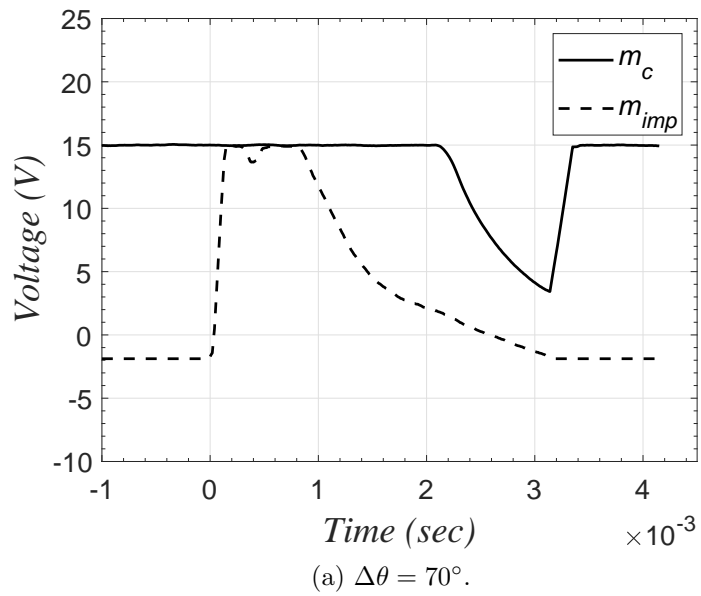


Figure 4.10: Flat surface experimental readout for detachment of the contact mass.

Similarly, for the second set of collision experiments on an inclined surface, Fig. 4.11 depicts the detachment of the contact mass for all $\Delta\theta$.

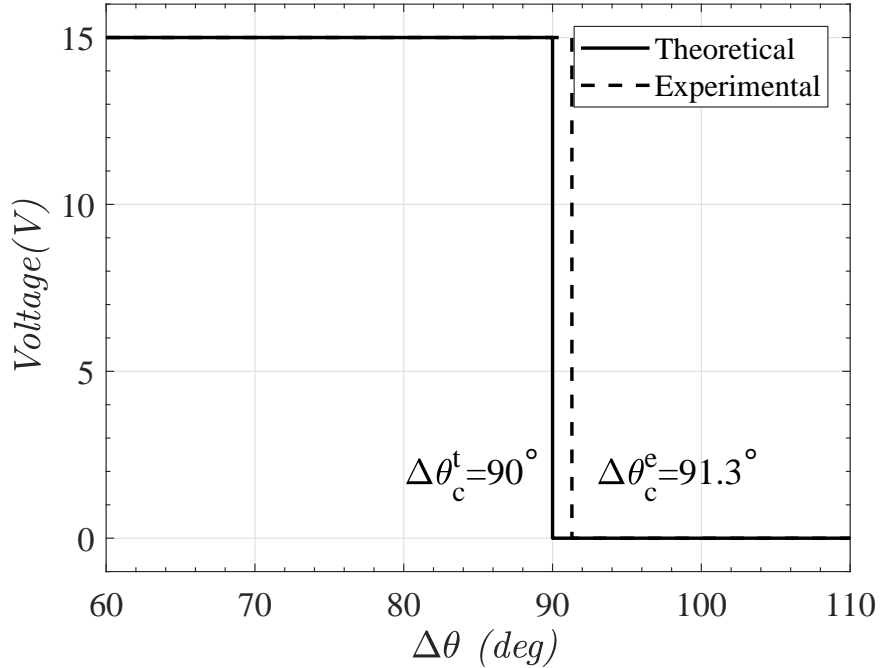
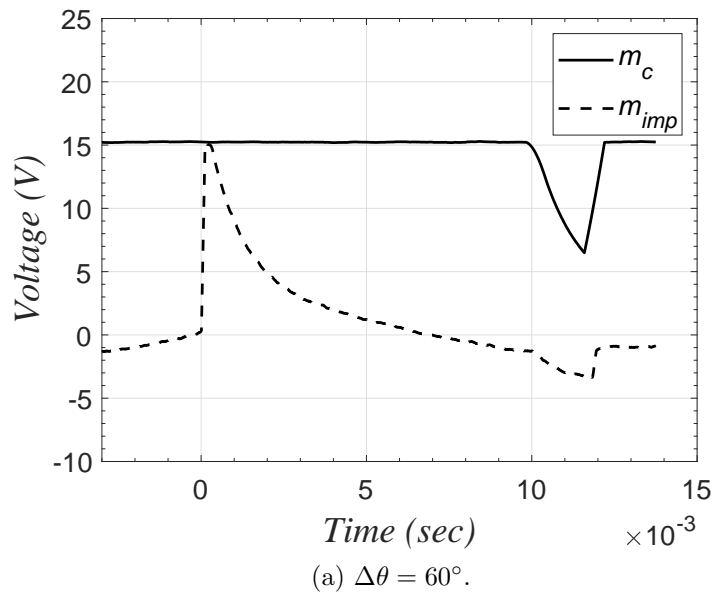


Figure 4.11: Inclined surface experimental and theoretical prediction for the detachment and non-detachment of the contact mass

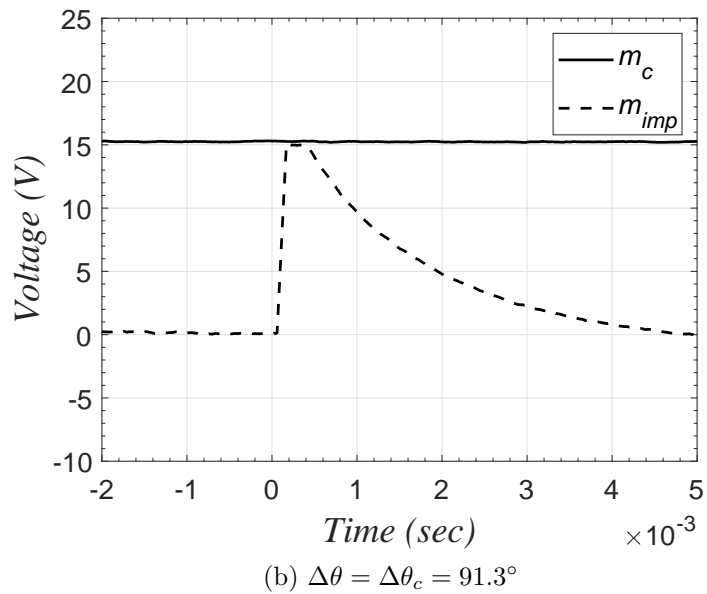
For the collisions on an inclined wall the theoretical prediction shows that the critical configuration is reached when $\Delta\theta_c^t = 90^\circ$. After performing the collision experiments on the inclined surface it was shown that the critical configuration is reached when $\Delta\theta_c^e = 91.3^\circ$, a deviation of 1.3° from the theoretical prediction. For the collision sets on the inclined wall we can observe the regions separating the detachment, and non-detachment of the contact mass at the 90° (see Fig. 4.11).

Figure 4.12 depicts the experimental readout of the oscilloscope for the detachment of the contact mass from the flat surface. Figure 4.12a shows the detachment case for 60° angle. After the collision event is over the contact mass

detaches from the surface and voltage drops. Figure 4.12b, however, depicts the case of 91.3° . By observation, one can see that the contact mass doesn't rebound from the surface, which satisfies the critical configuration condition.



(a) $\Delta\theta = 60^\circ$.



(b) $\Delta\theta = \Delta\theta_c = 91.3^\circ$

Figure 4.12: Inclined surface experimental readout for detachment of the contact mass for 25° inclination angle

Five additional inclination angles are experimentally studied including: 5° , 10° , 15° , 20° , and 25° . The objective is to experientially show that varying the

inclination angle has no effect on the critical configuration. Figure 4.13 depicts the experimental critical configuration compared to the theoretical one. We note that zero inclination angle corresponds to the impact on a flat surface. In addition, for all collision experiments on both flat and inclined surfaces, the mean value and the standard deviation of the critical configuration are 91.3° and 1.705° respectively.

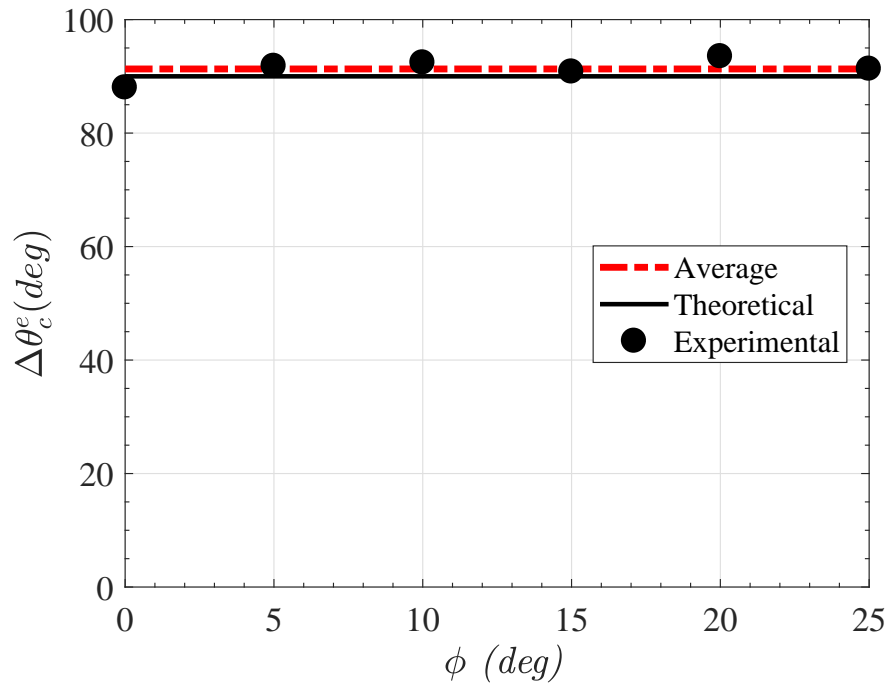


Figure 4.13: Variation of experimental $\Delta\theta_c^e$ with the inclination angles

Chapter 5

Conclusions

In this dissertation, we presented solution methods for solving the two and multibody impact problems. In addition, we solved the rigid body collision problem of planar kinematic chains with multiple contacts with external surfaces. In the first chapter of the dissertation, we presented a literature review on the topics presented in the dissertation.

In chapter two, we developed a method to calculate the COR for the B-C collisions. We conducted a set of experiments for the B-B and B-C collisions and obtained the corresponding experimental kinematic COR. We used three different materials including: steel, wood, and rubber. We discovered unexpected variations between the experimentally measured B-B and B-C CORs of the same collision pairs. This also showed that the COR was not necessarily related only to the local compliance. We proposed a discretization method to investigate the variation between the B-B and B-C CORs. We used three models to calculate the B-C COR based on the local B-B COR. These models are: rigid body, bimodal linear, and bimodal Hertz.

Furthermore, for each material and configuration, we ran stiffness analysis tests and obtained the corresponding experimental stiffness values. Based on the experimental data, we categorized the collision pairs into three categories: identical material, Hard-Soft, and Soft-Hard. Here, the concept of hardness is strictly related to the stiffness of the colliding body. Based on the simulation

results, we found that the bimodal Hertz model produced the most accurate outcomes. Then, we investigated the effect of the number of segments on the B-C COR for each category. For identical materials, when we simultaneously increased the number of segments of the balls and the cylinders, the percentage error between the experimental and theoretical B-C CORs decreased. Recalling that the ball is the softer member, increasing the number of segments of the ball does leads to better error outcomes. Meanwhile, for a Hard-Soft pair, increasing the number of segments of the softer member (cylinder) again caused the percentage error to drop. Increasing the segmentation of the ball, however, did not have an effect on the experimental errors. For Soft-Hard pair, increasing the number of segments of the ball decreased the percentage error, but increasing the number of segments of the cylinder did not have an effect. Based on these results, we concluded that in all cases, increasing the number of segments of the softer material leads to smaller experimental errors.

In addition, we conducted numerical simulations for all collision pairs. The number of segments j_S was varied between 1 to 50 and j_H was varied from 1 to 10. For each iteration of j_H , we calculated the average percentage error (APE) of all six combinations in each category. Subsequently, the minimum average percentage error (APE_m) of the B-C COR for each category was found. Then, we fixed j_H that corresponded to APE_m . Finally, we obtained a relationship between the stiffness ratio and the number of segments of the softer material. Then, a curve fit equation for this relationship was found. This relationship was used to identify the minimum number of segments needed to achieve APE_m for a particular B-C collision. We conducted two additional sets of collision experiments to validate the obtained relationship and the proposed

method. The percentage error between the theoretical and experimental B-C COR for the two addition sets of experiments were 0.24% and 4.2%.

In chapter three, we developed a method to calculate the post-impact velocities of balls and cylinders connected in a chain. We conducted sets of B-B experiments and obtained their kinematic COR. In addition, we conducted the collision experiments for three, four, and five-body chains and obtained their pre- and post-impact velocities. We used three main types of materials including: steel, wood, and rubber. We proposed a discretization method that can be used to accurately calculate the post-impact velocities of each of the colliding bodies. We used the bimodal Hertz contact force model and employed the B-B COR between the contacting pairs to compute the post-impact outcomes of the colliding bodies in the chain.

In addition, we conducted stiffness analysis tests and obtained the corresponding experimental stiffness values for each material and configuration. Based on our previous work of B-C collisions, we discovered a relationship, which related the stiffness ratio and the number of segments of the softer material. In addition, this relationship allowed us to determine the number of segments required to estimate the B-C COR for a given collision pair. In the present work, we used this relationship to determine the required number of segments of the softer material for any ball and cylinder connected in a given chain. The segmentation procedure allowed the best post-impact velocity outcomes. We applied the segmentation procedure on three, four, and five-body chains.

For the three-body chain of B-B-C, we performed the numerical simulation runs and the average *APE* of all collision combinations was approximately

3.4%. For B-C-B, however, the average *APE* of all collision pairs was about 3.5%. For the four-body chain of B-C-B-C, we performed the numerical simulation runs for all collisions and the overall average *APE* was approximately 4.81%. Finally, for the five-body chain, we used different combinations of the balls and cylinders arrangements. The average *APE* of the five-body chain was 6.17%.

In chapter four, we considered the rigid body collision of a general planar kinematic chain with external surfaces. The linear and angular momentum principles with a set of complementary equations were used to study the problem. In this type of problem, one mass of the chain, called the *impacting mass*, strikes an external surface. Meanwhile, k other *contacting masses* of the chain are in unilateral contact with other arbitrary external surfaces. The collision causes each contacting masses either to interact with or bounce off their respective surfaces. First, we showed that the conditions which define detachment of interaction are well-defined and produce unique solutions, In addition, for each contacting mass, there are specific chain configurations, called critical configurations, where the two conditions are simultaneously true.

We applied the proposed methods to obtain critical configurations of two numerical examples: a three- and a five-mass chains. Finally, we experimentally verified the existence of critical configurations for a three-mass chain on flat and inclined surfaces with different inclination angles.

BIBLIOGRAPHY

- [1] Y. Hurmuzlu and D. B. Marghitu, “Rigid body collisions of planar kinematic chains with multiple contact points,” *The International Journal of Robotics Research*, vol. 13, no. 1, pp. 82–92, 1994.
- [2] R. W. F. and S. L. D., *Engineering Mechanics Dynamics*. New York: John Wiley and Sons, 1996.
- [3] M. T. Wang, Yu and Mason, “Two-dimensional rigid-body collisions with friction,” *Journal of Applied Mechanics*, vol. 59, no. 3, pp. 635–642, 1992.
- [4] W. Stronge, “Unraveling paradoxical theories for rigid body collisions,” *Journal of Applied Mechanics*, vol. 58, no. 4, pp. 1049–1055, 1991.
- [5] G. Werner, *Impact : The Theory and Physical Behaviour of Colliding Solids*. Mineola: Dover Publication, 2001.
- [6] H. M. Lankarani and P. E. Nikravesh, “A Contact Force Model With Hysteresis Damping for Impact Analysis of Multibody Systems,” *Journal of Mechanical Design*, vol. 112, no. 3, p. 369, 1990.
- [7] J. B. Keller, “Impact with friction.” *Trans. Asme J. Appl. Mech.*, vol. 53, no. 1 , Mar. 1986, pp. 1–4, 1986.
- [8] G. Gilardi and I. Sharf, “Literature survey of contact dynamics modelling,” *Mechanism and Machine Theory*, vol. 37, no. 10, pp. 1213–1239, 2002.
- [9] P. Barkan, *Impact Design. Mechanical Design and Systems Handbook*. New York: McGraw-Hill, 1974, vol. 31.
- [10] H. M. Lankarani, “Canonical equations of motion and estimation of parameters in the analysis of impact problems,” *Ph. D. Thesis, University of Arizona, Ann Arbor, AZ*, 1988.

- [11] J. Wittenburg, *Dynamics of systems of rigid bodies*. Springer-Verlag, 2013.
- [12] H. M. Lankarani and P. E. Nikravesh, “Continuous contact force models for impact analysis in multibody systems,” *Nonlinear Dynamics*, vol. 5, no. 2, pp. 193–207, 1994.
- [13] S.-W. Kim, “Contact dynamics and force control of flexible multi-body systems,” *Ph. D. Thesis, McGill University, Montreal, Canada*, no. August, 1999.
- [14] N. Isaac, *Philosophiae naturalis principia mathematica*. G. Brookman, 1833.
- [15] W. Edmund, *A treatise on the analytical dynamics of particles and rigid bodies : with an introduction to the problem of three bodies*, 4th ed. New York: Dover Publication, 1944.
- [16] R. M. Brach, *Mechanical impact dynamics : rigid body collisions*. New York: J. Wiley, 1991.
- [17] R. Brach, “Formulation of rigid body impact problems using generalized coefficients,” *International Journal of Engineering Science*, vol. 36, no. 1, pp. 61–71, 1998.
- [18] H. Palas, W. Hsu, and A. Shabana, “On the Use of Momentum Balance and the Assumed Modes Method in Transverse Impact Problems,” *Journal of vibration and acoustics*, vol. 114, no. 3, pp. 364–373, 1992.
- [19] K. Hwang and A. Shabana, “Effect of mass capture on the propagation of transverse waves in rotating beams,” *Journal of Sound and Vibration*, vol. 186, no. 3, pp. 495–525, 1995.
- [20] C. E. Smith, “a Continuous Force Model for the Impact,” vol. 58, no. September 1991, pp. 754–758, 2014.
- [21] D. A. Kane, Thomas R and Levinson, *Dynamics, theory and applications*. McGraw Hill, 1985.
- [22] D. T. Greenwood, *Principles of dynamics*. Prentice-Hall Englewood Cliffs, NJ, 1988.

- [23] R. A. Wehage, E. J. Haug, and R. R. Beck, “Generalized coordinate partitioning in dynamic analysis of mechanical systems,” Iowa university college of engineering, Tech. Rep., 1981.
- [24] V. Ceanga and Y. Hurmuzlu, “A New Look at an Old Problem: Newton’s Cradle,” *Journal of Applied Mechanics*, vol. 68, no. 4, p. 575, 2001.
- [25] F. P. Beer, E. R. Johnston Jr, D. F. Mazurek, P. J. Cornwell, E. R. Eisenberg, and S. Sanghi, *Vector mechanics for engineers*. Tata McGraw-Hill Education, 1972.
- [26] G. Dietl, P and Wensing, J and Van Nijen, “Rolling bearing damping for dynamic analysis of multi-body systems—experimental and theoretical results,” *Proceedings of the Institution of Mechanical Engineers, Part K: Journal of Multi-body Dynamics*, vol. 214, 2000.
- [27] P. Pereira, M Seabra and Nikravesh, “Impact dynamics of multibody systems with frictional contact using joint coordinates and canonical equations of motion,” *Nonlinear Dynamics*, vol. 9, no. 1-2, pp. 53–71, 1996.
- [28] O. Ma, “Contact dynamics modelling for the simulation of the Space Station manipulators handling payloads,” *Proceedings of 1995 IEEE International Conference on Robotics and Automation*, vol. 2, pp. 1252–1258.
- [29] Y. T. Wang and R. V. Kumar, “Analysis and simulation of mechanical systems with multiple frictional contacts,” University of Pennsylvania Department of Computer and Information Sciences, Tech. Rep. June, 1991.
- [30] M. T. Mason and Y. Wang, “On the inconsistency of rigid-body frictional planar mechanics,” *Proceedings. 1988 IEEE International Conference on Robotics and Automation*, pp. 524–528, 1987.
- [31] W. Howard and V. Kumar, “A minimum principle for the dynamic analysis of systems with frictional contacts,” *Proceedings IEEE International Conference on Robotics and Automation*, pp. 437–442, 1993.
- [32] D. Atanackovic, TM and Spasic, “On viscoelastic compliant contact-impact models,” *Journal of applied mechanics*, vol. 71, no. 1, pp. 134–138, 2004.

- [33] H. Hertz, *Miscellaneous papers, translated from first German edition (1895) by DE Jones and JA Schott.* London: London: MacMillan, 1896.
- [34] F. Dubowsky, S and Freudenstein, “Dynamic analysis of mechanical systems with clearances—part 1: formation of dynamic model,” *Journal of Engineering for industry*, vol. 93, no. 1, pp. 305—309, 1971.
- [35] V. Kraus, Peter R and Kumar, “Compliant contact models for rigid body collisions,” in *Robotics and Automation, 1997. Proceedings., 1997 IEEE International Conference on*, 1997, pp. 1382—1387.
- [36] M. K. Vukobratović and V. Potkonjak, “Dynamics of contact tasks in robotics. Part I: General model of robot interacting with environment,” *Mechanism and Machine Theory*, vol. 34, no. 6, pp. 923–942, 1999.
- [37] K. Mirza, M. D. Hanes, and D. E. Orin, “Dynamic simulation of enveloping power grasps,” *Robotics and Automation, 1993. Proceedings., 1993 IEEE International Conference on*, pp. 430—435, 1993.
- [38] J. Alves, N. Peixinho, M. T. Da Silva, P. Flores, and H. M. Lankarani, “A comparative study of the viscoelastic constitutive models for frictionless contact interfaces in solids,” *Mechanism and Machine Theory*, vol. 85, pp. 172–188, 2015.
- [39] M. Machado, P. Moreira, P. Flores, and H. M. Lankarani, “Compliant contact force models in multibody dynamics: evolution of the Hertz contact theory,” vol. 53, pp. 99–121, 2012.
- [40] K. H. Hunt and F. R. E. Crossley, “Coefficient of Restitution Interpreted as Damping in Vibroimpact,” *Journal of Applied Mechanics*, vol. 42, no. 2, p. 440, 1975.
- [41] D. W. Marhefka and D. E. Orin, “A compliant contact model with nonlinear damping for simulation of robotic systems,” *IEEE Transactions on Systems Man and Cybernetics Part A Systems and Humans*, vol. 29, no. 6, pp. 566–572, 1999.
- [42] A. Khurshid, YA and Shabana, “A continuous force model for the impact analysis of flexible multibody systems,” *Mechanism and Machine Theory*, vol. 22, no. 3, pp. 213–224, 1987.

- [43] T. W. Lee and A. C. Wang, “On The Dynamics of Intermittent-Motion Mechanisms. Part 1: Dynamic Model and Response,” *Journal of Mechanisms Transmissions and Automation in Design*, vol. 105, no. 3, p. 534, 1983.
- [44] I. Zhang, Yuning and Sharf, “Compliant force modelling for impact analysis,” *ASME 2004 International Design Engineering Technical Conferences and Computers and Information in Engineering Conference*, pp. 595–601, 2004.
- [45] T. W. Wang, AC and Lee, “On the Dynamics of Intermittent-Motion Mechanisms. Part 2: Geneva Mechanisms, Ratchets, and Escapements,” *Journal of Mechanisms, Transmissions, and Automation in Design*, vol. 105, no. 3, pp. 541—551, 1983.
- [46] O. o. Sorensen, Soren E and Hansen, Michael R and Ebbesen, Morten K and Mouritsen, “Implicit identification of contact parameters in a continuous chain model,” *Modeling, Identification and Control*, vol. 32, no. 1, pp. 1–15, 2011.
- [47] J. Najafabadi, Seyed Ali Modarres and Kovecses, Jozsef and Angeles, “Generalization of the energetic coefficient of restitution for contacts in multibody systems,” *Journal of Computational and Nonlinear Dynamics*, vol. 3, no. 4, 2008.
- [48] Y. Gonthier, J. McPhee, C. Lange, and J. C. Piedboeuf, “A regularized contact model with asymmetric damping and dwell-time dependent friction,” *Multibody System Dynamics*, vol. 11, no. 3, pp. 209–233, 2004.
- [49] D. Herbert, RG and McWhannell, “Shape and frequency composition of pulses from an impact pair,” *Journal of Engineering for Industry*, vol. 99, no. 3, pp. 513–518, 1977.
- [50] G. H. Ristow, “Simulating granular flow with molecular dynamics,” *Journal de Physique I*, vol. 2, no. 5, pp. 649–662, 1992.
- [51] J. Shäfer, S. Dippel, and D. E. Wolf, “Force Schemes in Simulations of Granular Materials,” *Journal de Physique I*, vol. 6, no. 1, pp. 5–20, 1996.
- [52] J. Lee and H. J. Herrmann, “Angle of repose and angle of marginal stability: Molecular dynamics of granular particles,” *Journal of Physics A: Mathematical and General*, vol. 26, no. 2, pp. 373–383, 1993.

- [53] A. S. Yigit, A. G. Ulsoy, and R. A. Scott, “Spring-dashpot models for the dynamics of a radially rotating beam with impact,” *Journal of Sound and Vibration*, vol. 142, no. 3, pp. 515–525, 1990.
- [54] S. Abrate, *Impact on composite structures*. Cambridge university press, 2005.
- [55] C. Lim and W. Stronge, “Oblique elastic-plastic impact between rough cylinders in plane strain,” *International Journal of Engineering Science*, vol. 37, no. 1, pp. 97–122, 1999.
- [56] C. T. Lim and W. J. Stronge, “Normal elastic-plastic impact in plane strain,” *Mathematical and Computer Modelling*, vol. 28, no. 4-8, pp. 323–340, 1998.
- [57] W. J. Stronge, R. James, and B. Ravani, “Oblique impact with friction and tangential compliance,” *Philosophical Transactions of the Royal Society A: Mathematical, Physical and Engineering Sciences*, vol. 359, no. 1789, pp. 2447–2465, 2001.
- [58] K. A. Ismail and W. J. Stronge, “Impact of Viscoplastic Bodies: Dissipation and Restitution,” *Journal of Applied Mechanics*, vol. 75, no. 6, p. 061011, 2008.
- [59] Y. Hurnuzlu, “An energy-based coefficient of restitution for planar impacts of slender bars with massive external surfaces,” *Journal of Applied Mechanics*, vol. 65, no. 4, pp. 952–962, 1998.
- [60] R. Cross, “The bounce of a ball,” *American Journal of Physics*, vol. 67, no. 3, pp. 222–227, 1999.
- [61] Stronge W. J., *Impact Mechanics*. Cambridge, UK: Cambridge University Press, 2000.
- [62] P. S. D, *Recherches sur la probabilite des jugements en matirre criminelle et en matiere civile precedees des regles generales du calcul des probabilites par SD Poisson*. Bachelier, 1837.
- [63] W. J. Stronge, “Rigid body collisions with friction,” *Proceedings of the Royal Society of London. Series A: Mathematical and Physical Sciences*, vol. 431, no. 1881, pp. 169–181, 1990.
- [64] G. Barnes, “Study of collisions: Part I: A survey of the periodical literature,” *American Journal of Physics*, vol. 26, no. 5, pp. 5–12, 1957.

- [65] A. J. Morin, *Notions fondamentales de mecanique et donnees d exp erience*. Hachette, 1860.
- [66] R. E. John, *The advanced part of A treatise on the dynamics of a system of rigid bodies. Being part II. of a treatise on the whole subject*, 6th ed. New York: Dover Publication, 1955.
- [67] D. Stoianovici and Y. Hurmuzlu, “A critical study of the applicability of rigid-body collision theory,” *Journal of Applied Mechanics*, vol. 63, no. 2, pp. 307–316, 1996.
- [68] D. Auerbach, “Colliding rods: Dynamics and relevance to colliding balls,” *American Journal of Physics*, vol. 62, no. 6, p. 522, 1994.
- [69] A. A. Freschi, R. Hessel, M. Yoshida, and D. L. Chinaglia, “Compression waves and kinetic energy losses in collisions between balls and rods of different lengths,” *American Journal of Physics*, vol. 82, no. 4, pp. 280–286, 2014.
- [70] B. Hu, W. Schiehlen, and P. Eberhard, “Comparison of Analytical and Experimental Results for Longitudinal Impacts on Elastic Rods,” *Journal of Vibration and Control*, vol. 9, no. 1-2, pp. 157–174, 2003.
- [71] W. Schiehlen, R. Seifried, and P. Eberhard, “Elastoplastic phenomena in multibody impact dynamics,” *Computer Methods in Applied Mechanics and Engineering*, vol. 195, no. 50-51, pp. 6874–6890, 2006.
- [72] W. Schiehlen and R. Seifried, “Three approaches for elastodynamic contact in multibody systems,” *Multibody System Dynamics*, vol. 12, no. 1, pp. 1–16, 2004.
- [73] R. Seifried, B. Hu, and P. Eberhard, “Numerical and experimental investigation of radial impacts on a half-circular plate,” *Multibody System Dynamics*, vol. 9, no. 3, pp. 265–281, 2003.
- [74] A. K. Belyaev, C.-C. Ma, N. F. Morozov, P. E. Tovstik, T. P. Tovstik, and A. O. Shurpatov, “Dynamics of a rod undergoing a longitudinal impact by a body,” *Vestnik St. Petersburg University: Mathematics*, vol. 50, no. 3, pp. 310–317, 2017.
- [75] W. Maenhauta and J. D. Reuckb, “Analytical solutions of impact problems of rod structures with springs,” vol. 104, no. 97, pp. 328–332, 1995.

- [76] S. Wang, Y. Wang, Z. Huang, and T. X. Yu, “Dynamic Behavior of Elastic Bars and Beams Impinging on Ideal Springs,” *Journal of Applied Mechanics*, vol. 83, no. 3, p. 31002, 2015.
- [77] R. Yigit, AS and Ulsoy, AG and Scott, “Dynamics of a radially rotating beam with impact, Part 1 Theoretical and computational model,” *Journal of Vibration and Acoustics*, vol. 112, no. 1, pp. 65—70, 1990.
- [78] A. Gau, Wei-Hsin and Shabana, “Use of the generalized impulse momentum equations in analysis of wave propagation,” *Journal of vibration and acoustics*, vol. 113, no. 4, pp. 532—542, 1991.
- [79] H. M. Flores, Paulo and Ambrosio, Jorge and Claro, JC Pimenta and Lankarani, *Kinematics and dynamics of multibody systems with imperfect joints: models and case studies*. Springer Science & Business Media, 2008, vol. 34, no. September.
- [80] P. E. Nikravesh, *Computer-aided analysis of mechanical systems*. Prentice-hall Englewood Cliffs, NJ, 1988.
- [81] P. Nikravish, *Planar multibody dynamics: formulation, programming and applications*. CRC press, 2007.
- [82] A. A. Shabana, “Flexible Multibody Dynamics: Review of Past and Recent Developments,” *Multibody System Dynamics*, vol. 1, no. 2, pp. 189–222, 1997.
- [83] D. Verscheure, I. Sharf, H. Bruyninckx, J. Swevers, and J. De Schutter, “Identification of contact parameters from stiff multi-point contact robotic operations,” *International Journal of Robotics Research*, vol. 29, no. 4, pp. 367–385, 2010.
- [84] E. Askari, P. Flores, D. Dabirrahmani, and R. Appleyard, “Study of the friction-induced vibration and contact mechanics of artificial hip joints,” *Tribology International*, vol. 70, pp. 1–10, 2014.
- [85] A. A. Shabana, K. E. Zaazaa, J. L. Escalona, and J. R. Sany, “Development of elastic force model for wheel/rail contact problems,” *Journal of Sound and Vibration*, vol. 269, no. 1-2, pp. 295–325, 2004.
- [86] J. A. C. Ambrósio, M. A. Neto, and R. P. Leal, “Optimization of a complex flexible multibody systems with composite materials,” *Multibody System Dynamics*, vol. 18, no. 2, pp. 117–144, 2007.

- [87] J. Ambrósio and P. Verissimo, “Sensitivity of a vehicle ride to the suspension bushing characteristics,” *Journal of Mechanical Science and Technology*, vol. 23, no. 4, pp. 1075–1082, 2009.
- [88] “Energy trapping and shock disintegration in a composite granular medium,” *Physical Review Letters*, vol. 96, no. 5, pp. 1–4, 2006.
- [89] S. K. Dwivedy and P. Eberhard, “Dynamic analysis of flexible manipulators, a literature review,” *Mechanism and Machine Theory*, vol. 41, no. 7, pp. 749–777, 2006.
- [90] H. T. Pham and D. A. Wang, “A constant-force bistable mechanism for force regulation and overload protection,” *Mechanism and Machine Theory*, vol. 46, no. 7, pp. 899–909, 2011.
- [91] I. Gonzalez-Perez, J. L. Iserte, and A. Fuentes, “Implementation of Hertz theory and validation of a finite element model for stress analysis of gear drives with localized bearing contact,” *Mechanism and Machine Theory*, vol. 46, no. 6, pp. 765–783, 2011.
- [92] D. Dopico, A. Luaces, M. Gonzalez, and J. Cuadrado, “Dealing with multiple contacts in a human-in-the-loop application,” *Multibody System Dynamics*, vol. 25, no. 2, pp. 167–183, 2011.
- [93] K. D. Bhalerao and K. S. Anderson, “Modeling intermittent contact for flexible multibody systems,” *Nonlinear Dynamics*, vol. 60, no. 1-2, pp. 63–79, 2010.
- [94] T. A. Walkiewicz, “Linear Collisions,” *American Journal of Physics*, vol. 40, no. 1, p. 133, 1972.
- [95] W. Johnson, “Simple Linear Impact,” *ImechE. IJMEE*, vol. 4, no. 2, pp. pp. 167–181, 1976.
- [96] B. Han, Inhwan and Gilmore, “Multi-body impact motion with friction—Analysis, simulation, and experimental validation,” *Journal of Mechanical Design*, vol. 115, no. 3, pp. 412–422, 1993.
- [97] B. Brogliato, “Nonsmooth impact mechanics: models, dynamics and control,” *Lecture Notes in Control and Information Science*, vol. 210, 1996.

- [98] N. D. Newby, “Linear collisions with harmonic oscillator forces: the inverse scattering problem,” *American Journal of Physics*, vol. 47, no. 2, pp. 161–165, 1979.
- [99] E. J. Hinch and S. Saint-Jean, “The fragmentation of a line of balls by an impact,” *Proceedings of the Royal Society A: Mathematical, Physical and Engineering Sciences*, vol. 455, no. 1989, pp. 3201–3220, 1999.
- [100] C. Cholet, “Chocs de Solids Rigid,” Ph.D. dissertation, Ph. D. thesis, University of Paris, Paris, France, 1998.
- [101] J. J. Moreau, “Some numerical methods in multibody dynamics : application to granular materials,” 2018.
- [102] W. J. Stronge, “Chain reaction from impact on aggregate of elasto-plastic rigid bodies,” *International Journal of Impact Engineering*, vol. 28, no. 3, pp. 291–302, 2003.
- [103] W. Stronge, “Generalized impulse and momentum applied to multibody impact with friction,” *Mechanics of Structures and Machines*, vol. 29, no. 2, pp. 239–260, 2001.
- [104] R. Singh, A. Shukla, and H. Zervas, “Explosively generated pulse propagation through particles containing natural cracks,” *Mechanics of Materials*, vol. 23, no. 4, pp. 255–270, 1996.
- [105] G. Laird, “An investigation of ball-on-ball impact,” *Experimental Mechanics*, vol. 29, pp. 300–306, 1989.
- [106] W. Stronge, “Chain reaction from impact on coaxial multibody systems,” *Journal of applied mechanics*, vol. 67, no. 3, pp. 632–635, 2000.
- [107] M. Gharib, A. Celik, and Y. Hurmuzlu, “Shock Absorption Using Linear Particle Chains With Multiple Impacts,” *Journal of Applied Mechanics*, vol. 78, no. 3, p. 031005, 2011.
- [108] C. Liu, Z. Zhao, and B. Brogliato, “Frictionless multiple impacts in multibody systems. I. Theoretical framework,” *Proceedings of the Royal Society A: Mathematical, Physical and Engineering Sciences*, vol. 464, no. 2100, pp. 3193–3211, 2008.

- [109] C. Liu, Z. Zhao, and Brogliato, “Theoretical Analysis and Numerical Algorithm for Frictionless Multiple Impacts in Multibody Systems,” 2008.
- [110] Y. Hurmuzlu, “Dynamics of bipedal gait: Part i—objective functions and the contact event of a planar five-link biped,” *Journal of Applied Mechanics*, vol. 60, no. 2, pp. 331–336, 1993.
- [111] Y. Hurmuzlu and T.-H. Chang, “Rigid body collisions of a special class of planar kinematic chains,” *Systems, Man and Cybernetics, IEEE Transactions on*, vol. 22, no. 5, pp. 964–971, 1992.
- [112] Y. Hurmuzlu and G. Moskowitz, “The role of impact in the stability of bipedal locomotion,” *Dynamics and Stability of Systems*, vol. 1, no. 3, pp. 217–234, 1986.
- [113] Y. Hurmuzlu, “Dynamics of bipedal gait: Part ii—stability analysis of a planar five-link biped,” *Journal of Applied Mechanics*, vol. 60, no. 2, pp. 337–343, 1993.
- [114] A. Chatterjee and A. Ruina, “A new algebraic rigid-body collision law based on impulse space considerations,” *Journal of Applied Mechanics*, vol. 65, pp. 939–951, 1998.
- [115] S. Goyal, P. Elliot, and F. Sinden, “Simulation of dynamics of interacting rigid bodies including friction i: General problem and contact model,” *Engineering with computers*, vol. 10, no. 3, pp. 162–174, 1994.
- [116] D. B. Marghitu and Y. Hurmuzlu, “Three-dimensional rigid-body collisions with multiple contact points,” *Journal of applied mechanics*, vol. 62, no. 3, pp. 725–732, 1995.
- [117] A. Tavakoli, M. Gharib, and Y. Hurmuzlu, “Collision of two mass baton with massive external surfaces,” *Journal of applied mechanics*, vol. 79, no. 5, 2012.
- [118] A. Tavakoli and Y. Hurmuzlu, “Robotic locomotion of three generations of a family tree of dynamical systems. part i: Passive gait patterns,” *Nonlinear Dynamics*, vol. 73, no. 3, pp. 1969–1989, 2013.
- [119] Y. Hurmuzlu and G. G. D. Moskowitz, “Bipedal locomotion stabilized by impact and switching: I. two-and three-dimensional, three-element

- models,” *Dynamics and Stability of Systems*, vol. 2, no. 2, pp. 73–96, 1987.
- [120] Y. Hurmuzlu and G. Moskowitz, “Bipedal locomotion stabilized by impact and switching: Ii. structural stability analysis of a four-element bipedal locomotion model,” *Dynamics and Stability of Systems*, vol. 2, no. 2, pp. 97–112, 1987.
 - [121] D. M. Flickinger and A. Bowling, “Simultaneous oblique impacts and contacts in multibody systems with friction,” *Multibody System Dynamics*, vol. 23, no. 3, pp. 249–261, 2010.
 - [122] L. Meirovitch, *Methods of analytical dynamics*. Courier Corporation, 2010.
 - [123] Y. Khulief and A. Shabana, “Dynamic analysis of constrained system of rigid and flexible bodies with intermittent motion,” *Journal of Mechanisms, Transmissions, and Automation in Design*, vol. 108, no. 1, pp. 38–45, 1986.
 - [124] P. Razzaghi and N. Assadian, “Study of the triple-mass tethered satellite system under aerodynamic drag and j2 perturbations,” *Advances in Space Research*, vol. 56, no. 10, pp. 2141–2150, 2015.
 - [125] B. Brogliato, *Nonsmooth mechanics : models, dynamics and control*, 2nd ed. London: Springer, 1999.
 - [126] K. Alluhydan, P. Razzaghi, and Y. Hurmuzlu, “On planar impacts of cylinders and balls,” *Journal of Applied Mechanics*, pp. 1–11, 2019.
 - [127] M. Gharib and Y. Hurmuzlu, “A New Contact Force Model for Low Coefficient of Restitution Impact,” *Journal of Applied Mechanics*, vol. 79, no. 6, p. 64506, 2012.
 - [128] E. Ermolin and A. Kazakov, “Impulse-based approach for rigid body collisions simultaneous resolution,” in *International Conference Graphicon*, 2005.
 - [129] C. Liu, Z. Zhao, and B. Brogliato, “Frictionless multiple impacts in multibody systems. ii. numerical algorithm and simulation results,” *Proceedings of the Royal Society A: Mathematical, Physical and Engineering Sciences*, vol. 465, no. 2101, pp. 1–23, 2008.

- [130] N. S. Nguyen and B. Brogliato, *Multiple impacts in dissipative granular chains*. Springer, 2014, vol. 3.
- [131] V. Bhatt and J. Koechling, “Three-dimensional frictional rigid-body impact,” *Journal of applied mechanics*, vol. 62, no. 4, pp. 893–898, 1995.
- [132] H. M. Lankarani and M. F. Pereira, “Treatment of impact with friction in planar multibody mechanical systems,” *Multibody System Dynamics*, vol. 6, no. 3, pp. 203–227, 2001.
- [133] Z. Zhao, C. Liu, and B. Brogliato, “Planar dynamics of a rigid body system with frictional impacts. ii. qualitative analysis and numerical simulations,” *Proceedings of the Royal Society A: Mathematical, Physical and Engineering Science*, vol. 465, no. 2107, pp. 2267–2292, 2009.
- [134] B. Brogliato, *Impacts in mechanical systems: analysis and modelling*. Springer Science & Business Media, 2000, vol. 551.
- [135] C. Glocker and F. Pfeiffer, “Multiple impacts with friction in rigid multibody systems,” *Nonlinear Dynamics*, vol. 7, no. 4, pp. 471–497, 1995.
- [136] B. Brogliato, H. Zhang, and C. Liu, “Analysis of a generalized kinematic impact law for multibody-multicontact systems, with application to the planar rocking block and chains of balls,” *Multibody System Dynamics*, vol. 27, no. 3, pp. 351–382, 2012.
- [137] A. Blumentals, B. Brogliato, and F. Bertails-Descoubes, “The contact problem in lagrangian systems subject to bilateral and unilateral constraints, with or without sliding coulomb’s friction: A tutorial,” 2014.
- [138] F. Aghili, “Modeling and analysis of multiple impacts in multibody systems under unilateral and bilateral constrains based on linear projection operators,” *Multibody System Dynamics*, pp. 1–22, 2018.
- [139] T. Winandy and R. I. Leine, “A maximal monotone impact law for the 3-ball newton’s cradle,” *Multibody System Dynamics*, vol. 39, no. 1-2, pp. 79–94, 2017.

- [140] S. Ahmed, H. Lankarani, and M. Pereira, “Frictional impact analysis in open-loop multibody mechanical systems,” *Journal of Mechanical Design*, vol. 121, p. 119, 1999.
- [141] A. Tavakoli and Y. Hurmuzlu, “Robotic locomotion of three generations of a family tree of dynamical systems. part ii: Impulsive control of gait patterns,” *Nonlinear Dynamics*, pp. 1–22, 2013.
- [142] J.-J. E. Slotine, W. Li *et al.*, *Applied nonlinear control*. Prentice hall Englewood Cliffs, NJ, 1991, vol. 199, no. 1.
- [143] V. Acary and B. Brogliato, “Concurrent multiple impacts modelling: case study of a 3-ball chain,” in *Computational Fluid and Solid Mechanics 2003*. Elsevier, 2003, pp. 1842–1847.
- [144] D. Jalon, J. Garcia, and E. Bayo, *Kinematic and dynamic simulation of multibody systems: the real-time challenge*. Springer Science & Business Media, 2012.
- [145] V. A. Lubarda, “The Bounds on the Coefficients of Restitution for the Frictional Impact of Rigid Pendulum Against a Fixed Surface,” *Journal of Applied Mechanics*, vol. 77, no. 1, p. 11006, 2010.
- [146] W. Stronge, “Energy dissipated in planar collision,” *Journal of applied mechanics*, vol. 59, p. 681, 1992.
- [147] T. Kane, “A dynamics puzzle,” *Stanford Mechanics Alumni Club Newsletter*, vol. 6, pp. 1–4, 1984.
- [148] F. Veluswami, MA and Crossley, “Multiple Impacts of a Ball Between Two Plates Part 1: Some Experimental Observations,” *Journal of Engineering for Industry*, vol. 97, no. 3, pp. 820–827, 1975.
- [149] J. P. Nobre, A. M. Dias, and R. Gras, “A study on elasto-plastic impact friction,” *Wear*, vol. 230, no. 2, pp. 133–145, 1999.
- [150] V. Acary and B. Brogliato, *Numerical methods for nonsmooth dynamical systems: applications in mechanics and electronics*. Springer Science & Business Media, 2008, vol. 35.
- [151] B. Brogliato, “Inertial couplings between unilateral and bilateral holonomic constraints in frictionless lagrangian systems,” *Multibody System Dynamics*, vol. 29, no. 3, pp. 289–325, 2013.

- [152] R. M. Brach, “Rigid body collisions,” *Journal of Applied Mechanics*, vol. 56, no. 1, pp. 133–138, 1989.
- [153] F. Reuleaux, *Kinematics of machinery: outlines of a theory of machines*. Courier Dover Publications, 2012.
- [154] Y. Nakamura and M. Ghodoussi, “Dynamics computation of closed-link robot mechanisms with nonredundant and redundant actuators,” *Robotics and Automation, IEEE Transactions on*, vol. 5, no. 3, pp. 294–302, 1989.
- [155] N. Karandikar and O. Vargas, “Kinetic chains: a review of the concept and its clinical applications,” *PM&R*, vol. 3, no. 8, pp. 739–745, 2011.
- [156] P. Razzaghi, E. Al Khatib, and S. Bakhtiari, “Dynamics analysis and gnc design of flexible systems for space debris active removal,” *Advances in Space Research*, 2019.
- [157] E. Al Khatib, W. M. Al-Masri, S. Mukhopadhyay, M. A. Jaradat, and M. Abdel-Hafez, “A comparison of adaptive trajectory tracking controllers for wheeled mobile robots,” in *Mechatronics and its Applications (ISMA), 2015 10th International Symposium on*. IEEE, 2015, pp. 1–6.
- [158] E. I. Al Khatib, M. A. Jaradat, M. Abdel-Hafez, and M. Roigari, “Multiple sensor fusion for mobile robot localization and navigation using the extended kalman filter,” in *Mechatronics and its Applications (ISMA), 2015 10th International Symposium on*. IEEE, 2015, pp. 1–5.
- [159] A. G. Khiabani and R. Babazadeh, “Design of robust fractional-order lead–lag controller for uncertain systems,” *IET Control Theory & Applications*, vol. 10, no. 18, pp. 2447–2455, 2016.
- [160] A. G. Khiabani and A. Heydari, “Optimal switching of voltage source inverters using approximate dynamic programming,” in *ASME 2018 Dynamic Systems and Control Conference*. American Society of Mechanical Engineers, 2018, pp. V001T01A006–V001T01A006.
- [161] R. Babazadeh, A. G. Khiabani, and H. Azmi, “Optimal control of segway personal transporter,” in *2016 4th International Conference on Control, Instrumentation, and Automation (ICCIA)*. IEEE, 2016, pp. 18–22.